

## Original Article

# Pyroptosis impacts the prognosis and treatment response in gastric cancer via immune system modulation

Wanli Yang<sup>1\*</sup>, Liaoran Niu<sup>1\*</sup>, Xinhui Zhao<sup>2\*</sup>, Lili Duan<sup>1\*</sup>, Xiaoqian Wang<sup>1</sup>, Yiding Li<sup>1</sup>, Junfeng Chen<sup>1</sup>, Wei Zhou<sup>1</sup>, Yujie Zhang<sup>3</sup>, Daiming Fan<sup>1</sup>, Liu Hong<sup>1</sup>

<sup>1</sup>State Key Laboratory of Cancer Biology and National Clinical Research Center for Digestive Diseases, Xijing Hospital of Digestive Diseases, Fourth Military Medical University, Xi'an, Shaanxi, China; <sup>2</sup>Department of Thyroid and Breast Surgery, Xi'an No. 3 Hospital, The Affiliated Hospital of Northwest University, Northwest University, Xi'an, Shaanxi, China; <sup>3</sup>Department of Histology and Embryology, School of Basic Medicine, Xi'an Medical University, Xi'an, Shaanxi, China. \*Equal contributors.

Received February 2, 2022; Accepted March 24, 2022; Epub April 15, 2022; Published April 30, 2022

**Abstract:** Pyroptosis plays a vital role in the development of cancers; however, its role in regulating immune cell infiltration in tumor microenvironment (TME) and pyroptosis-related molecular subtypes remain unclear. Herein, we comprehensively analyzed the molecular subtypes mediated by the pyroptosis-related genes (PRGs) in gastric cancer (GC). Three pyroptosis patterns were determined with distinct TME cell-infiltrating characteristics and prognosis. Principal component analysis was performed to establish the pyroptosis score. The high pyroptosis score group was featured by increased activated CD4<sup>+</sup> T cell infiltration, better prognosis, elevated tumor mutation burden, higher immune and stromal scores, and enhanced response to immunotherapy. However, the low pyroptosis score group was characterized by poorer survival, decreased immune infiltration, and glycerolipid and histidine metabolism pathways. Additionally, high pyroptosis score was confirmed as an independent favorable prognostic factor for overall survival. Three cohorts designed to analyze the response to immunotherapy verified that patients with higher pyroptosis score showed treatment benefit. In summary, our study demonstrated that pyroptosis regulates the complex TME. Assessing the pyroptosis patterns will advance our understanding on TME features and tumor immunology and provide the rationale for designing personalized immunotherapy strategies.

**Keywords:** Pyroptosis, gastric cancer, immunotherapy, tumor microenvironment, prognosis

## Introduction

Gastric cancer (GC) ranks as the fourth most common cancer worldwide and claims about 11,010 lives in the United States in 2020 [1]. Metastasis, local recurrences, and multidrug resistance are the major causes of death in patients with advanced GC [2]. Due to the lack of ideal diagnostic biomarkers, most GC patients are diagnosed at late stage, and radical surgery can't be performed. Thus, chemotherapy plays a crucial role in the management of GC, especially for the advanced GC patients. Recently, immunotherapy is emerging as a promising treatment option for GC [3]. Immunotherapy uses patient's own immune system to identify and eliminate the cancer cells. The most successful immunotherapy used so far

is to target the immune checkpoint blockade such as programmed cell death-1/Ligand 1 (PD-1/L1) [4, 5]. Nevertheless, only a small fraction of patients have benefited from the immunotherapy [6, 7]. Therefore, it is in urgent need to identify the prognostic biomarkers and improve the effectiveness of immunotherapy. Previous studies have argued that genetic variation, epigenetic regulation, and environmental factors play crucial roles in the tumor initiation and progression [8, 9]. However, increasing evidence demonstrates that the tumor microenvironment (TME) is also a key regulatory factor in tumor progression [10, 11]. Tumor cells can directly or indirectly interact with the TME components, which, in turn promotes the malignant phenotypes of tumor cells [10, 12, 13]. Effective immunotherapy is based on the infil-

tration of immune cells in tumor sites, prediction of the response to immunotherapy based on the characterization of TME cell infiltration has become an important area of research, and novel immunotherapeutic drugs are currently being developed and tested [6, 7]. Hence, TME is important for the management of tumor progression, the development of personalized immunotherapy, and the prediction of prognosis and the response to immunotherapy [11, 14].

To personalize and optimize the treatments for patients with GC, an accurate prognosis prediction is also crucial for the GC management. To date, the tumor node metastasis (TNM) staging system is commonly adopted to predict the prognosis of cancer patients [15]. Nevertheless, increasing evidence showed the unsatisfactory discriminative capacity of staging system [16, 17]. There is controversy over whether the risk factors other than TNM factors are important predictors of clinical outcomes [17]. Recently, increasing prognostic biomarkers have been identified for GC [2]. Nevertheless, the existing biomarkers may lack sufficient specificity and sensitivity in prognosis judgement [2]. A comprehensive understanding of the TME landscape and different tumor immune phenotypes as well as the biomarkers or molecular signatures will be helpful in guiding the development of cancer treatment and prognosis prediction, which would be a great complement to the TNM staging system.

Pyroptosis has been reported as a pro-inflammatory cell death characterized by cellular swelling, plasma membrane rupture, water influx, osmotic lysis, and the release of the intracellular pro-inflammatory contents [18]. Although it shares some features with apoptosis, including caspase dependence, nuclear condensation, and DNA damage [18], pyroptosis has unique features. For example, pyroptosis is morphologically different from apoptosis as it presents the features of lysis and cell swelling [19]. Pyroptosis can be triggered mainly by two pathways—canonical pathway and non-canonical pathway. The canonical pathway is activated when pathogens, pathogen associated molecular patterns (PAMPs), and damage associated molecular patterns (DAMPs) activates the inflammasome sensors such as nucleotide oligomerization domain (NOD)-like receptor family, pyrin domain-containing-1 and 3 (NLRP1, NLRP3), or absent in melanoma-2

(AIM2) and recruits caspase 1 (CASP1) to activate Gasdermin D (GSDMD), which then forms a pore in the plasma membrane [20, 21]. As for the non-canonical pathway, lipopolysaccharide (LPS) and PAMPs directly activate CASP4, CASP5, and CASP11, causing pyroptosis via cleaving GSDMD. Subsequently, the activated GSDMD initiates pore formation in the cell membrane, finally inducing the cell death [20]. Pyroptosis is initially identified as an infection defending mechanism. Recent studies have revealed its important role in the development of various tumors [22, 23]. For example, caspase-3/GSDME pathway is considered as a switch between apoptosis and pyroptosis in cancer [24]. Recent studies also reveal the significant roles of pyroptosis in regulating immunology and tumor immune microenvironment (TIME) [25]. GSDMD is reported to enhance the phagocytosis of tumor cells by tumor-associated macrophages, tumor-infiltrating natural-killer, and CD8+ T lymphocytes and promote neutrophil death [26]. Furthermore, PD-L1-regulated GSDMC expression can switch apoptosis to pyroptosis in cancer cells and facilitate tumor necrosis [27]. However, most of studies only explored the function of a single or several pyroptosis-related genes (PRGs), while comprehensive analysis on the correlation of PRGs and TME characterizations is scarce. In this study, we comprehensively assessed the correlation between the pyroptosis-related molecular patterns and the TME cell-infiltrating characteristics through analyzing the genomic data of 989 GC cases. Three distinct pyroptosis-related molecular patterns were identified with different prognosis and TME characteristics, indicating the importance of pyroptosis-related molecular clusters in modulating the characterizations of TME. Moreover, we established a pyroptosis score system to quantify the pyroptosis clusters for each GC patient. The pyroptosis score may be helpful in selecting the personalized immunotherapy and predicting the prognosis of GC patients.

### Materials and methods

#### Materials

TRIzol reagent: Invitrogen, USA.

PrimeScript™ RT Master Mix (Perfect Real Time) Kit: TaKaRa, Dalian, China.

SYBR® Premix Ex Taq™ II (Tli RNaseH Plus): TaKaRa, Dalian, China.

## Prognostic role of pyroptosis-related genes in gastric cancer

Anti-GSDMC antibody: 27630-1-AP; Proteintech Group, Inc., USA.

HRP-conjugated secondary antibodies: Sigma-Aldrich, USA.

DAB substrate liquid: Thermo Fisher Scientific, USA.

### *Dataset collection and preprocessing*

[Figure S1](#) presented the workflow of our study. Gene profiling data and full clinical information were searched in Gene-Expression Omnibus (GEO) (<http://www.ncbi.nlm.nih.gov/geo/>) and The Cancer Genome Atlas (TCGA) (<https://portal.gdc.cancer.gov/>) databases. Datasets without survival information were censored. Five eligible GC cohorts (GSE15459, GSE34942, GSE57303, GSE62254, and TCGA-Stomach Adenocarcinoma (STAD)) were selected in the study. GEO database are available in GPL570 platform (Affymetrix Human Genome U133 Plus 2.0 Array). The raw “CEL” files of these GEO datasets were downloaded, and “affy” and “simpleaffy” packages were used to perform the background adjustment and quantile normalization. For TCGA-STAD dataset, gene expression profiling of RNA seq data (FPKM value) was obtained from the Genomic Data Commons (GDC, <https://portal.gdc.cancer.gov/>) website. Subsequently, the fragments per kilobase million (FPKM) values were transformed into transcripts per kilobase million (TPM). The “ComBat” algorithm of “sva” package was applied to correct the batch effects due to the non-biological technical bias. [Table S1](#) presented the information of all enrolled datasets of GC patients. The genomic mutation data (copy number variation (CNV) and somatic mutation data) of TCGA-STAD were downloaded from the UCSC Xena database (<https://gdc.xenahubs.net/>). The CNV landscape of 33 PRGs in human chromosomes was plotted using the “Rcircos” package.

### *Unsupervised clustering for PRGs*

Thirty-three PRGs were extracted from the prior reviews [28-31] ([Table S2](#)). These genes are known to be involved in the pyroptosis signaling, and encoding the core components of the pyroptosis machinery. Thus, they are collectively termed as PRGs. 30 overlapping PRGs were extracted from five integrated datasets to construct pyroptosis-related molecular patterns by

unsupervised clustering analysis ([Table S3](#)). The optimal number of clusters and their stability were evaluated based on the consensus clustering algorithm. The “ConsensusClusterPlus” package was used to conduct the above steps and 1000 times repetitions were performed to guarantee the classification stability [32].

### *Gene set variation analysis (GSVA) and functional enrichment*

GSVA enrichment was performed to decipher the biological process among the different pyroptosis clusters using “GSVA” R packages. The biological signatures (c2.cp.kegg.v7.2.symbols) were downloaded from the MSigDB database (<http://www.gsea-msigdb.org/gsea/msigdb>) for GSVA enrichment analysis. Adjusted *P*-value  $P < 0.05$  was regarded as statistically significant. Functional enrichment for PRGs was performed using the “clusterProfiler” R package with false discovery rate (FDR)-value cutoff below 0.05.

### *Estimation of immune cell infiltration*

The single sample gene set enrichment analysis (ssGSEA) was performed to quantify the relative abundance of different immune cell types in the TME as reported [33]. Marker genes for each tumor-infiltrating immune cell type were selected based on previous publications [34]. The enrichment score was calculated by ssGSEA analysis and normalized to unity distribution from 0 to 1 to represent the relative abundance of each immune cell type.

### *Identification of pyroptosis molecular pattern-related differential expression genes (DEGs)*

To identify the pyroptosis molecular pattern-related DEGs, we classified GC patients into three different pyroptosis molecular patterns based on the expression of 30 PRGs. The “limma” R package was utilized to screen the DEGs in GC patients in the distinct clusters [35]. The criteria for selecting the pyroptosis molecular pattern-related DEGs were set at adjusted *p*-value  $< 0.001$ .

### *Estimation of STromal and Immune cells in MAlignant Tumour tissues using Expression data (ESTIMATE)*

By performing the ESTIMATE algorithm, the ESTIMATE score, stromal score, and immune

## Prognostic role of pyroptosis-related genes in gastric cancer

score were calculated to evaluate the levels of infiltrating stromal and immune cells [36]. The differences in the ESTIMATE score, stromal score, and immune score among the different groups was compared using Wilcoxon rank-sum test.

### *Development of the pyroptosis score*

Pyroptosis scoring system was established to evaluate the pyroptosis-related molecular patterns of individual patient with GC by using principal components analysis (PCA) algorithm. Briefly, the overlapping DEGs screened from different pyroptosis clusters were used to select the overall survival (OS)-related DEGs by using the univariate Cox regression analysis. The OS-related DEGs were extracted for further analysis. The consensus clustering algorithm was used for identify the number of pyroptosis gene clusters as well as their stability using the OS-related DEGs. Then, PCA was performed to construct the pyroptosis-related gene signature (pyroptosis score). Both principal component 1 and 2 were extracted and served as the signature score. We subsequently used a formula similar to previous studies to define the pyroptosis score [37, 38]:  $\text{pyroptosis score} = \sum(\text{PC1}_i + \text{PC2}_i)$ , where  $i$  represents the expression of final determined pyroptosis phenotype-related prognostic DEGs.

### *Analysis of somatic alteration data*

Mutation data of GC patients in the TCGA-STAD cohort were downloaded from TCGA database (<https://www.cancer.gov/tcga/>). The total number of non-synonymous mutations (including frameshift mutation, inflame mutation, missense mutation, nonsense mutation, and splice site mutation) was counted to determine the mutational burden of GC [33]. The “maftool” package was used to identify and present the GC driver genes [39]. The distribution difference of somatic alterations between the low and high pyroptosis score group in TCGA-STAD cohort was also evaluated. The top 20 driver genes with the highest alteration frequency in these two groups were compared as reported [40].

### *Prediction of drug sensitivity for GC patients*

The Genomics of Drug Sensitivity in Cancer (GDSC; <https://www.cancerrxgene.org/>) data-

base was used to estimate the sensitivity of each patient to different chemotherapy drugs [41]. “pRRophetic” package was utilized to quantify the half-maximal inhibitory concentration (IC50) of drugs [42].

### *Identification of small molecule drugs for GC patients*

The “limma” package was applied to screen the DEGs between the low and high pyroptosis score groups with  $p$ -value  $< 0.05$  and  $|\log_{2}\text{FC}| > 1.0$  and visualized by volcano plot. “ClusterProfiler” package was used for Kyoto Encyclopedia of Genes and Genomes (KEGG) and Gene Ontology (GO) enrichment analyses. An adjusted  $p$ -value  $< 0.05$  was considered statistically significant. The upregulated and downregulated DEGs were then uploaded into the Connectivity map (CMap) database (<http://portals.broadinstitute.org/cmap/>) [43]. Small molecular drug candidates were identified by CMap mode-of-action (MoA) analysis.

### *Validation of pyroptosis score in predicting response to immunotherapy*

The immunophenogram was established to predict the response to anti-PD-1/PD-L1 therapy in pan-cancer [34]. Immunophenoscore (IPS) was calculated by the immunophenogram among the four cancer subtypes. The clinical data containing IPS information of TCGA-STAD cohort were downloaded from The Cancer Immunome Atlas database (TCIA, <https://tcia.at/home>) [34]. We compared IPS (cytotoxic T lymphocyte-associated antigen-4 (CTLA4)<sub>negative</sub>+PD-1<sub>negative</sub>, CTLA4<sub>positive</sub>+PD-1<sub>negative</sub>, CTLA4<sub>negative</sub>+PD-1<sub>positive</sub>, CTLA4<sub>positive</sub>+PD-1<sub>positive</sub>) between the high and low pyroptosis score groups in each subtype. A high IPS in PD-1<sub>positive</sub>/CTLA4<sub>positive</sub> subtype predicted a better response to anti-PD-1/PD-L1/anti-CTLA4 therapy.

Three immunotherapy cohorts were enrolled in this study. The gene expression profiles and complete clinical information were downloaded from the GEO database. These three cohorts had 26 patients with metastatic melanoma treated with anti-PD-1 antibody (GSE78220 cohort) [44], 27 patients with advanced non-small cell lung carcinoma patients treated with anti-PD-1/PD-L1 antibody (GSE135222 cohort) [45, 46], and 56 patients with advanced mela-

## Prognostic role of pyroptosis-related genes in gastric cancer

noma treated with anti-CTLA4 and anti-PD-1 (GSE91061 cohort) antibodies [47]. The gene expression profiles of GEO datasets were curated and converted to the TPM format for further analysis.

### *Tissues collection, RNA isolation, and quantitative reverse transcription PCR (RT-qPCR)*

20 paired GC and adjacent normal tissues were collected from the GC patients who underwent radical resection at the Xijing Hospital of Digestive Diseases of Fourth Military Medical University during March 2017 to October 2019. Written informed consent was obtained from all patients. The patients didn't receive other treatments prior to the surgery. After collection, the samples were immediately snap-frozen in liquid nitrogen and stored at  $-80^{\circ}\text{C}$ . The study was approved by the Ethics Committee of the Xijing Hospital of Fourth Military Medical University.

TRIzol reagent was used for total RNA isolation. cDNA was synthesized using the PrimeScript<sup>TM</sup> RT Master Mix (Perfect Real Time) Kit. RT-qPCR reaction was performed using SYBR<sup>®</sup> Premix Ex Taq<sup>TM</sup> II (Tli RNaseH Plus). mRNA expression was normalized with internal control GAPDH. Relative RNA expression was calculated by the  $2^{-\Delta\Delta\text{Ct}}$  method. The primer sequences used were: GAPDH Forward primer: 5'-GACAGTCAGCCGCATCTTCT-3'; Reverse primer: 5'-GCGCCCAATACGACCAAATC-3'. GSDMC Forward primer: 5'-CCTGGTGGTGCCATCCTAAA-3'; Reverse primer: 5'-GATGCTCCTTACCAGCTCCT-3'.

### *Immunohistochemistry (IHC) assay*

IHC of GSDMC was performed on the tissue microarray (OD-CT-DgStm01-003) provided by Shanghai Outdo Biotech (Shanghai, China). Briefly, the slides were incubated with primary antibody and HRP-conjugated secondary antibody. The signal was visualized by DAB staining and scanned by 3D-histech scanner (3DHISTECH Ltd., Hungary) equipped with a Panoramic Viewer (3DHISTECH Ltd., Hungary) and a Caseviewer software (3DHISTECH Ltd., Hungary). The IHC results were independently evaluated and scored by two pathologists. The IHC signal was scored based on the total proportion of cells stained positively and the intensity of signal in cells. The intensity was

scored as follows: 0, negative; 1, weak; 2, medium; or 3, strong. The proportion was scored as follows: 0, negative; 1, 1-25%; 2, 26-50%; 3, 51-75%; or 4, 76-100%. The IHC scores were obtained by multiplying the proportion score with the intensity score, which were in the range of 0-12.

### *Statistical analysis*

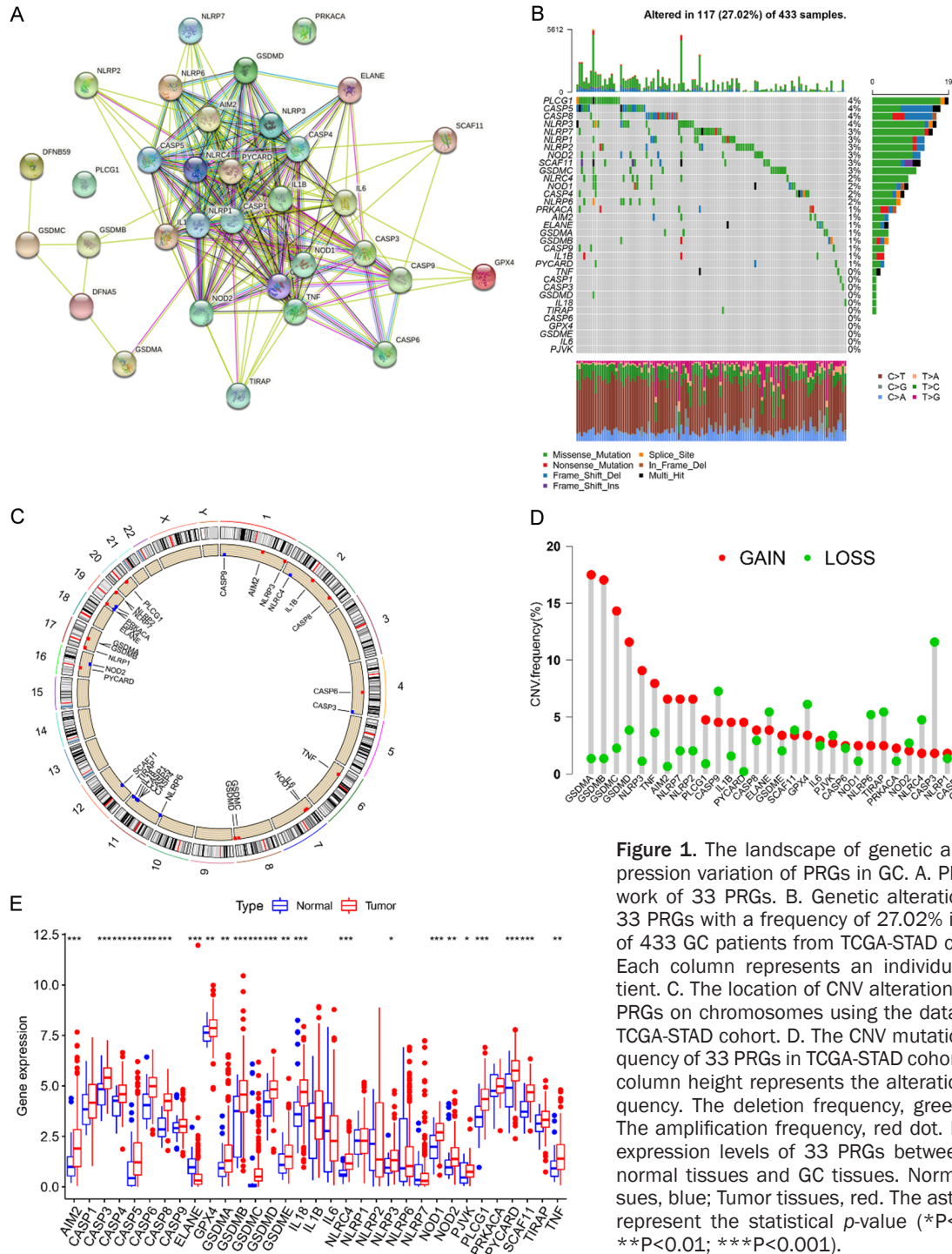
All statistical analysis in this study was conducted using R 4.0.2 software. The Perl language and R 4.0.2 software were used to process the data. The "RCircos" package was used to plot the copy number variation landscape of 33 PRGs in human chromosomes. For two group comparison, Student's t tests and Wilcoxon rank-sum test were used to estimate the statistical significance of normally distributed variables and non-normally distributed variables, respectively. One-way ANOVA and Kruskal-Wallis tests were conducted for multiple group comparison. The "survminer" package was utilized to identify the cut-off point of each subgroup. The survival curve for OS analysis was constructed using the Kaplan-Meier method and compared by the log-rank tests. Univariate and multivariate Cox regression analysis were conducted to determine the effect of clinicopathological factors and pyroptosis score on OS. Two-sided *p*-value less than 0.05 was considered statistically significant.

## Results

### *Landscape of genetic variation of pyroptosis-related genes in GC*

To explore the importance of PRGs in GC progression, we examined the genetic variation of PRGs in GC. Thirty-three PRGs that have been reported till now were included in our analysis [46] (Table S2). We used STRING (<https://www.string-db.org/>) to construct the protein-protein interaction (PPI) network [49]. As shown in Figure 1A, there were broad interactions among these genes. Somatic mutations were frequently observed in PRGs in GC patients. Out of 433 GC cases we examined, 117 samples (27.02%) had mutations in PRGs, including missense mutations, nonsense mutations, deep deletions, and etc. (Figure 1B). Among these PRGs, phospholipase cgamma 1 (PLCG1), CASP5, CASP8, and NLRP3 exhibited the highest mutation rates (4%), whereas tumor necro-

# Prognostic role of pyroptosis-related genes in gastric cancer



**Figure 1.** The landscape of genetic and expression variation of PRGs in GC. A. PPI network of 33 PRGs. B. Genetic alterations of 33 PRGs with a frequency of 27.02% in 117 of 433 GC patients from TCGA-STAD cohort. Each column represents an individual patient. C. The location of CNV alteration of 33 PRGs on chromosomes using the data from TCGA-STAD cohort. D. The CNV mutation frequency of 33 PRGs in TCGA-STAD cohort. The column height represents the alteration frequency. The deletion frequency, green dot; The amplification frequency, red dot. E. The expression levels of 33 PRGs between the normal tissues and GC tissues, blue; Tumor tissues, red. The asterisks represent the statistical *p*-value (\**P*<0.05; \*\**P*<0.01; \*\*\**P*<0.001).

sis factor (TNF), CASP1, CASP3, GSDMD, interleukin 18 (IL18), TIR domain-containing adaptor protein (TIRAP), CASP6, glutathione peroxidase 4 (GPX4), GSDME, IL6, and pejkavin (PJK) had the lowest mutation rates (0%). **Figure 1C** showed the location of CNV of these PRGs on chromosomes. GSDMA, GSDMB,

GSDMC, and GSDMD genes had a relatively high frequency of amplification, while CASP3, CASP9, elastase, neutrophil expressed (ELANE), and GPX4 genes mainly had CNV deletions (**Figure 1D**). We also analyzed the mutation co-occurrence across all PRGs and identified several co-occurring mutation patterns in

several PRGs, such as the co-occurring mutation between NLRP6 and CASP5, or NOD1 and NLRC4, as well as PLCG1 and CASP5 (Figure S2A). More importantly, our three-dimensional PCA (3D-PCA) showed that the 33 PRGs could completely distinguished GC patients from normal controls (Figure S2B). As shown in Figure 1E, most PRGs showed higher mRNA expression in GC tissues compared with that in the normal tissues. Particularly, the expression of PRGs with CNV amplification such as GSDMA, GSDMB, GSDMC, GSDMD, NLRP3, TNF and absent in melanoma 2 (AIM2), except for ELANE, was markedly increased in GC tissues compared to that in normal controls (Figure 1E). Moreover, we performed Spearman correlation analysis to explore the co-expression correlation among these PRGs. As shown in Figure S2C, CASP1 and CASP3 showed a significant positive correlation with most of other PRGs. KEGG pathway enrichment analysis of these PRGs was also performed, and we found signaling pathways such as NOD-like receptor-, TNF-, and IL17-signaling pathway were significantly enriched (Figure S2D), suggesting that these PRGs may play significant roles in the development and progression of GC. In addition, the expression levels of some PRGs were closely associated with The Cancer Genome Atlas (TCGA) molecular subtypes (Figure S3A), suggesting that the PRGs might contribute to the heterogeneity of GC. These results were further validated in the GSE62254 cohort (Figure S3B). Collectively, these findings indicated the high heterogeneity in the genetic alteration of PRGs in GC.

### *Prognostic role of PRGs and pyroptosis-related molecular patterns in GC patients*

To further investigate the function of PRGs in GC development and progression, four independent GEO datasets (GSE15459, GSE34942, GSE57303, and GSE62254) and a TCGA-STAD dataset containing patient OS and clinical data were merged into one meta-cohort (Table S1). After analyzing the gene expression data, 30 overlapping PRGs were selected for further analysis (Table S3). First, the prognostic value of these PRGs was investigated using a univariate Cox regression model (Table S4), and PRGs related to OS of patients were summarized in Figure S4. The prognostic significance and the interactions of these PRGs were

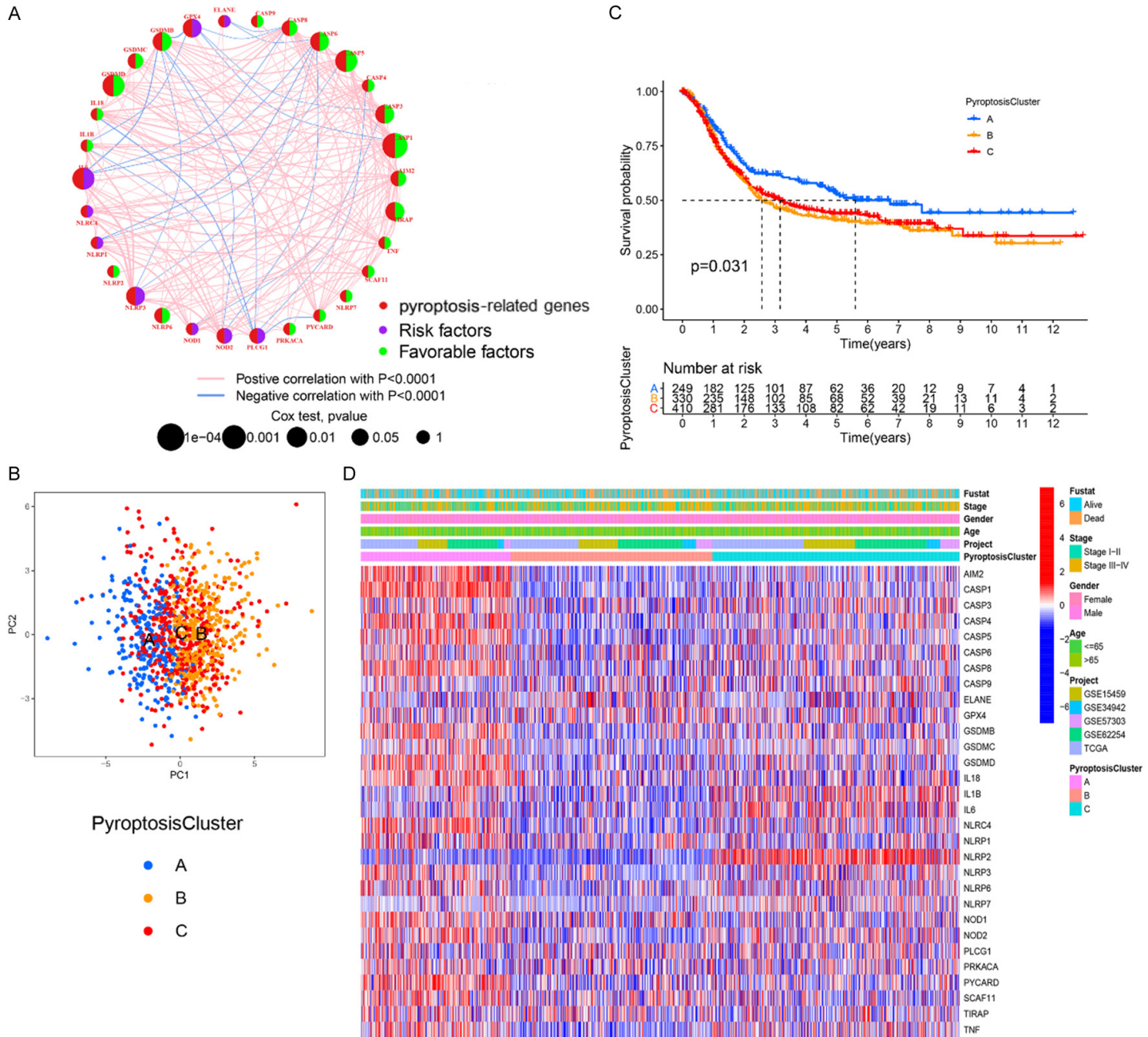
then depicted in a network plot (Figure 2A). We found that these PRGs showed a remarkably co-expression correlation. Since PLCG1, CASP5, CASP8, and NLRP3 genes exhibited a relatively higher mutation frequency, we analyzed the difference in the expression of PRGs between these wild type and mutants, respectively. We found a differential expression of PRGs, e.g., CASP3 was markedly upregulated in mutant as compared to wild type (Figures S5, S6, S7, S8). These results suggested that the crosstalk among the PRGs might play a significant role in the formation of pyroptosis-related molecular patterns.

Based on the above findings, we applied consensus clustering analysis to classify samples with qualitatively different pyroptosis-related molecular patterns by the mRNA expression profiles of overlapping PRGs, and we identified three pyroptosis-related molecular patterns using the R package of “ConsensusClusterPlus”, including 249 patients in pyroptosis Cluster-A, 330 cases in pyroptosis Cluster-B and 410 cases in pyroptosis Cluster-C (Figure S9A-D). PCA results showed that the three Clusters can be completely separated (Figure 2B). In addition, prognostic analysis for the three pyroptosis-related molecular patterns revealed that the pyroptosis Cluster-A pattern had survival advantage over the other two Clusters (Figure 2C). We observed a clear difference in the expression of PRGs between different pyroptosis-related molecular patterns. The expression of AIM2, CASP1, CASP4, CASP8, and IL18 was markedly upregulated in the pyroptosis Cluster-A subtype while ELANE and GPX4 was significantly increased in pyroptosis Cluster-B. IL1B, IL6 and NLRP2 levels were evidently elevated in pyroptosis Cluster-C (Figure 2D). The different clinicopathological characteristics of GC patients in these three Clusters were also shown in Figure 2D.

### *Immunological characteristics of distinct pyroptosis-related molecular patterns in GC*

We further performed gene set variation analysis (GSVA) enrichment analysis to assess gene set enrichment and evaluate the pathway enrichment in these three pyroptosis-related molecular patterns. As shown in Figure S10A-C, pyroptosis Cluster-A was prominently enriched in the pathways related to the activation of

# Prognostic role of pyroptosis-related genes in gastric cancer





## Prognostic role of pyroptosis-related genes in gastric cancer

**Figure 2.** Characteristics of pyroptosis-related molecular patterns. A. The interaction network of PRGs in GC. The size of circle represents the effects of PRGs on the clinical outcome of GC patients ( $P < 0.0001$ ,  $P < 0.001$ ,  $P < 0.01$ ,  $P < 0.05$  and  $P < 1$ , Cox test). Green dots in the circle, favorable factors of prognosis. Purple dots in the circle, unfavorable factors of prognosis; B. PCA of the mRNA expression profiles of PRGs confirms the three pyroptosis clusters (blue, pyroptosis Cluster A; yellow, pyroptosis Cluster B; red, pyroptosis Cluster C). C. Survival analyses for the three pyroptosis-related molecular patterns based on 989 GC patients from five cohorts (GSE15459, GSE34942, GSE57303, GSE62254, and TCGA-STAD) including 249 patients in pyroptosis Cluster A, 330 patients in pyroptosis Cluster B, and 410 patients in pyroptosis Cluster C (Log-rank test,  $P = 0.031$ ). D. Heatmap presents the correlation between the three pyroptosis clusters and clinicopathological characteristics of GC patients.

immune system, including natural killer (NK) cell mediated cytotoxicity, NOD-like receptor signaling pathway, graft-versus-host disease, antigen processing and presentation, and allograft rejection. On the other hand, pathways related to basal cell carcinoma, propanoate metabolism, taurine and hypotaurine metabolism, cardiac muscle contraction and ribosome were enriched in Pyroptosis Cluster-B. Pyroptosis Cluster-C was mainly associated with biological processes related to steroid biosynthesis, terpenoid backbone biosynthesis, maturity onset diabetes of the young, nitrogen metabolism, protein export and several immune-related pathways such as NOD-like receptor signaling pathway, graft-versus-host disease, and allograft rejection. Based on the GSVA enrichment analysis, we found that these three pyroptosis-related molecular patterns had markedly distinct TME cell infiltration characteristics. Consistently, TME cell infiltration analyses showed that pyroptosis Cluster-C was mainly enriched in immune cell infiltration such as natural killer cell, immature dendritic cell, neutrophil, and plasmacytoid dendritic cell (Figure S11A). Nevertheless, GC patients in this subtype didn't have survival advantage (Figure 2C). One possible explanation was that the immune cells were limited in the stroma of tumor microenvironment and couldn't reach the tissue parenchyma, as a result, the anti-tumor immune response was inhibited by the stromal elements in the pyroptosis Cluster-C [50]. We also found a low level of major histocompatibility complex (MHC) class I and myeloid-derived suppressor cells (MDSCs) in pyroptosis Cluster-C whereas pyroptosis Cluster-B was associated with the absence of activated CD8+ T cells, low MHC class I expression, and fatty acid metabolism (Figure S11A, S11B). Based on these results, we categorized these three pyroptosis Clusters as immune-excluded phenotype (pyroptosis Cluster-C), immune-inflamed phenotype (pyroptosis Cluster-A), and immune-desert phenotype (pyroptosis Cluster-

B) according to the previous published criteria (Figure S11A, S11B). Moreover, the correlation between the characteristics of tumor immune microenvironment (TIME) and pyroptosis-related molecular patterns were explored. As shown in Figure S11A, S11B, clear differences in the immune cell infiltration and immune functions were found among the three Clusters. Anti-tumor lymphocyte subpopulations, including activated B cells, activated CD4+ T cells, activated CD8+ T cells, and NK T cells were significantly enriched in the pyroptosis Cluster-A subtype as compared with other subtypes. Additionally, we found that patients in the pyroptosis Cluster-A pattern had markedly higher ESTIMATE score ( $P < 0.001$ , Figure S11C), immune score ( $P < 0.001$ , Figure S11D) and stromal score ( $P < 0.01$ , Figure S11E) than pyroptosis Cluster-B or Cluster-C had, suggesting the critical roles of PRGs in the tumor immunology.

Similarly, Spearman's correlation analyses were applied to analyze the specific correlation between PRGs and TME infiltration cell type. As shown in Figure S12A, GSDMC had a relatively higher correlation with the activated CD8+ T cells and activated CD4+ T cells, therefore, we focused our analysis on the role of GSDMC in tumor immunology. We first found that patients in GSDMC high expression group showed a relatively longer OS than those in GSDMC low expression group (Figures S4K, S12B and S12C). Second, gene set enrichment analysis (GSEA) suggested the enrichment of several immune-related pathways such as antigen processing and presentation pathway, cytokine-cytokine receptor interaction pathway, janus kinase/signal transducer and activator of transcription (JAK-STAT) signaling pathway, NK cell mediated cytotoxicity pathway, and retinoic acid-inducible gene-1 (RIG-I)-like receptor signal pathway in GSDMC high expression group (Figure S12D). Next, we detected the mRNA and protein expression levels of GSDMC in GC

and the adjacent normal tissues. In consistent with the data in TCGA dataset, RT-qPCR result showed that the mRNA expression of GSDMC in GC tissues was significantly higher than that in the adjacent normal tissues (Figure S12E). However, the IHC results indicated that GSDMC protein level was much lower in the GC tissues (Figure S12F, S12G). We speculated that this discrepancy might result from the post-translational modifications, epigenetic modifications, and other modulations. Lastly, we investigated the difference in TME infiltrating immune cells between the high and low GSDMC expression groups. The results showed that patients with high GSDMC had markedly increased infiltration in resting memory CD4+ T cells, activated memory CD4+ T cells, regulatory T cells (TReg cells), resting NK cells, activated dendritic cell, and neutrophils than patients with low GSDMC (Figure S13A). To support this, we used ESTIMATE algorithm to evaluate the overall infiltration of immune cells between the patients with high and low GSDMC expression. Figure S13B showed the higher immune scores in GSDMC high group. The correlations between GSDMC expression and several immune cells were shown in Figure S13C.

### *Pyroptosis molecular pattern related DEGs and pyroptosis gene cluster in GC*

In order to further explore the underlying genetic alterations within each pyroptosis-related molecular pattern, we performed differential expression analysis among these three patterns using the “limma” package and identified 346 overlapping DEGs (Figure 3A; Table S5). We then conducted the KEGG pathway enrichment and GO enrichment analyses for these DEGs. The significant enrichment KEGG pathways and GO terms were summarized in Figure S14A and S14B, respectively. These DEGs showed the enrichment of pathways associated with immune response and inflammatory response, further suggesting the role of pyroptosis in the immunology regulation within the TME (Figure S14A, S14B). Then, the prognostic value of these DEGs in GC patients were explored via a univariate Cox regression analysis, and 143 OS-related DEGs were screened (Table S6). The unsupervised clustering analysis was performed, and the GC patients were clustered into three different genomic subtypes with different clinicopathologic charac-

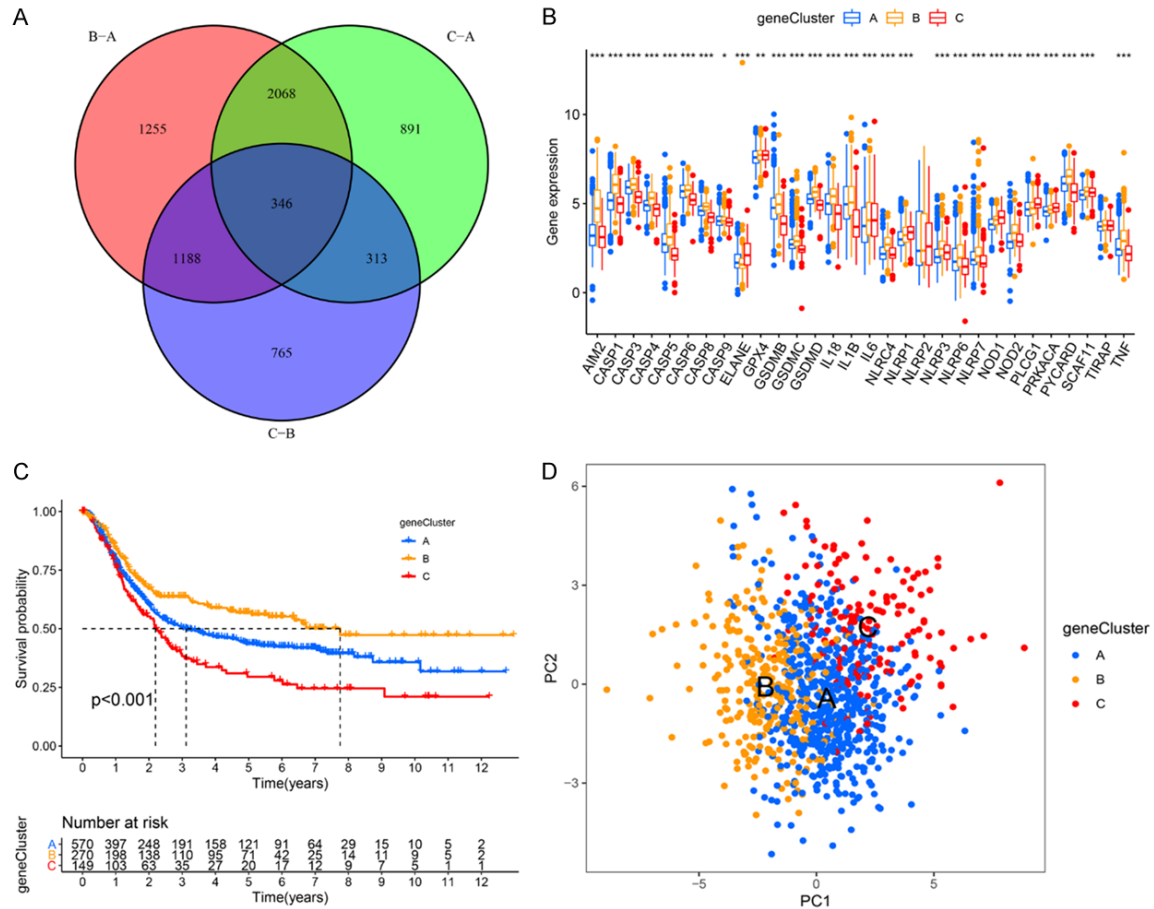
teristics (gene Clusters A-C; Figures S14C, S15A-D). The expression of PRGs and the OS in these three pyroptosis gene clusters were markedly different (Figure 3B, 3C). Patients in Cluster B had the best OS, while Cluster C exhibited the worst prognosis among these three clusters ( $P < 0.001$ , Figure 3C). In consistent, GC patients with death status were markedly concentrated in the Cluster A and gene Cluster C, and clinical stage III-IV cases were also enriched in Cluster A (Figure S14C). These results suggested the potential prognostic value of the pyroptosis gene Clusters. We also observed that patients in Clusters A and C subtypes were enriched in the advanced age subtype (age >65). PCA analysis confirmed the separation of these clusters (Figure 3D).

Subsequently, we investigated whether these three pyroptosis gene Clusters exhibited different TME characteristics. As shown in Figure S16A, compared to pyroptosis gene Clusters A and C, Cluster B was particularly enriched in immune cell infiltration including active B cells, activated memory CD4+ T cells, activated memory CD8+ T cells, NK cells. Additionally, Cluster B was the highest in the scores of antigen presenting cell (APC) co-stimulation, chemokine receptors (CCR), check point, cytolytic activity, human leukocyte antigen (HLA), inflammation promoting, MHC class I, parainflammation, T cell co-stimulation and type I Interferon (IFN) response and the lowest in type II IFN response score (Figure S16B). Patients in Cluster-B had relative higher ESTIMATE score ( $P < 0.001$ , Figure S16C), immune score ( $P < 0.001$ , Figure S16D) and stromal score ( $P < 0.01$ , Figure S16E) than patients in Cluster-A or Cluster-C. These data also confirmed our conclusion that there were indeed three distinct immune phenotype groups in GC with different clinicopathologic and TME features.

### *Construction of pyroptosis scoring system and its clinical significance*

In order to quantify the pyroptosis-related molecular patterns of individual GC patient, we constructed a scoring system termed pyroptosis score based on the identified OS-related DEGs. The distribution of pyroptosis score and the survival status of GC patients in different gene Clusters and pyroptosis Clusters were shown in Figure 4A. Specifically, patients in

## Prognostic role of pyroptosis-related genes in gastric cancer

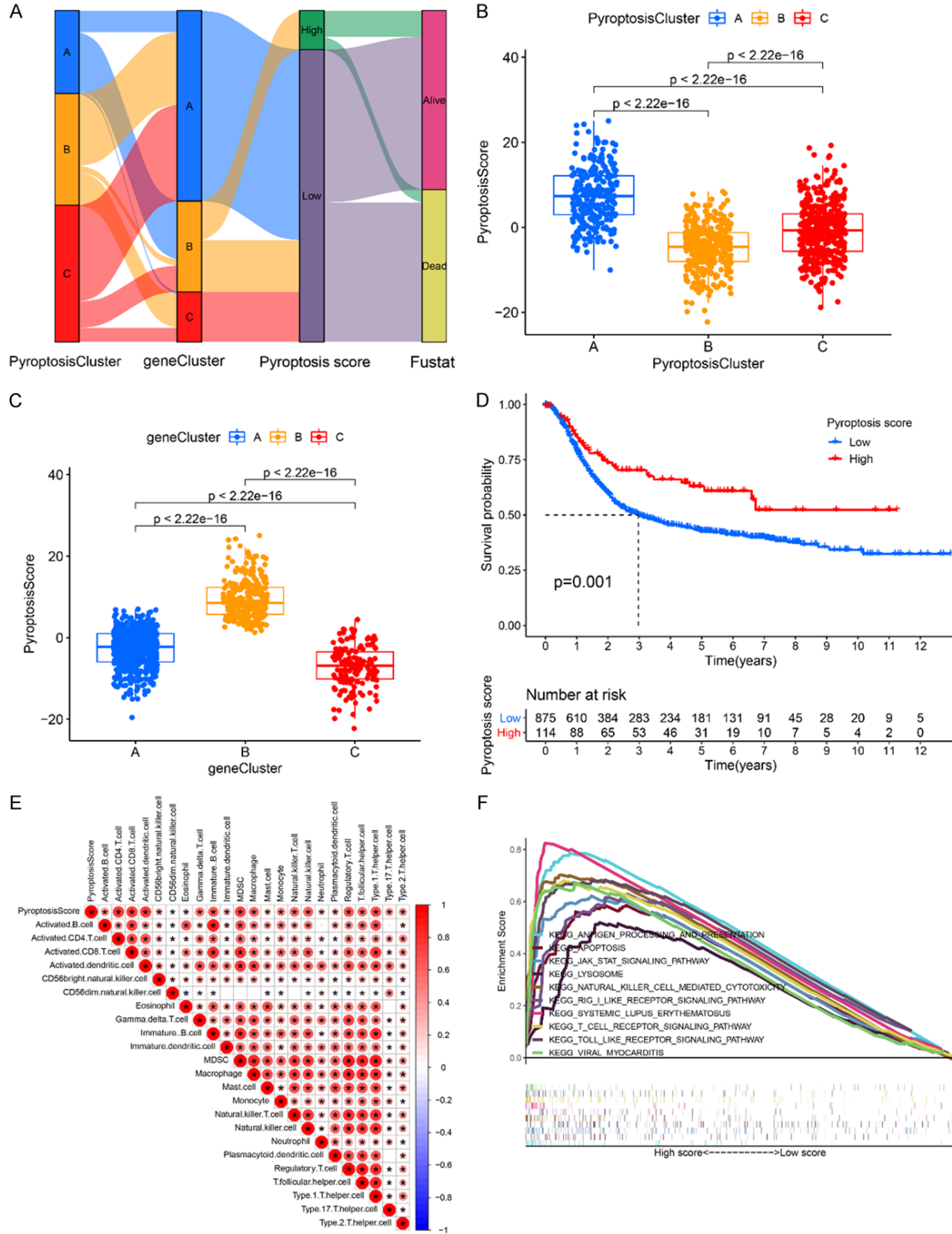


**Figure 3.** Characteristics of pyroptosis gene clusters. A. Venn diagram presents 346 DEGs among the three pyroptosis clusters. B. The expression levels of PRGs among the three pyroptosis gene clusters. \* $P < 0.05$ ; \*\* $P < 0.01$ ; \*\*\* $P < 0.001$ . C. Survival analyses for the pyroptosis gene clusters based on 989 GC patients including 570 patients in pyroptosis gene Cluster A, 270 patients in pyroptosis gene Cluster B, and 149 patients in pyroptosis gene Cluster C (Log-rank test,  $P < 0.01$ ). D. PCA of the mRNA expression profiles of PRGs confirms the pyroptosis gene clusters (blue, gene Cluster A; yellow, gene Cluster B; red, gene Cluster C).

pyroptosis Cluster A had the highest pyroptosis score among the three clusters ( $P < 2.2 \times 10^{-16}$ ) (Figure 4B). At the same time, the highest pyroptosis score was also observed in pyroptosis gene Cluster B ( $P < 2.2 \times 10^{-16}$ , Figure 4C). Figure 4D showed that patients with high pyroptosis score usually exhibited a better outcome than those with low pyroptosis score ( $P = 0.001$ ). We further assessed the prognostic role of pyroptosis score in GC patients that were subgrouped by clinicopathological features (age, grade, and stage). As shown in Figure S17A-E, GC patients with higher pyroptosis score in subgroups of age  $\leq 65$ , age  $> 65$ , and male group had dramatically better OS than patients with lower pyroptosis score ( $P < 0.05$ ), suggesting that the pyroptosis score could also separate the patients with different

OS. GC patients with stage I-II, stage III-IV, and female group also showed similar trend but it was not statistically significant (Figure S17C, S17E and S17F). The prognostic value of the pyroptosis score was further confirmed in the meta-GEO cohort ( $n = 618$ ), TCGA-STAD cohort ( $n = 371$ ), GSE62254 cohort ( $n = 300$ ), GSE57303 cohort ( $n = 70$ ), and GSE34942 cohort ( $n = 56$ ) (Figure S18A-E). The relationships between the pyroptosis score and the clinical features were also explored (Figure S19A-H). The results showed that high pyroptosis score group had higher percentage of alive patients during the follow-up (Figure S19A, S19B). However, no visible difference was observed in percent weight between the two groups considering the features of gender, age, and stage (Figure S19C-H). Furthermore, we explored the

# Prognostic role of pyroptosis-related genes in gastric cancer



**Figure 4.** Construction of pyroptosis score system. A. Alluvial diagram shows the distribution of GC patients with different pyroptosis clusters, pyroptosis gene clusters, pyroptosis scores, and survival state. B. Differences in pyroptosis score among three pyroptosis clusters ( $P < 0.001$ , Kruskal-Wallis test). C. Differences in pyroptosis score among three pyroptosis gene clusters ( $P < 0.001$ , Kruskal-Wallis test). D. Kaplan-Meier curves for GC patient with high and low pyroptosis score. Log-rank test,  $P = 0.001$ . E. Correlations between pyroptosis score and different types of immune cells using Spearman analysis. F. GSEA identified several immune-related pathways enriched in the high pyroptosis score group.

## Prognostic role of pyroptosis-related genes in gastric cancer

relationship between the pyroptosis score and TME infiltrating immune cells by Spearman analysis. The heatmap of the correlation matrix showed that the pyroptosis score was positively correlated with the activated CD4+ T cells, activated CD8+ T cells, activated dendritic cells, immature B cells, MDSC, macrophage, NK T cells, NK cells, T-helper cell type 1 (Th1) cells, T-regulatory (Treg) cells, and T follicular helper (Tfh) cells (**Figure 4E**). GSEA analysis showed that antigen processing and presentation pathway, apoptosis, JAK-STAT signaling pathway, lysosome, NK cell mediated cytotoxicity pathway, and RIG-I-like receptor signal pathway, systemic lupus erythematosus, T cell receptor signaling pathway, toll like receptor signal pathway and viral myocarditis were significantly enriched in the high pyroptosis score group (**Figure 4F**), while low pyroptosis score group was mainly enriched in pathways involved in cytochrome P450 of drug metabolism, glycerolipid and histidine metabolism, maturity-onset diabetes of the young, and reclamation of bicarbonate in the proximal tubule (**Figure S20**). Moreover, we also explored the correlation between the characteristics of TIME and pyroptosis score. As shown in **Figure S21A**, high pyroptosis score group was significantly enriched in immune cell infiltration including activated B cells, activated CD4+ T cells, activated CD8+ T cells, NK cells, etc. In addition, high pyroptosis score subtype showed higher APC co-stimulation, CCR, check point, cytolytic activity, HLA, inflammation promoting, MHC class I, parainflammation, T cell co-stimulation and type I IFN response scores and the lower type II IFN response score (**Figure S21B**). Importantly, we also observed that GC patients in the high pyroptosis score group had relative higher ESTIMATE score ( $P < 2.22 \times 10^{-16}$ ; **Figure S21C**), immune score ( $P < 2.22 \times 10^{-16}$ ; **Figure S21D**) and stromal score ( $P = 0.00032$ ; **Figure S21E**) as compared to those in low pyroptosis score group. In sum, we confirmed that the pyroptosis score was associated with TME and could be used to evaluate certain clinical features of GC patients.

### *Correlation between the pyroptosis and TCGA molecular subtypes of GC*

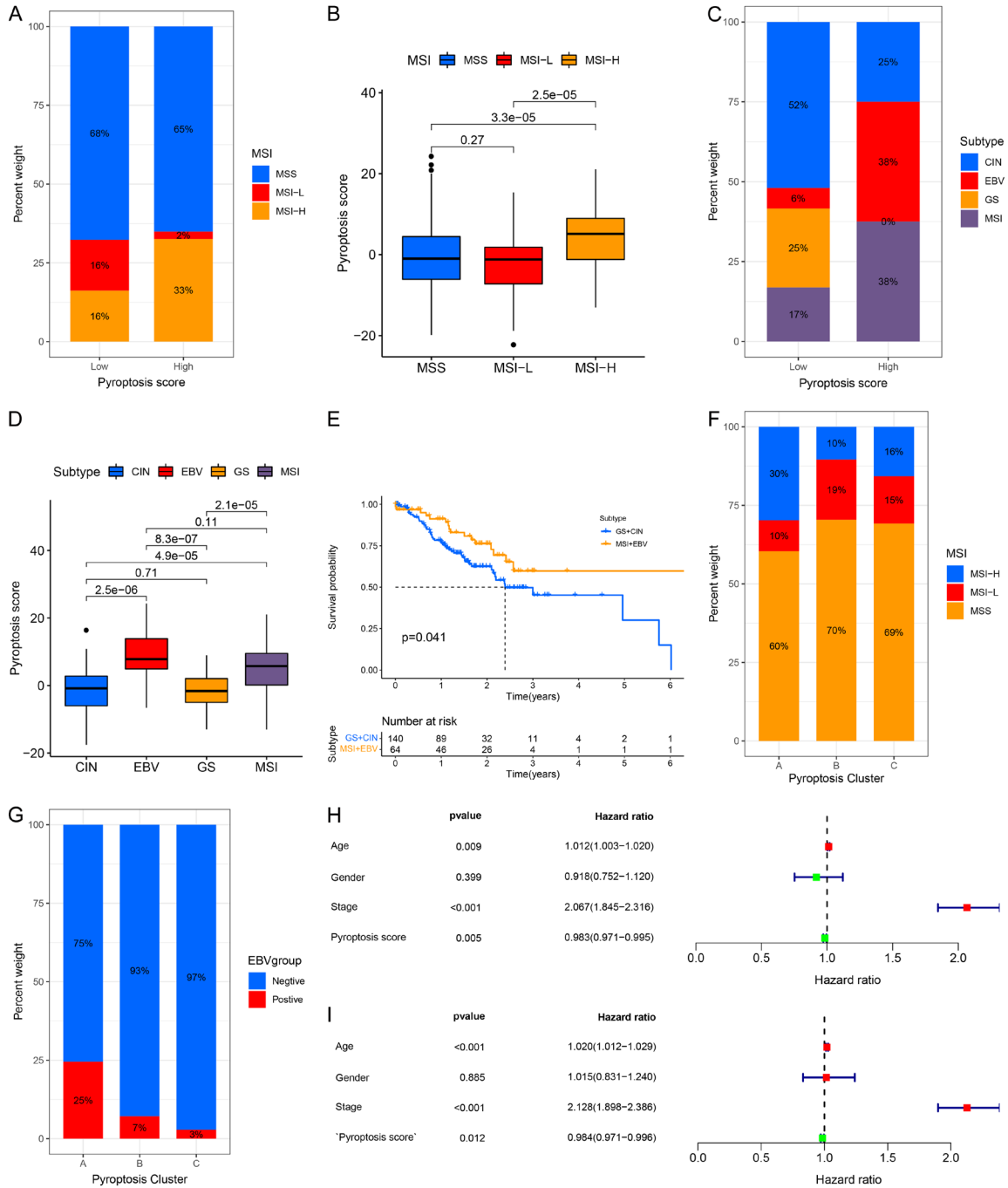
TCGA project classified GC into four molecular subtypes: Epstein-Barr virus (EBV) infection, chromosomal instability (CIN), genome stable (GS), and microsatellite instability (MSI) [51]. Studies also revealed that MSI patients or EBV-

positive cases usually showed better response to immune checkpoint blockade treatment [52]. Thus, we assessed the correlation between our pyroptosis score and TCGA molecular subtypes. First, the expression levels of PRGs in different groups were examined. As shown in **Figure S22A-D**, AIM2, CASP1, CASP3, CASP4, CASP5, and IL18 were markedly elevated, while PLCG1 was significantly downregulated in the MSI group in both the TCGA cohort and GSE-62254 cohort. The MSI-High subtype, featured by the better outcome, was associated with high pyroptosis score, whereas MSI-Low and MSS had a low pyroptosis score (**Figure 5A, 5B**). Moreover, the higher pyroptosis score was mainly concentrated on EBV infection and MSI subtype, which showed a better OS in GC patients (**Figure 5C-E**). The lower pyroptosis score was concentrated on the subtypes of CIN and GS group, which was associated with poorer OS (**Figure 5E**,  $P = 0.041$ ). Further analysis showed that patients in MSI-High subtype shared the features in pyroptosis Cluster-A, whilst cases with MSS subtype were like the pyroptosis Cluster-B and Cluster-C in TCGA cohort (**Figure 5F**). The levels of AIM2, CASP1, CASP4, GCDMB, GSDMC, GSDMD, IL18, NLR4, PLCG1 and PYD and CARD domain containing (PYCARD) was much higher, whereas CASP9, ELANE, and NLRP6 level was lower in EBV-positive patients than in EBV-negative patients (**Figure S22E**). Moreover, pyroptosis Cluster-A was concentrated on the EBV positive subtype compared to pyroptosis Cluster-B and Cluster-C (**Figure 5G**). Univariate Cox regression analysis showed that age, tumor stage, and pyroptosis score were closely associated with OS (HR=1.012 (95% CI: 1.003-1.020),  $P = 0.009$ ; HR=2.067 (95% CI: 1.845-2.316),  $P < 0.001$ ; HR=0.983 (95% CI: 0.971-0.995),  $P = 0.005$ , respectively) (**Figure 5H**). Multivariate Cox regression analysis indicated that age (HR=1.020 (95% CI: 1.012-1.029),  $P < 0.001$ ) and tumor stage (HR=2.128 (95% CI: 1.898-2.396),  $P < 0.001$ ) could be considered as independent risk factors for OS, while pyroptosis score acted as an independent favorable prognostic indicator for clinical outcome in GC (HR=0.984 (95% CI: 0.971-0.996),  $P < 0.001$ ) (**Figure 5I**).

### *Correlation between the pyroptosis scores and somatic variants*

It has been reported that high tumor mutation burden (TMB) tissues usually have an increas-

# Prognostic role of pyroptosis-related genes in gastric cancer



**Figure 5.** Characteristics of pyroptosis in TCGA molecular subtypes and identification of independent prognostic factors. A, B. Differences in pyroptosis score among different microsatellite subtypes. The Kruskal-Wallis test was used to compare the statistical difference between the three microsatellite subtypes. C, D. Differences in pyroptosis score among different TCGA-STAD molecular subtypes. The Kruskal-Wallis test was conducted to compare the statistical difference between the four TCGA-STAD molecular subtypes. E. Kaplan-Meier curves for GC patients in GS+CIN and MSI+EBV subtypes in the TCGA-STAD cohort. Log rank test, P=0.041. F. The proportion of three pyroptosis clusters in the MSS, MSI-High and MSI-Low subtypes. MSI, microsatellite instability; MSS, microsatellite stable. G. The proportion of three pyroptosis clusters in the EBV-positive and EBV-negative groups. H. Univariate Cox regression analysis of the clinicopathological factors and pyroptosis score in the TCGA-STAD cohort. I. Multivariate Cox regression analysis of the clinicopathological features and pyroptosis score in the TCGA-STAD cohort.

ed immune infiltration of CD8+ T cell [53, 54]. Some studies have shown that elevated TMB

level is associated with the prolonged survival time and improved response to PD-1-based

immunotherapy [53, 55, 56]. These findings suggest the clinical significance of TMB in cancer treatment. We therefore sought to investigate the correlation between our pyroptosis scores and TMB. First, the TMB level was compared between the high and the low pyroptosis score of GC patients. We found that GC patients in high pyroptosis score group had a markedly higher TMB than patients in the low pyroptosis score group had (**Figure 6A**,  $P=0.011$ ). Next, correlation analyses showed that the pyroptosis score was positively correlated with the TMB ( $R=0.13$ ,  $P=0.011$ , **Figure 6B**). We further found that GC patients with high TMB showed longer OS than those with low TMB ( $P<0.001$ , **Figure 6C**). Additionally, the synergistic effect of TMB and pyroptosis score in predicting prognosis of GC patients was evaluated (**Figure 6D**). Stratified survival analysis showed that GC patients with both high TMB status and high pyroptosis score had the longest OS time as compared with patients in other groups. Different TMB status caused significant differences in OS in both high and low pyroptosis score subgroups (**Figure 6D**,  $P<0.001$ ). Taken together, we concluded that the TMB status and pyroptosis score might act as promising prognostic markers in GC patients.

Moreover, the distribution of the somatic variants in GC driver genes between the low and high pyroptosis groups was analyzed. The maf-tools was applied to evaluate the GC driver genes. The top 20 driver genes with the highest alteration frequency in the low and high pyroptosis groups were shown in **Figure 6E**. Among them, AT-rich interaction domain 1A (ARID1A) ( $P<0.001$ ), lysine methyltransferase 2D (KMT2D) ( $P=0.002$ ), zinc finger homeobox 4 (ZFX4) ( $P=0.025$ ), and phosphatidylinositol-4,5-bisphosphate 3-kinase catalytic subunit alpha (PIK3CA) ( $P<0.001$ ) showed the highest difference in alteration frequency between the low and high pyroptosis score groups, indicating the cross-talk between pyroptosis phenotypes and individual somatic mutations.

### *Chemo sensitivity screening for patients with GC based on the pyroptosis score*

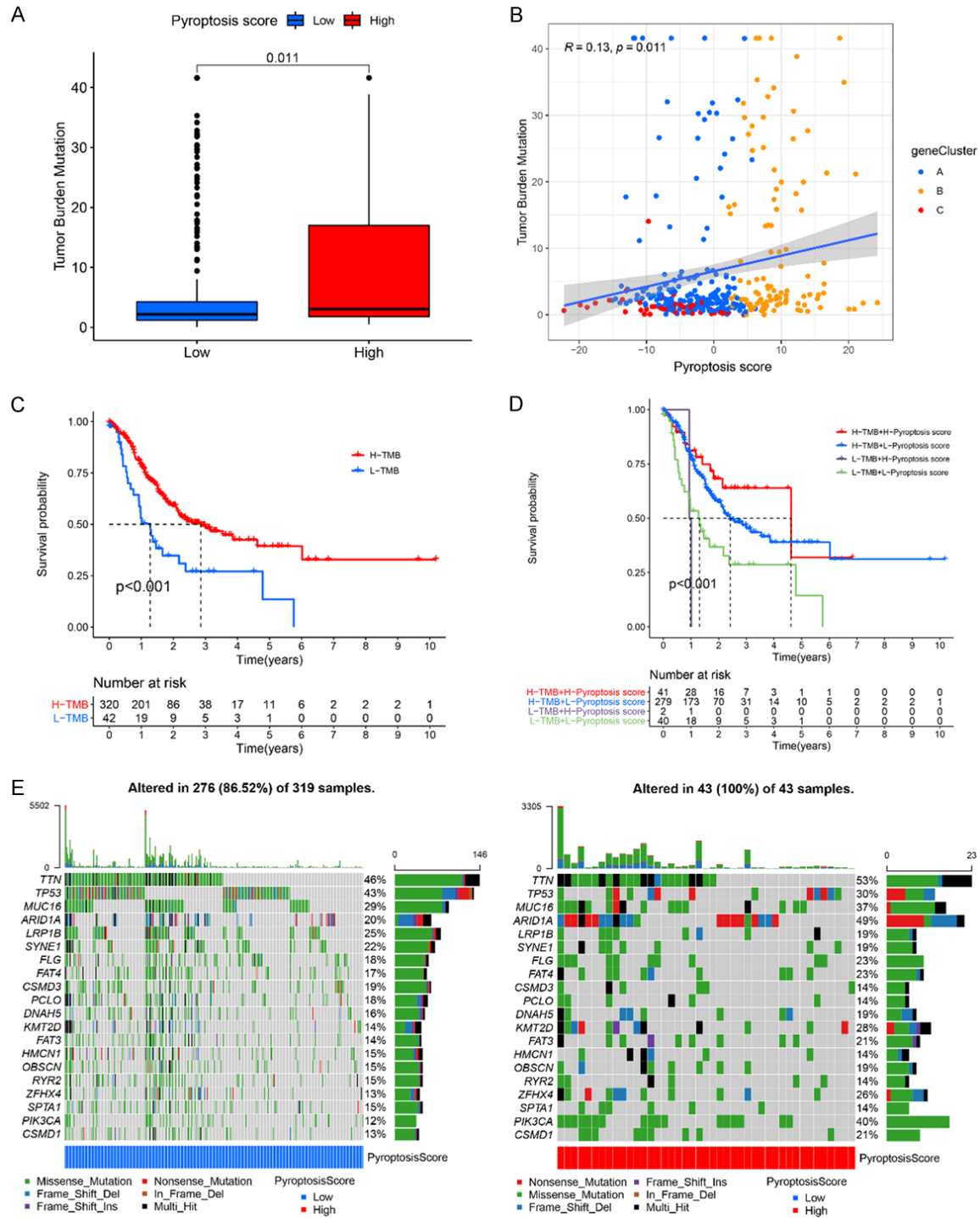
We evaluated the application of our pyroptosis score on predicting the response of GC patient to chemotherapeutic drugs. The estimated IC50 values were compared in different

groups for 16 chemotherapy drugs: Bleomycin (**Figure 7A**), Camptothecin (**Figure 7B**), Cisplatin (**Figure 7C**), Cytarabine (**Figure 7D**), Dasatinib (**Figure 7E**), Docetaxel (**Figure 7F**), Doxorubicin (**Figure 7G**), Etoposide (**Figure 7H**), Gemcitabine (**Figure 7I**), Imatinib (**Figure 7J**), Methotrexate (**Figure 7K**), Paclitaxel (**Figure 7L**), Rapamycin (**Figure 7M**), Sunitinib (**Figure 7N**), Vinblastine (**Figure 7O**), and Vinorelbine (**Figure 7P**). We found that IC50 values of 13 chemotherapy drugs were higher in the low pyroptosis score group than that in the high pyroptosis score group (**Figure 7A-D, G-I and K-P**). On the contrary, the estimated IC50 value of Imatinib ( $P=1.1e-07$ , **Figure 7J**) was significantly lower in the low pyroptosis score group than that in the high pyroptosis score group, suggesting that low pyroptosis patients were more sensitive to Imatinib.

### *Identification of potential small molecule compounds for patients with GC based on the pyroptosis score*

In order to identify the potential small molecule compounds for treating the GC patients, we screened the DEGs between the low and high pyroptosis score groups. A total of 309 DEGs were selected between the two groups with adjusted  $p$  value  $<0.05$  and  $|\logFC| >1.0$ , including 71 upregulated and 238 downregulated genes (**Figure S23A**; **Table S7**). GO enrichment analysis classified the DEGs into three functional subgroups: biological process (BP), cellular component (CC), and molecular function (MF). As shown in **Figure S23B**, the DEGs significantly enriched in the BP were related to regulation of innate immune response, T cell activation, positive regulation of innate immune response iron ion binding. In the CC group, the DEGs were mainly enriched in the tertiary granule membrane, secretory granule membrane, chromosomal region. DEGs related to cytokine receptor activity, helicase activity, tumor necrosis factor receptor superfamily binding was enriched in MF. KEGG analysis showed that the DEGs were obviously related to Epstein-Barr virus infection, influenza A, osteoclast differentiation, leishmaniasis, chemokine signaling pathway, Th1 and Th2 cell differentiation, measles, NOD-like receptor signaling pathway, allograft rejection, and NF-kappa B signaling pathway (**Figure S23C**). Finally, DEGs query in CMAP small molecule drug database identified 11 potential drugs,

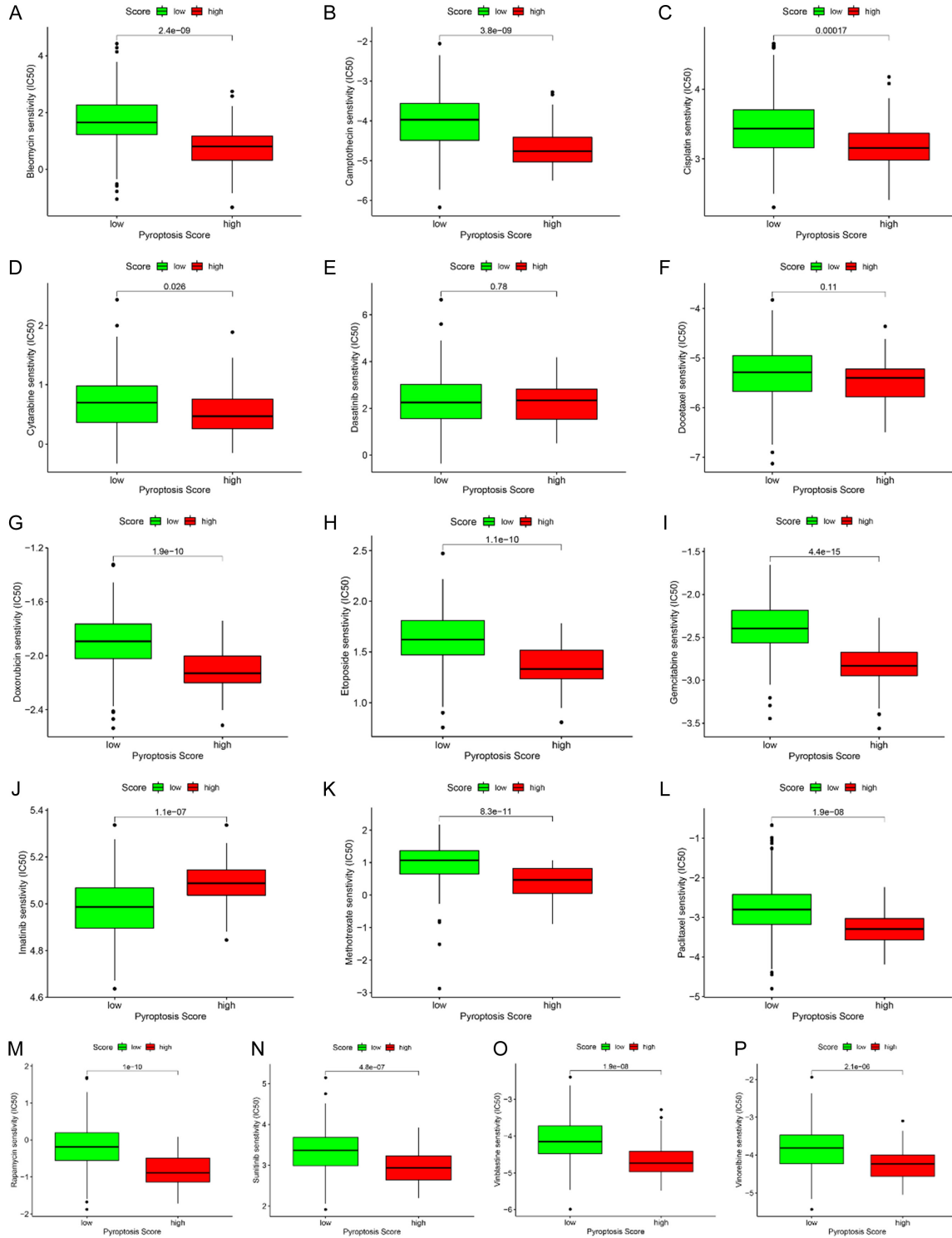
# Prognostic role of pyroptosis-related genes in gastric cancer



**Figure 6.** The correlation between the pyroptosis score and somatic variants. A. Difference of TMB level in the high and low pyroptosis score groups. Wilcoxon test,  $P=0.011$ . B. Scatterplots presents the positive correlation between pyroptosis score and mutation load in the TCGA-STAD cohort. Spearman correlation analysis,  $R=0.13$ ,  $P=0.011$ . C. Kaplan-Meier curves for GC patients with high and low TMB in the TCGA-STAD cohort. Log rank test,  $P < 0.001$ . D. Kaplan-Meier curves for GC patients with different TMB status and pyroptosis scores in the TCGA-STAD cohort. Log rank test,  $P < 0.001$ . E. Mutational landscape of significantly mutated genes in TCGA-STAD cohort stratified by low (left panel, blue) and high pyroptosis score (right panel, red) subgroups. Each column represents an individual GC patient.



## Prognostic role of pyroptosis-related genes in gastric cancer

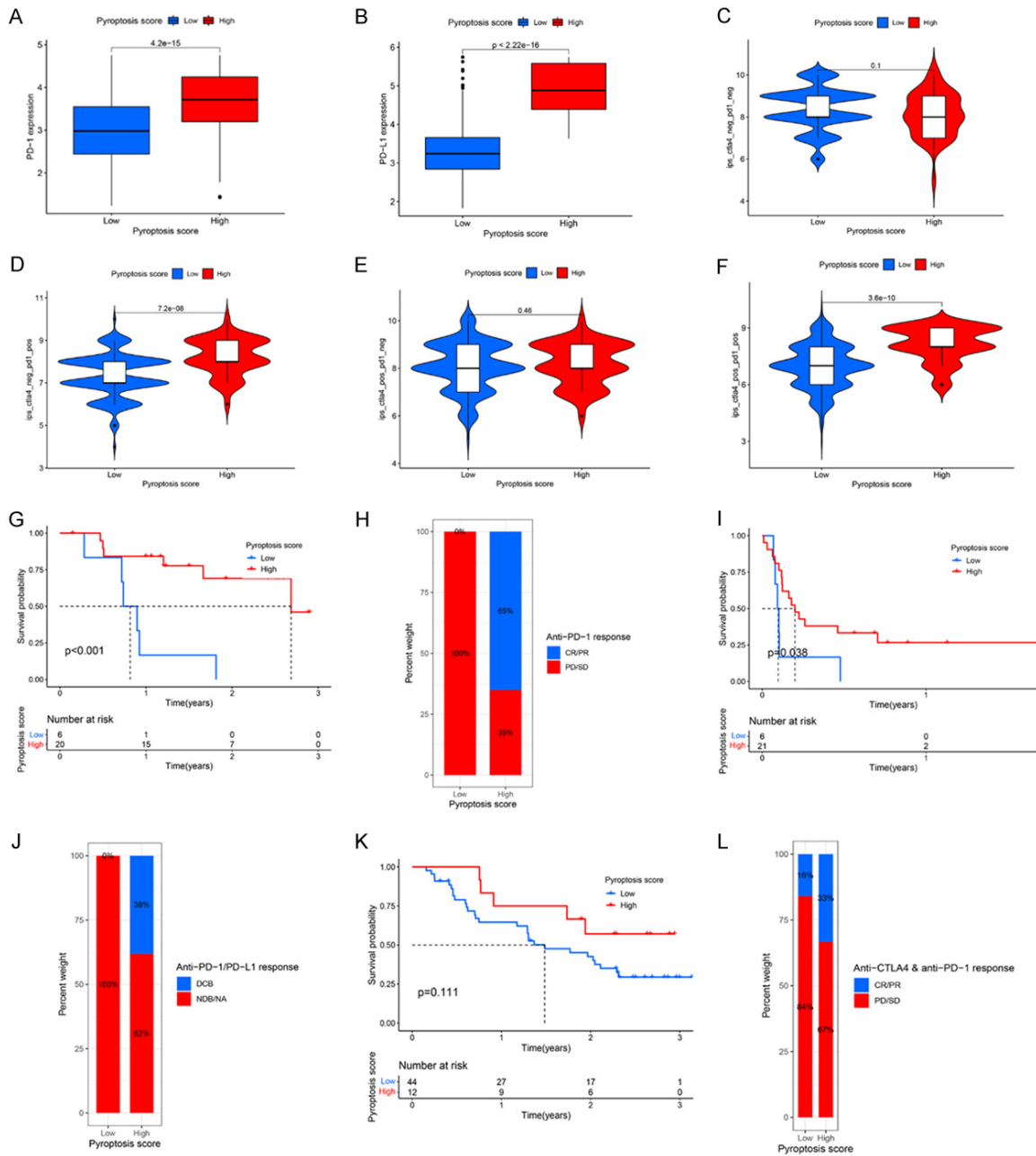


**Figure 7.** Identification of sensitive chemotherapy drugs based on the pyroptosis score. Box plots depicts the differences in the estimated IC50 levels of Bleomycin (A), Camptothecin (B), Cisplatin (C), Cytarabine (D), Dasatinib (E), Docetaxel (F), Doxorubicin (G), Etoposide (H), Gemcitabine (I), Imatinib (J), Methotrexate (K), Paclitaxel (L), Rapamycin (M), Sunitinib (N), Vinblastine (O), and Vinorelbine (P) between the high and low pyroptosis score groups.

including caffeic acid, puromycin and alimemazine (Figure S23D), which might provide new

clues for targeted therapy in GC patients in the future.

# Prognostic role of pyroptosis-related genes in gastric cancer



**Figure 8.** Prediction values of pyroptosis score in immunotherapeutic benefits. (A, B) Difference in PD-1 (A) and PD-L1 (B) expression between high and low pyroptosis score groups ( $P < 0.0001$ ). (C-F) Comparison of IPS between the GC patients with high and low pyroptosis score groups in the CTLA4 negative/positive or PD-1 negative/positive groups. CTLA4<sub>positive</sub> or PD1<sub>positive</sub> represents anti-CTLA4 or anti-PD-1/PD-L1 therapy, respectively. (G, H) Kaplan-Meier curves (G) and clinical response (H) to anti-PD-1 therapy for patients in high and low pyroptosis score groups from the GSE78220 cohort. (I, J) Kaplan-Meier curves (G) and clinical response (H) to anti-PD-1/PD-L1 therapy for patients in high and low pyroptosis score groups from the GSE135222 cohort. (K, L) Kaplan-Meier curves (K) and clinical response (L) to anti-CTLA4 and anti-PD-1 therapy for patients in high and low pyroptosis score groups from the GSE91061 cohort. CR, Complete Response; PR, Partial Response; SD, Stable Disease; PD, Progressive Disease; DCB, Durable Clinical Benefit; NDB, Non-Durable Benefit; NA, Not Determined.

## Predictive value of pyroptosis score in predicting response to immunotherapy

We first evaluated the expression of two crucial immune checkpoint inhibitors (PD-1 and PD-L1)

in the two pyroptosis score groups. The results showed that high pyroptosis score group was characterized by a markedly higher PD-1 and PD-L1 expression levels compared to the low pyroptosis score group (Figure 8A, 8B). Since

IPS has been reported to play important roles in predicting the response to immunotherapy [34], we assessed the predicting ability of pyroptosis score too. Immunophenogram analysis was used to explore the correlation between IPS and pyroptosis score in TCGA-STAD cohort (**Figure 8C, 8F**). Our results showed that in the CTLA4<sub>negative</sub>+PD-1<sub>positive</sub> and CTLA4<sub>positive</sub>+PD-1<sub>positive</sub> subtypes, the IPS in high pyroptosis group was significantly higher than that in low pyroptosis group (**Figure 8D, 8F**, both  $P < 0.0001$ ), suggesting that GC patients in high pyroptosis score group might benefit from treatment with anti-PD-1/PD-L1 antibodies alone or in combination with anti-CTLA4 blockers.

We further validated the correlation between pyroptosis score and the response to immunotherapy with another three independent cohorts (GSE78220, GSE135222, and GSE91061). The patients who received anti-PD-1 therapy in the GSE78220 cohort were divided into high and low pyroptosis score groups (**Figure 8G**). We found patients with high pyroptosis score had a better prognosis than patients with low pyroptosis score (GSE78220,  $P < 0.001$ , **Figure 8G**). Moreover, the response rate to anti-PD-1 therapy in the high pyroptosis score group was higher than that in the low pyroptosis score group (**Figure 8H**). Similar results were also observed in the GSE135222 cohort (**Figure 8I, 8J**). Patients in high pyroptosis score group showed obvious clinical advantages and significantly prolonged OS ( $P = 0.038$ , **Figure 8I, 8J**). Patients in GSE91061 cohort also showed similar trend, but it was not statistically significant (**Figure 8K, 8L**), partly due to the small sample size and tumor heterogeneity. Collectively, the above results strongly indicated that the pyroptosis score was closely related to the response to immunotherapy, and it might serve as a biomarker to help predict benefits of immunotherapy in GC patients.

### Discussion

Numerous studies have shown that pyroptosis plays a significant role in inflammation, innate immunity, and cancer biology [57], while the overall characteristics of TME mediated by integrated PRGs remain poorly understood. Thus, exploring the functions of distinct pyroptosis-related molecular patterns in the TME will advance our understanding of the interactions of PRGs on anti-tumor immune response and

assist doctors to make more effective immunotherapy strategies for GC patients.

In this study, we identified three distinct pyroptosis-related molecular patterns based on the mRNA expression profiles of pyroptosis genes. Distinct features in immune infiltrations, prognosis, and functions were observed among the three clusters. They can be classified as immune-inflamed phenotype (pyroptosis Cluster-A), immune-desert phenotype (pyroptosis Cluster-B), and immune-excluded phenotype (pyroptosis Cluster-C) according to the previously published studies [50]. Further, based on the OS-related DEGs that were correlated with the different pyroptosis clusters, we identified three pyroptosis gene clusters with distinct outcomes and functions and immune infiltrations for GC. By conducting PCA algorithms, we established the pyroptosis score to quantify the pyroptosis patterns in individual GC patient. The pyroptosis Cluster-A and pyroptosis gene Cluster B had the best clinical outcomes and had the highest pyroptosis score among three pyroptosis patterns and gene clusters. Importantly, GC patients with high pyroptosis scores usually exhibited longer OS time, suggesting that high pyroptosis score could contribute to better outcome for patients. Moreover, our results showed that pyroptosis score was an independent favorable indicator for predicting the prognosis of GC patients. Pyroptosis score was also closely associated with clinicopathological feature and molecular subtypes of GC patients. Recently, a pyroptosis-related signature has been developed for predicting the prognosis of GC patients, although this model didn't perform well in terms of all-time survival stages in immunotherapy cohort [58]. Still, our findings and the results from other groups warrant further investigation on the role of pyroptosis in GC.

We also investigated the specific functions of individual pyroptosis gene in tumor immunity. The crucial role of pyroptosis in tumor immunity has been reported [57]. Recently, increasing evidence has also revealed the dysregulation and dysfunction of the GSDM family members in various cancers [60, 61]. However, the diagnostic and prognostic roles of GSDM family members have not been clearly defined. Wei et al. reported that overexpression of GSDMC is a prognostic indicator for poor outcome in lung cancer [61]. Interestingly, our results showed that GSDMC was upregulated in GC tissues but

related to better prognosis. There are several possible explanations for this contradiction. First, the effect of GSDMC expression might be tissue-specific or context-dependent. Furthermore, tumor immune cell infiltration is an important defense mechanism in tumorigenesis, and it may in turn modulate the functions of tumor-associated genes. Our data showed that higher expression of GSDMC was closely related to the activation of immune-related pathways, higher levels of activated CD4<sup>+</sup> T cells and activated CD8<sup>+</sup> T cells, and higher immune scores, suggesting that GSDMC mediated pyroptosis may be widely involved in the tumor immunity. The biological functions and predictive roles of GSDMC need to be further validated in larger sample sets and by experimental studies.

Increasing evidence has shown that pyroptosis is important in inflammation and immunity. Consistent with these findings, our GSEA results demonstrated that antigen processing and presentation pathway, JAK-STAT signaling pathway, NK cell mediated cytotoxicity pathway, and T cell receptor signaling pathway were significantly enriched in, suggesting that pyroptosis is crucial in the immune response. TME mainly contains immune cells and stromal cells [12]. Here, we used ESTIMATE algorithm to assess the immune and stromal scores for GC patients based on the pyroptosis patterns, gene clusters, and pyroptosis score groups. Patients in pyroptosis Cluster A, gene Cluster B, and high pyroptosis score group had significantly higher ESTIMATE score, higher immune score, and higher stromal scores, indicating that pyroptosis participated in the modulation of TME. Therefore, targeting pyroptosis might be a promising treatment strategy. It is well known that accumulated genetic mutations can lead to carcinogenesis [62]. Higher TMB level has been reported to be related to better prognosis for cancer patients [63]. Consistently, our results verified that there was a significant difference in TMB level between the high and low pyroptosis score groups. In addition, patients with both high TMB status and high pyroptosis score had the longest OS time compared to other groups, suggesting TMB status and high pyroptosis score as the positive prognostic factors in GC patients.

Drug resistance remains the major challenge in GC treatment [2]. Therefore, it is of extreme importance to timely assess the drug resis-

tance and identify more effective drug treatment options. Our study showed that patients with low pyroptosis were more sensitive to Imatinib, and inhibiting pyroptosis might alleviate the drug resistance in these patients. Moreover, we identified 11 potential small molecule compounds for treating GC patients based on the pyroptosis score, although the activity of these novel pharmacological and genetic inhibitors for pyroptosis needs to be further validated.

Immunotherapy is emerging as a new and effective approach in the treatment of GC [3]. Our results showed that higher pyroptosis score was associated with higher expression levels of PD-1 and PD-L1 in GC patients. Additionally, IPS, a newly identified predictor for immune response, was significantly higher in GC patients treated with PD-1 antibody alone or in combination with CTLA-4 in the high pyroptosis score group than that in the low pyroptosis score group, indicating that pyroptosis score hold the potential in predicting the response to immunotherapy. We also validated the prognostic values of pyroptosis score in another three independent immunotherapy cohorts. Due to the lack of datasets for immunotherapy in GC, immunotherapy cohorts of melanoma and lung cancer were selected. Using the GSE78220 and GSE135222 cohorts, the predictive value of pyroptosis score was evaluated for response to anti-PD-1/PD-L1 immunotherapy. GC Patients in high pyroptosis score group were more likely to benefit from treatment with anti-PD-1/PD-L1 antibodies. Patients in GSE91061 datasets showed similar trends, but it was not statistically significant, possibly due to the tumor heterogeneity and small sample size. Therefore, the current results need to be confirmed in a larger sample GC cohort.

### Conclusion

In summary, we systematically studied the genetic and expression variation landscape of pyroptosis-related genes in GC, which advanced our understanding on the clinical features and implications of pyroptosis in GC. Three pyroptosis-related molecular patterns with distinct clinical prognosis and TME features were found in GC. Obvious differences in TME and the response to immunotherapy were also observed between the GC patients with high and low pyroptosis scores. Therefore, it is of

great significance to comprehensively assess the pyroptosis scores for individual GC patient, which may provide novel insight on optimizing the immunotherapy strategies.

### Acknowledgements

This study was supported in part by grant from the National Natural Science Foundation of China (No. 82073210), grant from the Scientific Foundation of Shaanxi Province (No. S2019ZDCXL01-02-01), grant from the National Clinical Research Center for Digestive Diseases (No. 2015BAI13B07). We appreciated STRING, GEO, TCGA, CMAP, UCSC Xena, MSigDB, TCIA, and GDSC databases for providing the platform or datasets.

### Disclosure of conflict of interest

None.

### Abbreviations

GC, Gastric Cancer; STAD, Stomach Adenocarcinoma; TME, Tumor Microenvironment; GEO, Gene-Expression Omnibus; TCGA, The Cancer Genome Atlas; PCA, Principal Component Analysis; CNV, Copy Number Variation; GSVA, Gene Set Variation Analysis; ssGSEA, single sample Gene Set Enrichment Analysis; DEGs, Differential Expression Genes; FDR, False Discovery Rate; OS, Overall Survival; KEGG, Kyoto Encyclopedia of Genes and Genomes; GO, Gene Ontology; BP, Biological Process; CC, Cellular Component; MF, Molecular Function; CIN, Chromosomal Instability; GS, Genome Stable; MSI, Microsatellite Instability; EBV, Epstein-Barr Virus; MSS, Microsatellite Stability; PRGs, Pyroptosis-Related Genes; PAMPs, Pathogen-Associated Molecular Patterns; DAMPs, Damage Associated Molecular Patterns; AIM2, Absent In Melanoma-2; GSDMD, Gasdermin D; IPS, Immunophenoscore; LPS, Lipopolysaccharide; TIME, Tumor Immune Microenvironment; ESTIMATE, Estimation of STromal and Immune cells in MAlignant Tumor tissues using Expression data; TMB, Tumor Mutation Burden; GDSC, Genomics of Drug Sensitivity in Cancer; IC50, Half Maximal Inhibitory Concentration; CMap, Connectivity Map; MoA, Mode-of-Action; DCs, Dendritic Cells; Tfh, Follicular Helper T cells; Th1, Type-1 T Helper Cells; Th2, Type-2 T Helper Cells; Treg, Regulatory T Cells; aDCs, Activated Dendritic

Cells; HR, Hazard Ratio; CI, Confidence Interval; pDCs, plasmacytoid Dendritic Cells; ZFX4, Zinc Finger Homeobox 4; JAK-STAT, Janus Kinase/Signal Transducer and Activator Of Transcription; RIG-I, Retinoic Acid-Inducible Gene-I; PYCARD, PYD and CARD Domain Containing; NLRP1, Nucleotide Oligomerization Domain (NOD)-Like Receptor Family, Pyrin Domain-Containing-1; APC, Antigen Presenting Cell; CCR, Chemokine Receptors; HLA, Human Leukocyte Antigen; TNF, Tumor Necrosis Factor; IL18, Interleukin 18; TIRAP, TIR Domain-Containing Adaptor Protein; GPX4, Glutathione Peroxidase 4; PJVK, Pejvakin; ELANE, Neutrophil Expressed; IFN, Interferon; PD-1/L1, Programmed Cell Death-1/Ligand 1; PIK3CA, Phosphatidylinositol-4,5-Bisphosphate 3-Kinase Catalytic Subunit Alpha; KMT2D, Lysine Methyltransferase 2D; ARID1A, AT-Rich Interaction Domain 1A; AIM2, Absent In Melanoma-2; CASP1, Caspase 1; CTLA4, Cytotoxic T Lymphocyte-Associated Antigen-4.

**Address correspondence to:** Daiming Fan and Liu Hong, State Key Laboratory of Cancer Biology and National Clinical Research Center for Digestive Diseases, Xijing Hospital of Digestive Diseases, Fourth Military Medical University, No. 127 Changle West Road, Xi'an 710032, Shaanxi, China. E-mail: hlhyhj@126.com (DMF); hongliufmmu@163.com (LH)

### References

- [1] Siegel RL, Miller KD and Jemal A. Cancer statistics, 2020. *CA Cancer J Clin* 2020; 70: 7-30.
- [2] Yang W, Ma J, Zhou W, Cao B, Zhou X, Yang Z, Zhang H, Zhao Q, Fan D and Hong L. Molecular mechanisms and theranostic potential of miRNAs in drug resistance of gastric cancer. *Expert Opin Ther Targets* 2017; 21: 1063-1075.
- [3] Johnston FM and Beckman M. Updates on management of gastric cancer. *Curr Oncol Rep* 2019; 21: 67.
- [4] Helmy KY, Patel SA, Nahas GR and Rameshwar P. Cancer immunotherapy: accomplishments to date and future promise. *Ther Deliv* 2013; 4: 1307-1320.
- [5] Zhuo M, Chi Y and Wang Z. The adverse events associated with combination immunotherapy in cancers: challenges and chances. *Asia Pac J Clin Oncol* 2020; 16: e154-e159.
- [6] Zhao Q, Cao L, Guan L, Bie L, Wang S, Xie B, Chen X, Shen X and Cao F. Immunotherapy for gastric cancer: dilemmas and prospect. *Brief Funct Genomics* 2019; 18: 107-112.

## Prognostic role of pyroptosis-related genes in gastric cancer

- [7] Coutzac C, Pernot S, Chaput N and Zaanani A. Immunotherapy in advanced gastric cancer, is it the future? *Crit Rev Oncol Hematol* 2019; 133: 25-32.
- [8] Spector LG, Pankratz N and Marcotte EL. Genetic and nongenetic risk factors for childhood cancer. *Pediatr Clin North Am* 2015; 62: 11-25.
- [9] Lewandowska AM, Rudzki M, Rudzki S, Lewandowski T and Laskowska B. Environmental risk factors for cancer-review paper. *Ann Agric Environ Med* 2019; 26: 1-7.
- [10] Hinshaw DC and Shevde LA. The tumor microenvironment innately modulates cancer progression. *Cancer Res* 2019; 79: 4557-4566.
- [11] Wu T and Dai Y. Tumor microenvironment and therapeutic response. *Cancer Lett* 2017; 387: 61-68.
- [12] Quail DF and Joyce JA. Microenvironmental regulation of tumor progression and metastasis. *Nat Med* 2013; 19: 1423-1437.
- [13] Maacha S, Bhat AA, Jimenez L, Raza A, Haris M, Uddin S and Grivel JC. Extracellular vesicles-mediated intercellular communication: roles in the tumor microenvironment and anti-cancer drug resistance. *Mol Cancer* 2019; 18: 55.
- [14] Zhou Z, He H, Wang K, Shi X, Wang Y, Su Y, Wang Y, Li D, Liu W, Shen L, Han W, Shen L, Ding J and Shao F. Granzyme A from cytotoxic lymphocytes cleaves GSDMB to trigger pyroptosis in target cells. *Science* 2020; 368: eaaz7548.
- [15] Birla R, Ganda C, Hoara P, Caragui A, Marica C, Vasiliu E and Constantinoiu S. Clinical and therapeutic implications of the 8th edition TNM classification of adenocarcinomas of the esophagogastric junction. *Chirurgia (Bucur)* 2018; 113: 747-757.
- [16] Zheng Y, Fu S, He T, Yan Q, Di W and Wang J. Predicting prognosis in resected esophageal squamous cell carcinoma using a clinical nomogram and recursive partitioning analysis. *Eur J Surg Oncol* 2018; 44: 1199-1204.
- [17] Du F, Sun Z, Jia J, Yang Y, Yu J, Shi Y, Jia B, Zhao J and Zhang X. Development and validation of an individualized nomogram for predicting survival in patients with esophageal carcinoma after resection. *J Cancer* 2020; 11: 4023-4029.
- [18] Fang Y, Tian S, Pan Y, Li W, Wang Q, Tang Y, Yu T, Wu X, Shi Y, Ma P and Shu Y. Pyroptosis: a new frontier in cancer. *Biomed Pharmacother* 2020; 121: 109595.
- [19] Schnappauf O, Chae JJ, Kastner DL and Aksentijevich I. The pyrin inflammasome in health and disease. *Front Immunol* 2019; 10: 1745.
- [20] Shojaie L, Iorga A and Dara L. Cell death in liver diseases: a review. *Int J Mol Sci* 2020; 21: 9682.
- [21] Galluzzi L, Vitale I, Aaronson SA, Abrams JM, Adam D, Agostinis P, Alnemri ES, Altucci L, Amelio I, Andrews DW, Annicchiarico-Petruzzelli M, Antonov AV, Arama E, Baehrecke EH, Barlev NA, Bazan NG, Bernassola F, Bertrand MJM, Bianchi K, Blagosklonny MV, Blomgren K, Borner C, Boya P, Brenner C, Campanella M, Candi E, Carmona-Gutierrez D, Cecconi F, Chan FK, Chandel NS, Cheng EH, Chipuk JE, Cidlowski JA, Ciechanover A, Cohen GM, Conrad M, Cubillos-Ruiz JR, Czabotar PE, D'Angiolella V, Dawson TM, Dawson VL, De Laurenzi V, De Maria R, Debatin KM, DeBerardinis RJ, Deshmukh M, Di Daniele N, Di Virgilio F, Dixit VM, Dixon SJ, Duckett CS, Dynlacht BD, El-Deiry WS, Elrod JW, Fimia GM, Fulda S, Garcia-Saez AJ, Garg AD, Garrido C, Gavathiotis E, Golstein P, Gottlieb E, Green DR, Greene LA, Gronemeyer H, Gross A, Hajnoczky G, Hardwick JM, Harris IS, Hengartner MO, Hetz C, Ichijo H, Jäättelä M, Joseph B, Jost PJ, Juin PP, Kaiser WJ, Karin M, Kaufmann T, Kepp O, Kimchi A, Kitsis RN, Klionsky DJ, Knight RA, Kumar S, Lee SW, Lemasters JJ, Levine B, Linkermann A, Lipton SA, Lockshin RA, López-Otín C, Lowe SW, Luedde T, Lugli E, MacFarlane M, Madeo F, Malewicz M, Malorni W, Manic G, Marine JC, Martin SJ, Martinou JC, Medema JP, Mehlen P, Meier P, Melino S, Miao EA, Molkentin JD, Moll UM, Muñoz-Pinedo C, Nagata S, Nuñez G, Oberst A, Oren M, Overholtzer M, Pagano M, Panaretakis T, Pasparakis M, Penninger JM, Pereira DM, Pervez S, Peter ME, Piacentini M, Pinton P, Prehn JHM, Puthalakath H, Rabinovich GA, Rehm M, Rizzuto R, Rodrigues CMP, Rubinsztein DC, Rudel T, Ryan KM, Sayan E, Scorrano L, Shao F, Shi Y, Silke J, Simon HU, Sistigu A, Stockwell BR, Strasser A, Szabadkai G, Tait SWG, Tang D, Tavernarakis N, Thorburn A, Tsujimoto Y, Turk B, Vanden Berghe T, Vandenabeele P, Vander Heiden MG, Villunger A, Virgin HW, Vousden KH, Vucic D, Wagner EF, Walczak H, Wallach D, Wang Y, Wells JA, Wood W, Yuan J, Zakeri Z, Zhivotovsky B, Zitvogel L, Melino G and Kroemer G. Molecular mechanisms of cell death: recommendations of the Nomenclature Committee on Cell Death 2018. *Cell Death Differ* 2018; 25: 486-541.
- [22] Man SM, Karki R and Kanneganti TD. Molecular mechanisms and functions of pyroptosis, inflammatory caspases and inflammasomes in infectious diseases. *Immunol Rev* 2017; 277: 61-75.
- [23] Liu X, Zhang Z, Ruan J, Pan Y, Magupalli VG, Wu H and Lieberman J. Inflammasome-activated gasdermin D causes pyroptosis by forming membrane pores. *Nature* 2016; 535: 153-158.
- [24] Jiang M, Qi L, Li L and Li Y. The caspase-3/GSDME signal pathway as a switch between

## Prognostic role of pyroptosis-related genes in gastric cancer

- apoptosis and pyroptosis in cancer. *Cell Death Discov* 2020; 6: 112.
- [25] Zhao P, Wang M, Chen M, Chen Z, Peng X, Zhou F, Song J and Qu J. Programming cell pyroptosis with biomimetic nanoparticles for solid tumor immunotherapy. *Biomaterials* 2020; 254: 120142.
- [26] Kambara H, Liu F, Zhang X, Liu P, Bajrami B, Teng Y, Zhao L, Zhou S, Yu H, Zhou W, Silberstein LE, Cheng T, Han M, Xu Y and Luo HR. Gasdermin D exerts anti-inflammatory effects by promoting neutrophil death. *Cell Rep* 2018; 22: 2924-2936.
- [27] Hou J, Zhao R, Xia W, Chang CW, You Y, Hsu JM, Nie L, Chen Y, Wang YC, Liu C, Wang WJ, Wu Y, Ke B, Hsu JL, Huang K, Ye Z, Yang Y, Xia X, Li Y, Li CW, Shao B, Tainer JA and Hung MC. PD-L1-mediated gasdermin C expression switches apoptosis to pyroptosis in cancer cells and facilitates tumour necrosis. *Nat Cell Biol* 2020; 22: 1264-1275.
- [28] Tan Y, Chen Q, Li X, Zeng Z, Xiong W, Li G, Li X, Yang J and Xiang B. Pyroptosis: a new paradigm of cell death for fighting against cancer. *J Exp Clin Cancer Res* 2021; 40: 153.
- [29] Kesavardhana S, Malireddi RKS and Kanneganti TD. Caspases in cell death, inflammation, and pyroptosis. *Annu Rev Immunol* 2020; 38: 567-595.
- [30] Karki R and Kanneganti TD. Diverging inflammatory signals in tumorigenesis and potential targeting. *Nat Rev Cancer* 2019; 19: 197-214.
- [31] Xia X, Wang X, Cheng Z, Qin W, Lei L, Jiang J and Hu J. The role of pyroptosis in cancer: pro-cancer or pro-“host”? *Cell Death Dis* 2019; 10: 650.
- [32] Wilkerson MD and Hayes DN. ConsensusClusterPlus: a class discovery tool with confidence assessments and item tracking. *Bioinformatics* 2010; 26: 1572-1573.
- [33] Chong W, Shang L, Liu J, Fang Z, Du F, Wu H, Liu Y, Wang Z, Chen Y, Jia S, Chen L, Li L and Chen H. m(6)A regulator-based methylation modification patterns characterized by distinct tumor microenvironment immune profiles in colon cancer. *Theranostics* 2021; 11: 2201-2217.
- [34] Charoentong P, Finotello F, Angelova M, Mayer C, Efremova M, Rieder D, Hackl H and Trajanoski Z. Pan-cancer immunogenomic analyses reveal genotype-immunophenotype relationships and predictors of response to checkpoint blockade. *Cell Rep* 2017; 18: 248-262.
- [35] Ritchie ME, Phipson B, Wu D, Hu Y, Law CW, Shi W and Smyth GK. Limma powers differential expression analyses for RNA-sequencing and microarray studies. *Nucleic Acids Res* 2015; 43: e47.
- [36] Yoshihara K, Shahmoradgoli M, Martinez E, Vegesna R, Kim H, Torres-Garcia W, Trevino V, Shen H, Laird PW, Levine DA, Carter SL, Getz G, Stemke-Hale K, Mills GB and Verhaak RG. Inferring tumour purity and stromal and immune cell admixture from expression data. *Nat Commun* 2013; 4: 2612.
- [37] Zhang B, Wu Q, Li B, Wang D, Wang L and Zhou YL. m(6)A regulator-mediated methylation modification patterns and tumor microenvironment infiltration characterization in gastric cancer. *Mol Cancer* 2020; 19: 53.
- [38] Zeng D, Li M, Zhou R, Zhang J, Sun H, Shi M, Bin J, Liao Y, Rao J and Liao W. Tumor microenvironment characterization in gastric cancer identifies prognostic and immunotherapeutically relevant gene signatures. *Cancer Immunol Res* 2019; 7: 737-750.
- [39] Mayakonda A, Lin DC, Assenov Y, Plass C and Koeffler HP. Maftools: efficient and comprehensive analysis of somatic variants in cancer. *Genome Res* 2018; 28: 1747-1756.
- [40] Zhang X, Shi M, Chen T and Zhang B. Characterization of the immune cell infiltration landscape in head and neck squamous cell carcinoma to aid immunotherapy. *Mol Ther Nucleic Acids* 2020; 22: 298-309.
- [41] Yang W, Soares J, Greninger P, Edelman EJ, Lightfoot H, Forbes S, Bindal L, Beare D, Smith JA, Thompson IR, Ramaswamy S, Futreal PA, Haber DA, Stratton MR, Benes C, McDermott U and Garnett MJ. Genomics of Drug Sensitivity in Cancer (GDSC): a resource for therapeutic biomarker discovery in cancer cells. *Nucleic Acids Res* 2013; 41: D955-961.
- [42] Geeleher P, Cox N and Huang RS. pRRophetic: an R package for prediction of clinical chemotherapeutic response from tumor gene expression levels. *PLoS One* 2014; 9: e107468.
- [43] Lamb J, Crawford ED, Peck D, Modell JW, Blat IC, Wrobel MJ, Lerner J, Brunet JP, Subramanian A, Ross KN, Reich M, Hieronymus H, Wei G, Armstrong SA, Haggarty SJ, Clemons PA, Wei R, Carr SA, Lander ES and Golub TR. The connectivity map: using gene-expression signatures to connect small molecules, genes, and disease. *Science* 2006; 313: 1929-1935.
- [44] Hugo W, Zaretsky JM, Sun L, Song C, Moreno BH, Hu-Lieskovan S, Berent-Maoz B, Pang J, Chmielowski B, Cherry G, Seja E, Lomeli S, Kong X, Kelley MC, Sosman JA, Johnson DB, Ribas A and Lo RS. Genomic and transcriptomic features of response to Anti-PD-1 therapy in metastatic melanoma. *Cell* 2016; 165: 35-44.
- [45] Kim JY, Choi JK and Jung H. Genome-wide methylation patterns predict clinical benefit of immunotherapy in lung cancer. *Clin Epigenetics* 2020; 12: 119.
- [46] Jung H, Kim HS, Kim JY, Sun JM, Ahn JS, Ahn MJ, Park K, Esteller M, Lee SH and Choi JK.

## Prognostic role of pyroptosis-related genes in gastric cancer

- DNA methylation loss promotes immune evasion of tumours with high mutation and copy number load. *Nat Commun* 2019; 10: 4278.
- [47] Riaz N, Havel JJ, Makarov V, Desrichard A, Urba WJ, Sims JS, Hodi FS, Martín-Algarra S, Mandal R, Sharfman WH, Bhatia S, Hwu WJ, Gajewski TF, Slingluff CL Jr, Chowell D, Kendall SM, Chang H, Shah R, Kuo F, Morris LGT, Sidhom JW, Schneck JP, Horak CE, Weinhold N and Chan TA. Tumor and microenvironment evolution during immunotherapy with nivolumab. *Cell* 2017; 171: 934-949.
- [48] Ye Y, Dai Q and Qi H. A novel defined pyroptosis-related gene signature for predicting the prognosis of ovarian cancer. *Cell Death Discov* 2021; 7: 71.
- [49] von Mering C, Huynen M, Jaeggi D, Schmidt S, Bork P and Snel B. STRING: a database of predicted functional associations between proteins. *Nucleic Acids Res* 2003; 31: 258-261.
- [50] Chen DS and Mellman I. Elements of cancer immunity and the cancer-immune set point. *Nature* 2017; 541: 321-330.
- [51] Sohn BH, Hwang JE, Jang HJ, Lee HS, Oh SC, Shim JJ, Lee KW, Kim EH, Yim SY, Lee SH, Cheong JH, Jeong W, Cho JY, Kim J, Chae J, Lee J, Kang WK, Kim S, Noh SH, Ajani JA and Lee JS. Clinical significance of four molecular subtypes of gastric cancer identified by the cancer genome atlas project. *Clin Cancer Res* 2017; 23: 4441-4449.
- [52] Kim TS, da Silva E, Coit DG and Tang LH. Intratumoral immune response to gastric cancer varies by molecular and histologic subtype. *Am J Surg Pathol* 2019; 43: 851-860.
- [53] Rizvi NA, Hellmann MD, Snyder A, Kvistborg P, Makarov V, Havel JJ, Lee W, Yuan J, Wong P, Ho TS, Miller ML, Rekhman N, Moreira AL, Ibrahim F, Bruggeman C, Gasmir B, Zappasodi R, Maeda Y, Sander C, Garon EB, Merghoub T, Wolchok JD, Schumacher TN and Chan TA. Cancer immunology. Mutational landscape determines sensitivity to PD-1 blockade in non-small cell lung cancer. *Science* 2015; 348: 124-128.
- [54] Blaesche F, Paul MC, Schuhmann MU, Rabsteyn A, Schroeder C, Casadei N, Matthes J, Mohr C, Lotfi R, Wagner B, Kaeuferle T, Feucht J, Willier S, Handgretinger R, Stevanović S, Lang P and Feuchtinger T. Low mutational load in pediatric medulloblastoma still translates into neoantigens as targets for specific T-cell immunotherapy. *Cytotherapy* 2019; 21: 973-986.
- [55] Braun DA, Hou Y, Bakouny Z, Ficial M, Sant' Angelo M, Forman J, Ross-Macdonald P, Berger AC, Jegede OA, Elagina L, Steinharter J, Sun M, Wind-Rotolo M, Pignon JC, Cherniack AD, Lichtenstein L, Neuberg D, Catalano P, Freeman GJ, Sharpe AH, McDermott DF, Van Allen EM, Signoretti S, Wu CJ, Shukla SA and Choueiri TK. Interplay of somatic alterations and immune infiltration modulates response to PD-1 blockade in advanced clear cell renal cell carcinoma. *Nat Med* 2020; 26: 909-918.
- [56] Sabbatino F, Marra A, Liguori L, Scognamiglio G, Fusciello C, Botti G, Ferrone S and Pepe S. Resistance to anti-PD-1-based immunotherapy in basal cell carcinoma: a case report and review of the literature. *J Immunother Cancer* 2018; 6: 126.
- [57] Tang R, Xu J, Zhang B, Liu J, Liang C, Hua J, Meng Q, Yu X and Shi S. Ferroptosis, necroptosis, and pyroptosis in anticancer immunity. *J Hematol Oncol* 2020; 13: 110.
- [58] Shao W, Yang Z, Fu Y, Zheng L, Liu F, Chai L and Jia J. The pyroptosis-related signature predicts prognosis and indicates immune microenvironment infiltration in gastric cancer. *Front Cell Dev Biol* 2021; 9: 676485.
- [59] Li L, Jiang M, Qi L, Wu Y, Song D, Gan J and Li Y. Pyroptosis, a new bridge to tumor immunity. *Cancer Sci* 2021; 112: 3979-3994.
- [60] Berkel C and Cacan E. Differential expression and copy number variation of gasdermin (GSDM) family members, pore-forming proteins in pyroptosis, in normal and malignant serous ovarian tissue. *Inflammation* 2021; 44: 2203-2216.
- [61] Wei J, Xu Z, Chen X, Wang X, Zeng S, Qian L, Yang X, Ou C, Lin W, Gong Z and Yan Y. Overexpression of GSDMC is a prognostic factor for predicting a poor outcome in lung adenocarcinoma. *Mol Med Rep* 2020; 21: 360-370.
- [62] Paul P, Malakar AK and Chakraborty S. The significance of gene mutations across eight major cancer types. *Mutat Res Rev Mutat Res* 2019; 781: 88-99.
- [63] Lee DW, Han SW, Bae JM, Jang H, Han H, Kim H, Bang D, Jeong SY, Park KJ, Kang GH and Kim TY. Tumor mutation burden and prognosis in patients with colorectal cancer treated with adjuvant fluoropyrimidine and oxaliplatin. *Clin Cancer Res* 2019; 25: 6141-6147.



# Prognostic role of pyroptosis-related genes in gastric cancer

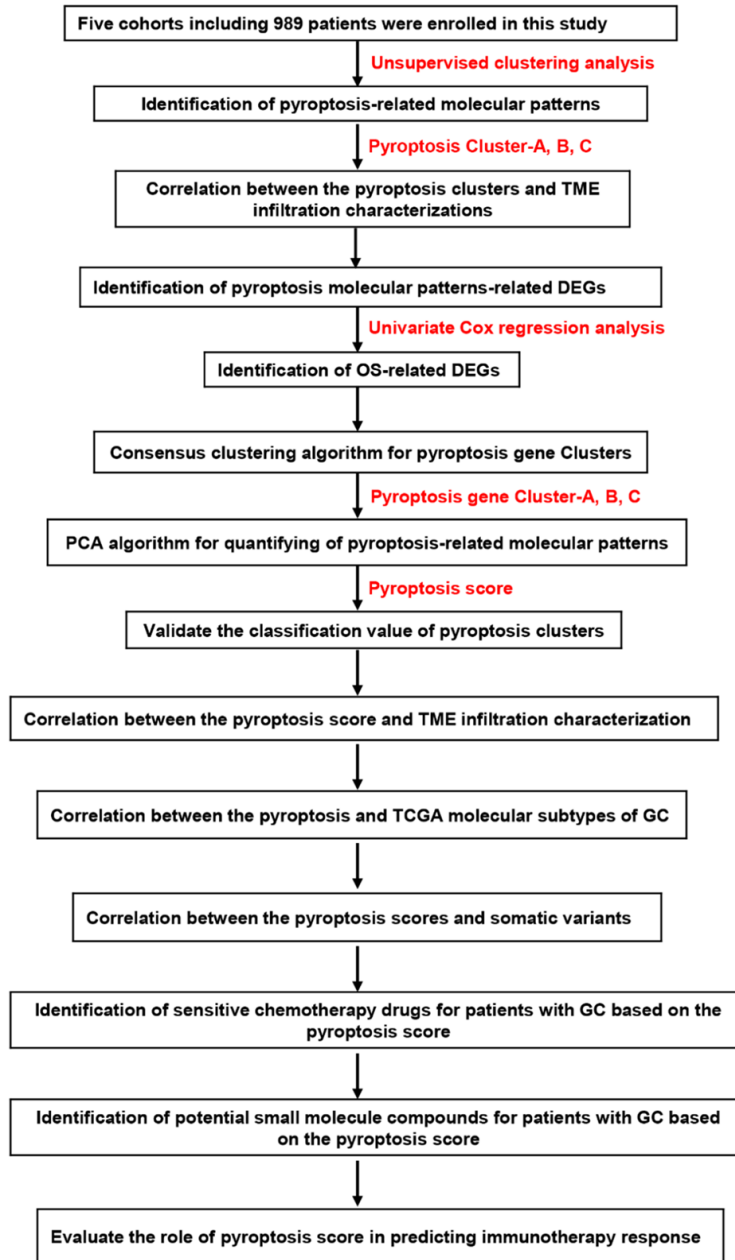


Figure S1. Workflow of the study design.

## Prognostic role of pyroptosis-related genes in gastric cancer

**Table S1.** Datasets of GC patients

Cohort	Platform	Number of patients	Survival data
GSE15459	Affymetrix Human Genome U133 Plus 2.0 Array	192	OS
GSE34942	Affymetrix Human Genome U133 Plus 2.0 Array	56	OS
GSE57303	Affymetrix Human Genome U133 Plus 2.0 Array	70	OS
GSE62254	Affymetrix Human Genome U133 Plus 2.0 Array	300	OS
TCGA:STAD	Illumina RNAseq	371	OS

**Table S2.** 33 acknowledged pyroptosis-related genes

Gene	Full name
AIM2	Absent in melanoma 2
CASP1	cysteine-aspartic acid protease-1
CASP3	cysteine-aspartic acid protease-3
CASP4	cysteine-aspartic acid protease-4
CASP5	cysteine-aspartic acid protease-5
CASP6	cysteine-aspartic acid protease-6
CASP8	cysteine-aspartic acid protease-8
CASP9	cysteine-aspartic acid protease-9
ELANE	elastase, neutrophil expressed
GPX4	glutathione peroxidase 4
GSDMA	gasdermin A
GSDMB	gasdermin B
GSDMC	gasdermin C
GSDMD	gasdermin D
GSDME	gasdermin E
IL18	interleukin 18
IL1B	interleukin 1 beta
IL6	interleukin 6
NLRC4	NLR family CARD domain containing 4
NLRP1	NLR family pyrin domain containing 1
NLRP2	NLR family pyrin domain containing 2
NLRP3	NLR family pyrin domain containing 3
NLRP6	NLR family pyrin domain containing 6
NLRP7	NLR family pyrin domain containing 7
NOD1	nucleotide binding oligomerization domain containing 1
NOD2	nucleotide binding oligomerization domain containing 2
PJVK	pejvakin/deafness, autosomal recessive 59
PLCG1	phospholipase C gamma 1
PRKACA	protein kinase cAMP-activated catalytic subunit alpha
PYCARD	PYD and CARD domain containing
SCAF11	SR-related CTD associated factor 11
TIRAP	TIR domain containing adaptor protein
TNF	tumor necrosis factor

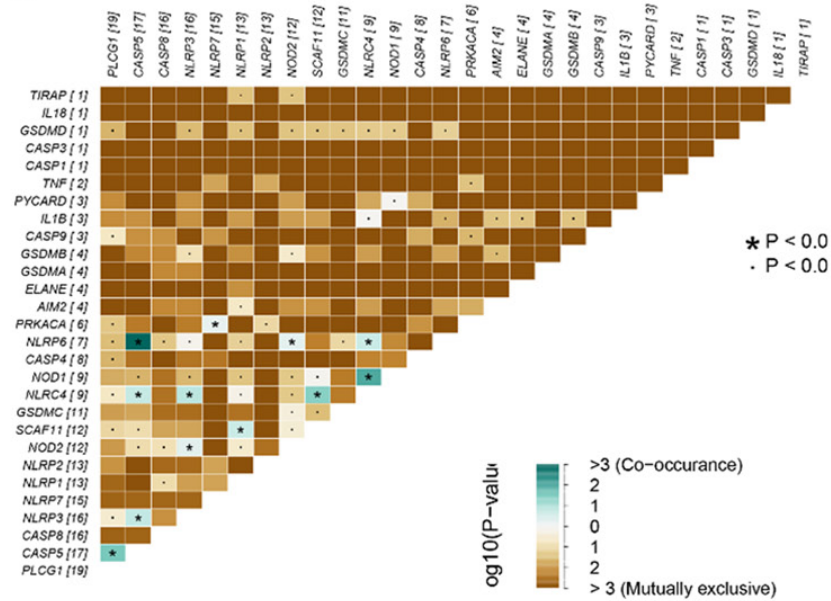
## Prognostic role of pyroptosis-related genes in gastric cancer

**Table S3.** 30 overlapping pyroptosis-related genes

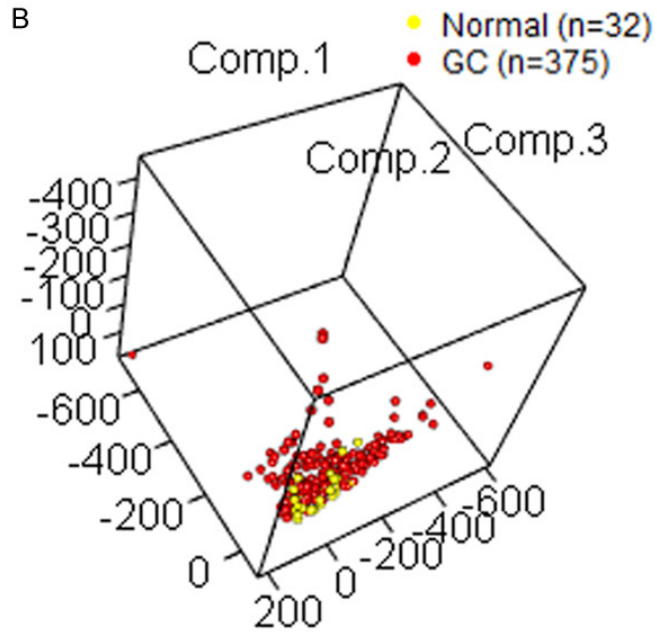
Gene	Full name
AIM2	Absent in melanoma 2
CASP1	cysteine-aspartic acid protease-1
CASP3	cysteine-aspartic acid protease-3
CASP4	cysteine-aspartic acid protease-4
CASP5	cysteine-aspartic acid protease-5
CASP6	cysteine-aspartic acid protease-6
CASP8	cysteine-aspartic acid protease-8
CASP9	cysteine-aspartic acid protease-9
ELANE	elastase, neutrophil expressed
GPX4	glutathione peroxidase 4
GSDMB	gasdermin B
GSDMC	gasdermin C
GSDMD	gasdermin D
IL18	interleukin 18
IL1B	interleukin 1 beta
IL6	interleukin 6
NLRC4	NLR family CARD domain containing 4
NLRP1	NLR family pyrin domain containing 1
NLRP2	NLR family pyrin domain containing 2
NLRP3	NLR family pyrin domain containing 3
NLRP6	NLR family pyrin domain containing 6
NLRP7	NLR family pyrin domain containing 7
NOD1	nucleotide binding oligomerization domain containing 1
NOD2	nucleotide binding oligomerization domain containing 2
PLCG1	phospholipase C gamma 1
PRKACA	protein kinase cAMP-activated catalytic subunit alpha
PYCARD	PYD and CARD domain containing
SCAF11	SR-related CTD associated factor 11
TIRAP	TIR domain containing adaptor protein
TNF	tumor necrosis factor

# Prognostic role of pyroptosis-related genes in gastric cancer

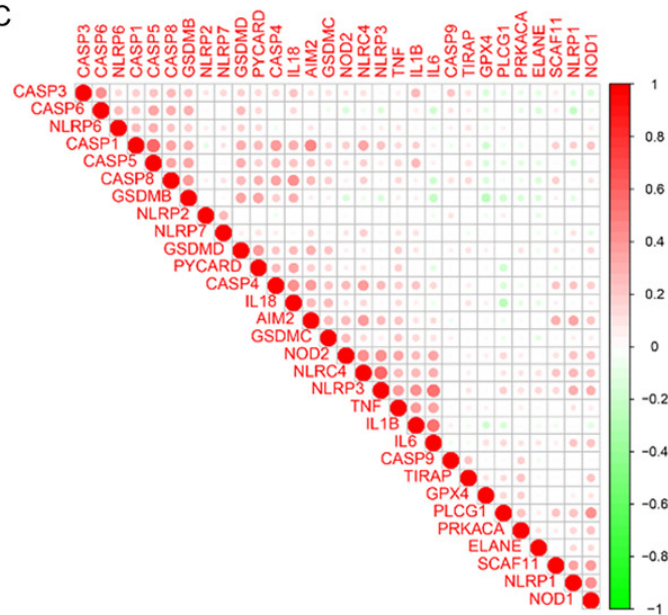
A



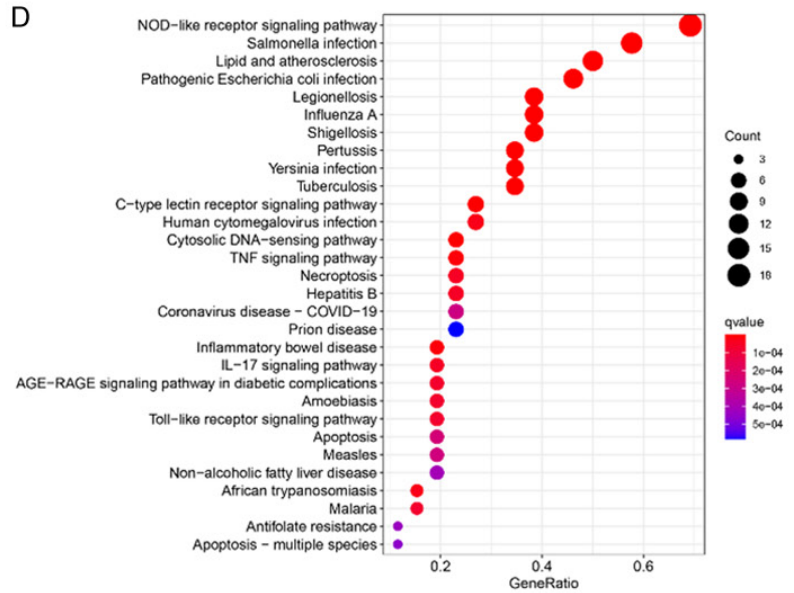
B



C

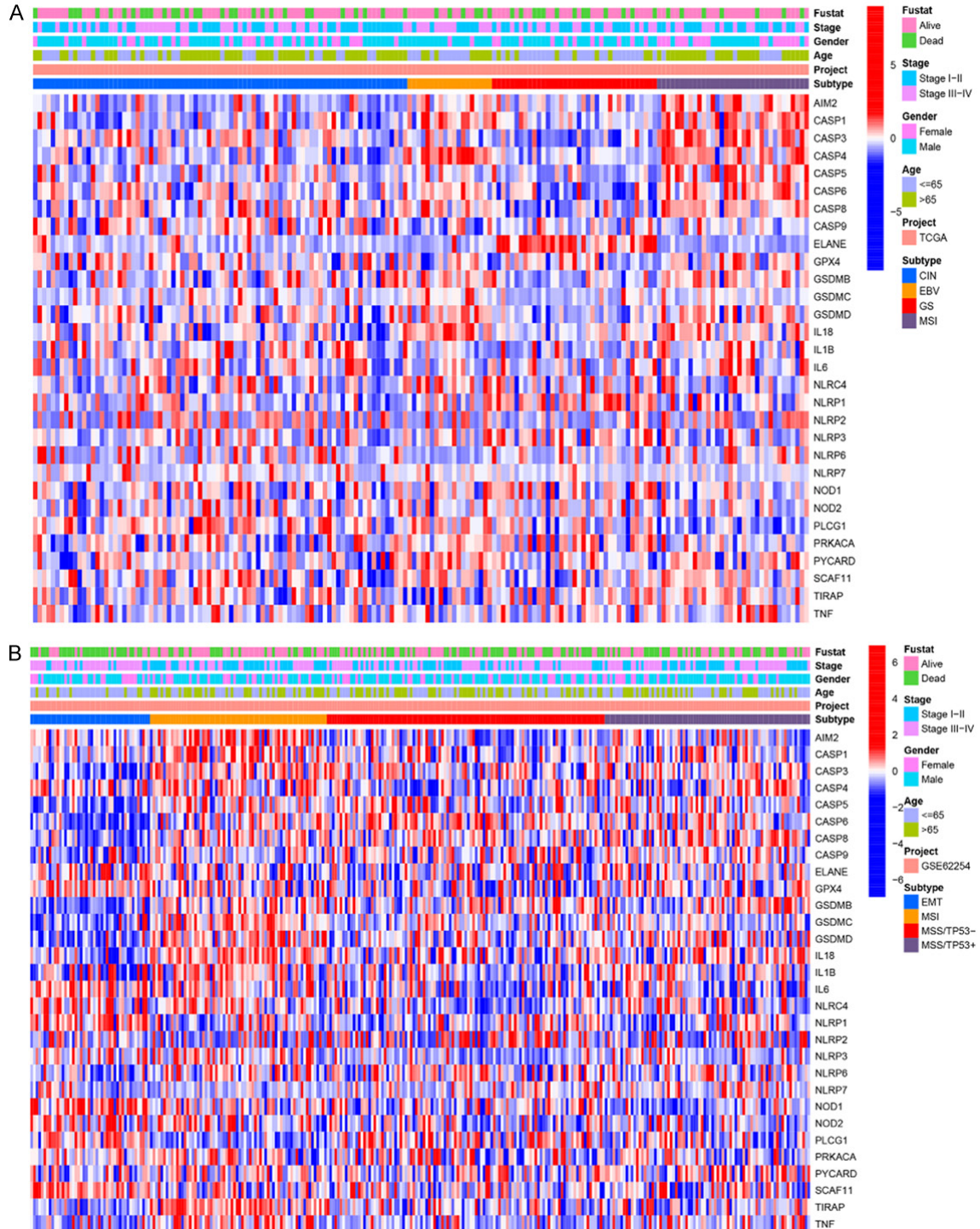


D



## Prognostic role of pyroptosis-related genes in gastric cancer

**Figure S2.** Characteristics of PGRs in GC. A. The mutation co-occurrence and mutually exclusion analyses for PGRs. Co-occurrence, green; Mutually exclusion, brown. B. Three-dimensional principal component analysis (3D-PCA) of the mRNA expression profiles of PRGs to distinguish tumors from normal samples in TCGA-STAD cohort. C. The correlations between these PGRs were evaluated using the Spearman correlation analysis in GC. D. KEGG pathway enrichment analysis of the 33 PRGs.



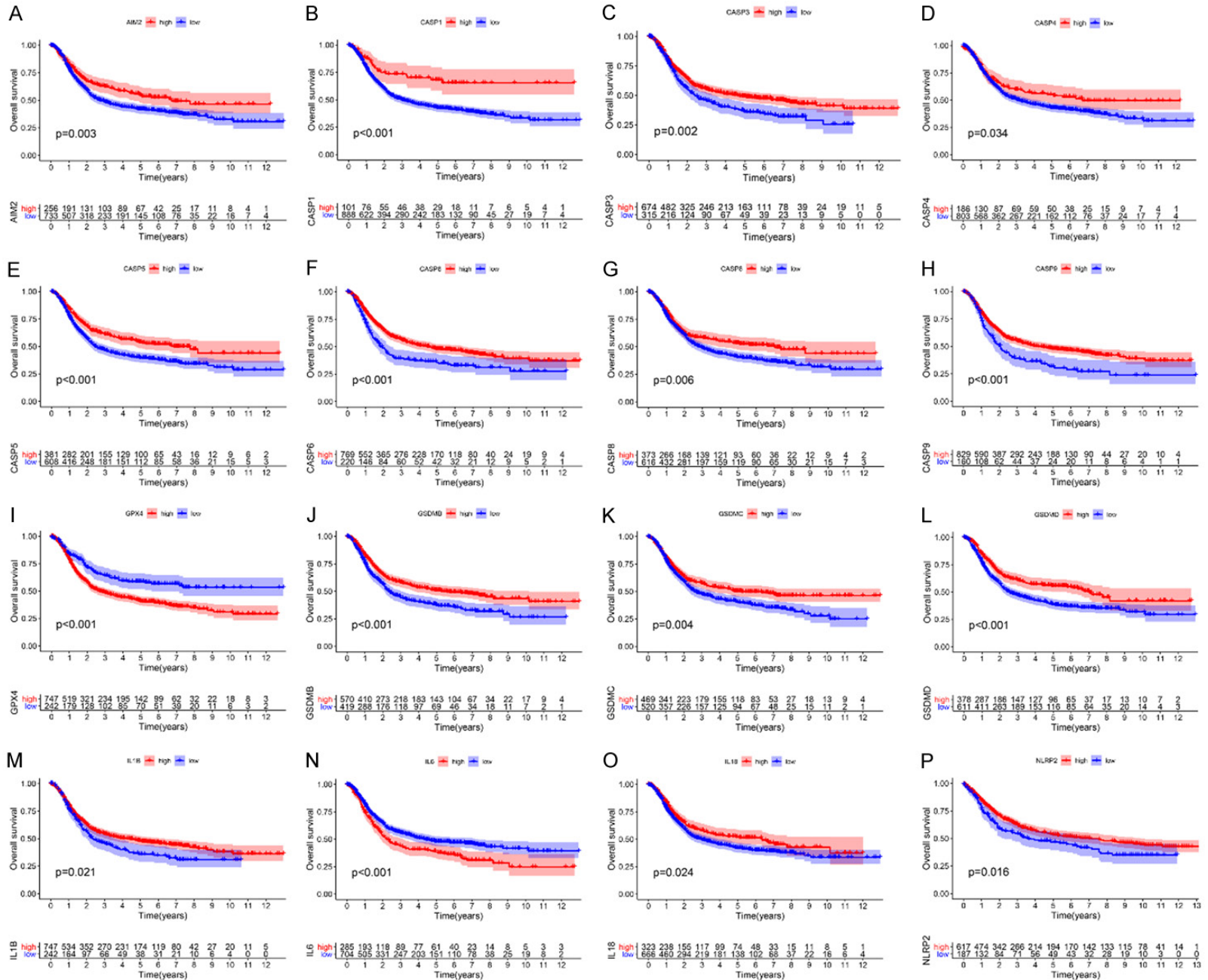
**Figure S3.** The expression of PGRs in TCGA molecular subtypes (A) and GSE62254 cohort subtypes (B).

## Prognostic role of pyroptosis-related genes in gastric cancer

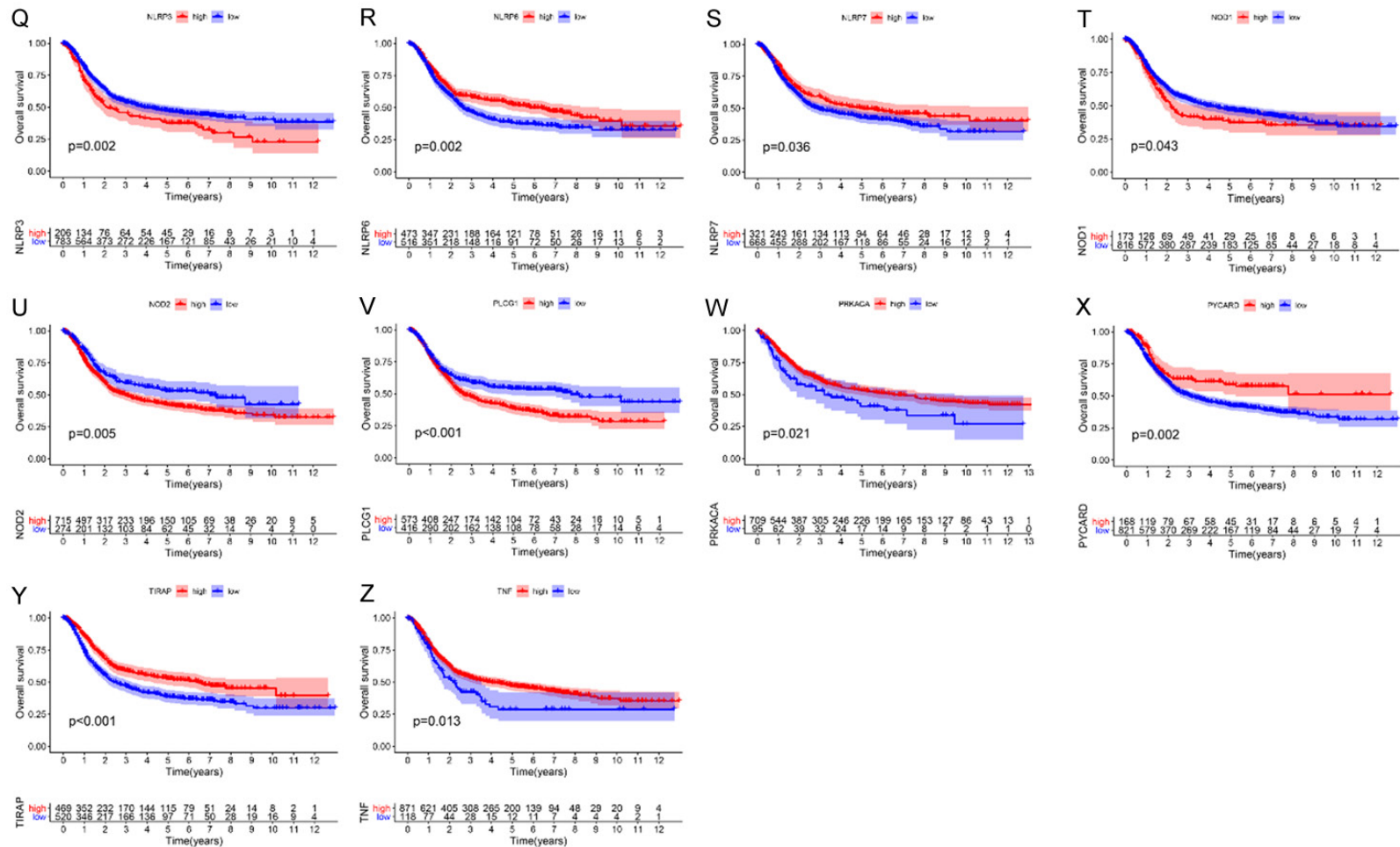
**Table S4.** Univariate Cox regression analysis of 30 PRGs in GC patients

Gene	HR	HR.95L	HR.95H	P-value	p-km
AIM2	0.9162	0.850929	0.986477	0.020285	0.002784
CASP1	0.813646	0.738252	0.896739	3.23E-05	0.000138
CASP3	0.791896	0.672539	0.932435	0.005122	0.002149
CASP4	0.926298	0.779201	1.101162	0.385538	0.034045
CASP5	0.826208	0.743883	0.917644	0.000364	6.20E-05
CASP6	0.758625	0.643263	0.894675	0.001029	4.25E-05
CASP8	0.766377	0.625849	0.938459	0.010038	0.005662
CASP9	0.791276	0.612488	1.022252	0.073206	0.000452
ELANE	1.057157	0.928772	1.20329	0.40012	0.145916
GPX4	1.29307	1.078449	1.550401	0.005511	1.97E-05
GSDMB	0.86055	0.784177	0.944361	0.001539	4.90E-05
GSDMC	0.848944	0.723394	0.996285	0.044904	0.003529
GSDMD	0.730325	0.60767	0.877739	0.000808	2.56E-05
IL18	0.947813	0.858823	1.046024	0.286657	0.024476
IL1B	0.986575	0.918594	1.059588	0.710612	0.020541
IL6	1.122685	1.052046	1.198068	0.000483	0.000552
NLRC4	1.072602	0.913468	1.259458	0.392344	0.116657
NLRP1	1.061701	0.914147	1.233072	0.432913	0.055706
NLRP2	0.997506	0.941941	1.05635	0.93196	0.154515
NLRP3	1.205337	1.065877	1.363046	0.002912	0.002096
NLRP6	0.902724	0.818304	0.995854	0.041061	0.002225
NLRP7	0.982512	0.881398	1.095225	0.750177	0.036066
NOD1	1.087384	0.894139	1.322395	0.401384	0.042653
NOD2	1.163598	1.021308	1.325712	0.022799	0.004966
PLCG1	1.233606	1.048437	1.451479	0.011407	0.000288
PRKACA	0.985863	0.770836	1.260871	0.909696	0.266301
PYCARD	0.943283	0.827467	1.07531	0.382335	0.001941
SCAF11	0.978412	0.773484	1.237634	0.855581	0.184893
TIRAP	0.689006	0.549698	0.863619	0.001228	1.25E-05
TNF	0.919229	0.818404	1.032475	0.155373	0.012761

# Prognostic role of pyroptosis-related genes in gastric cancer



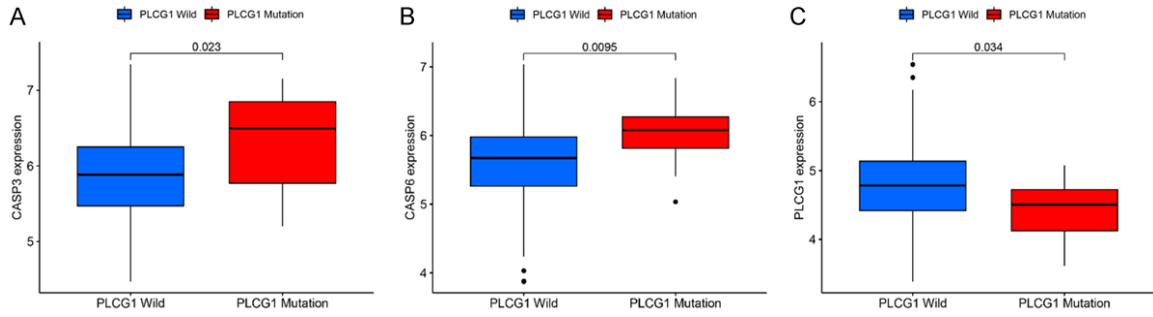
## Prognostic role of pyroptosis-related genes in gastric cancer



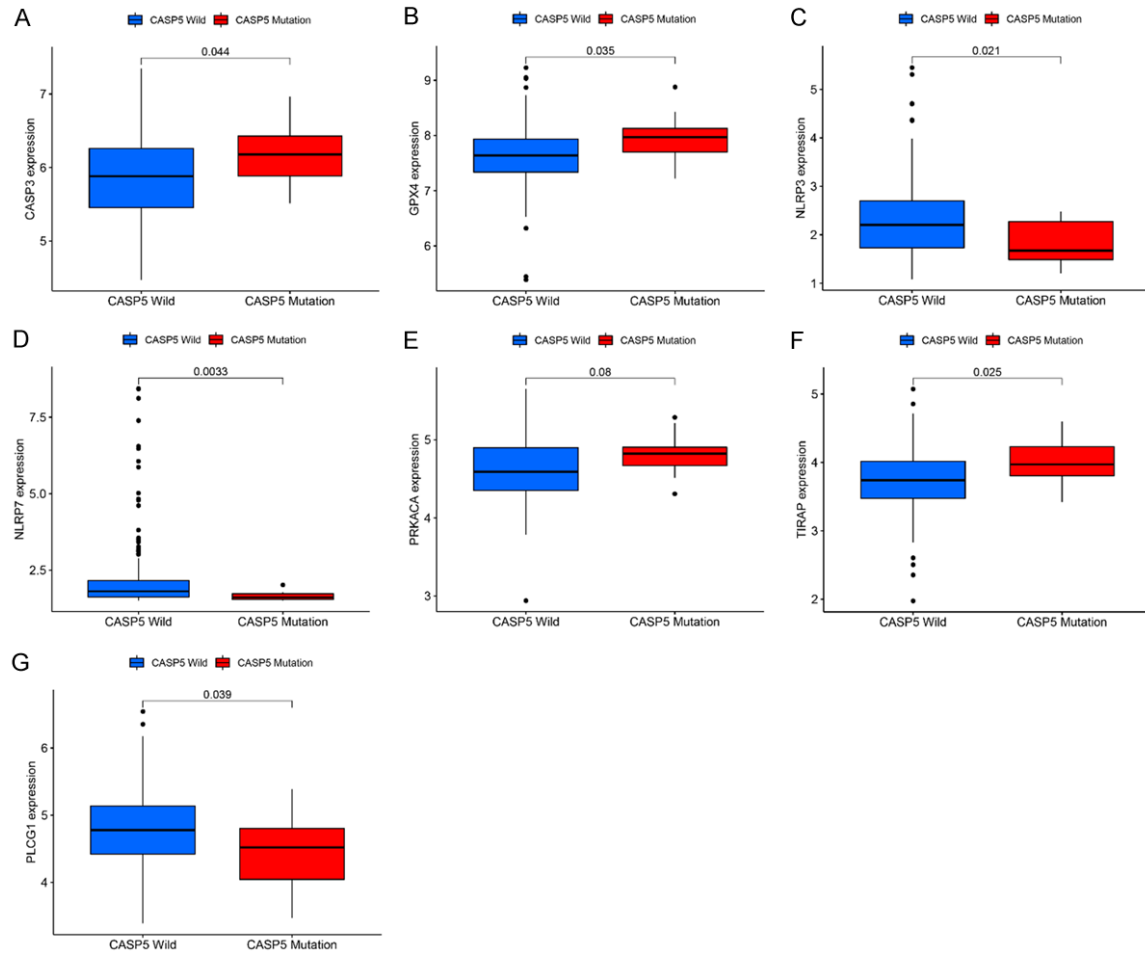
**Figure S4.** OS-related PRGs in gathered GC cohort. Kaplan-Meier curves for GC patients with high and low levels of AIM2 (A), CASP1 (B), CASP3 (C), CASP4 (D), CASP5 (E), CASP6 (F), CASP8 (G), CASP9 (H), GPX4 (I), GSDMB (J), GSDMC (K), GSDMD (L), IL1B (M), IL6 (N), IL18 (O), NLRP2 (P), NLRP3 (Q), NLRP6 (R), NLRP7 (S), NOD1 (T), NOD2 (U), PLCG1 (V), PRKACA (W), PYCARD (X), TIRAP (Y), TNF (Z) in gathered GC cohort.



## Prognostic role of pyroptosis-related genes in gastric cancer

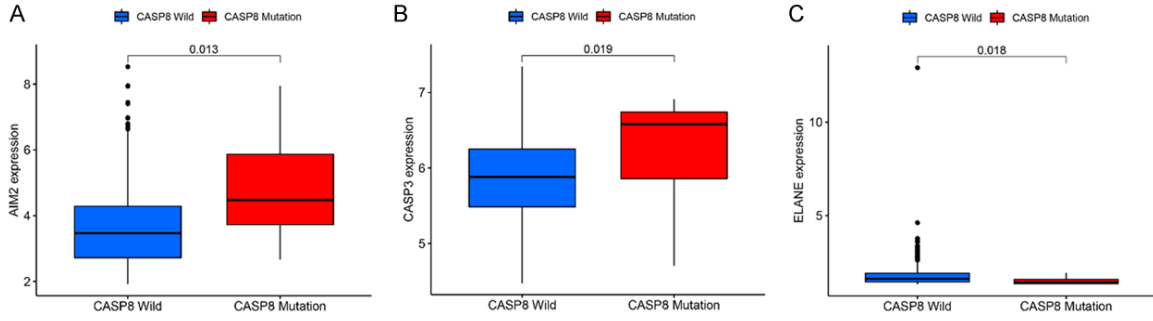


**Figure S5.** Difference in PRGs expression between PLCG1-mutant and wild types. (A-C) Expression levels of CASP3 (A), CASP6 (B), and PLCG1 (C) between PLCG1-mutant and wild types.

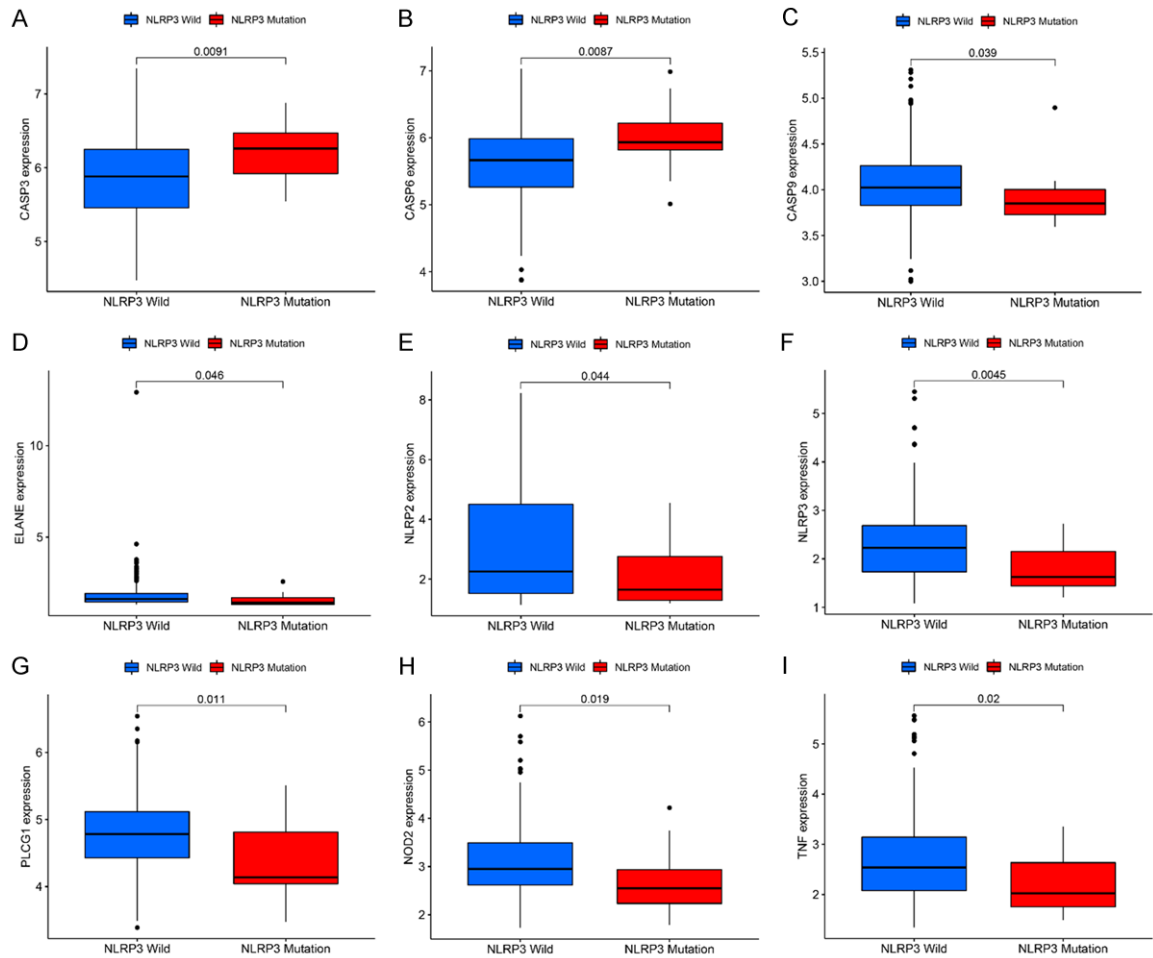


**Figure S6.** Difference in PRGs expression between CASP5-mutant and wild types. (A-G) Expression levels of CASP3 (A), GPX4 (B), NLRP3 (C), NLRP7 (D), PRKACA (E), TIRAP (F), and PLCG1 (G) between CASP5-mutant and wild types.

## Prognostic role of pyroptosis-related genes in gastric cancer

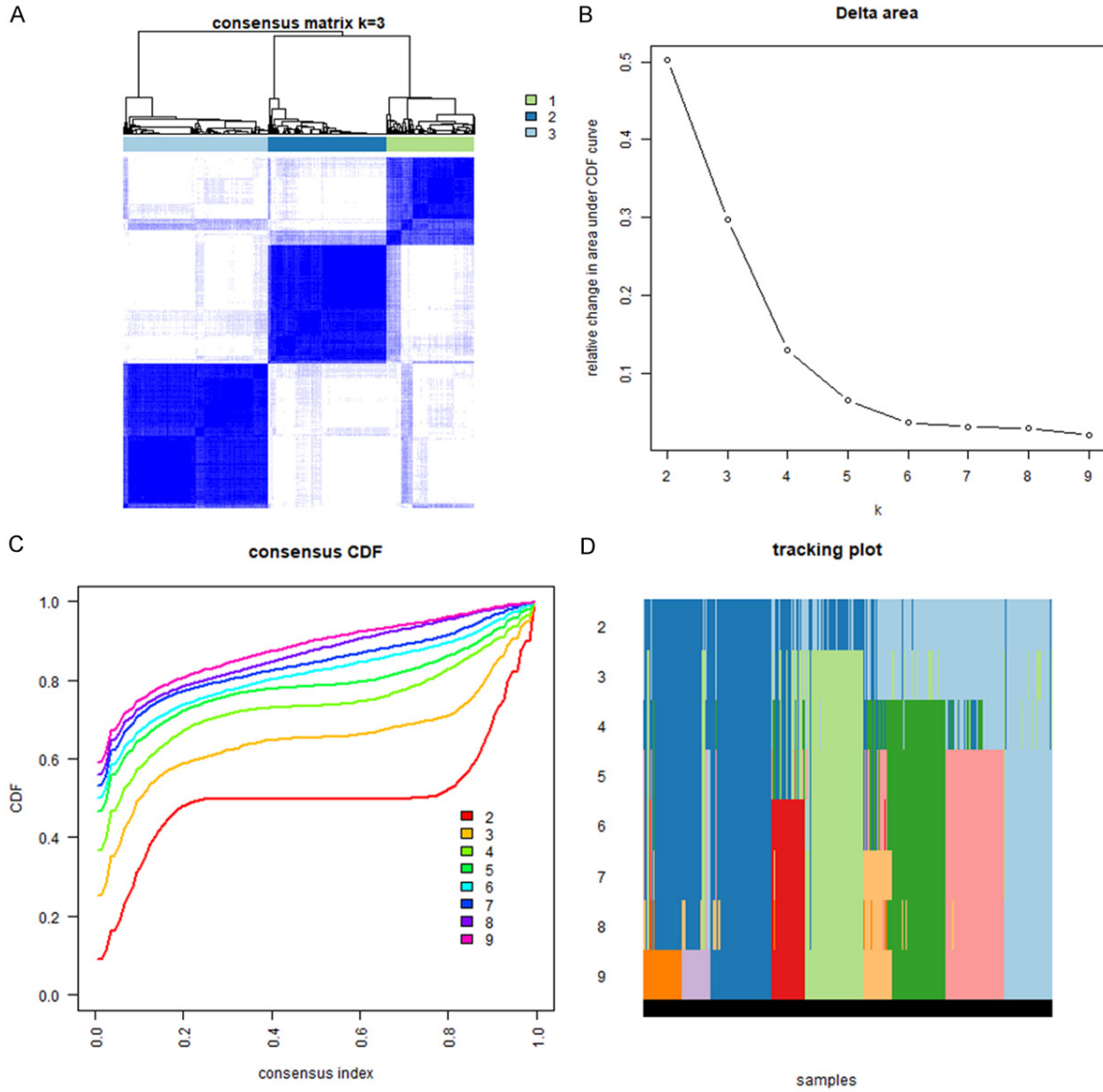


**Figure S7.** Difference in PRGs expression between CASP8-mutant and wild types. (A-C) Expression levels of AIM2 (A), CASP3 (B), and ELANE (C) between CASP8-mutant and wild types.



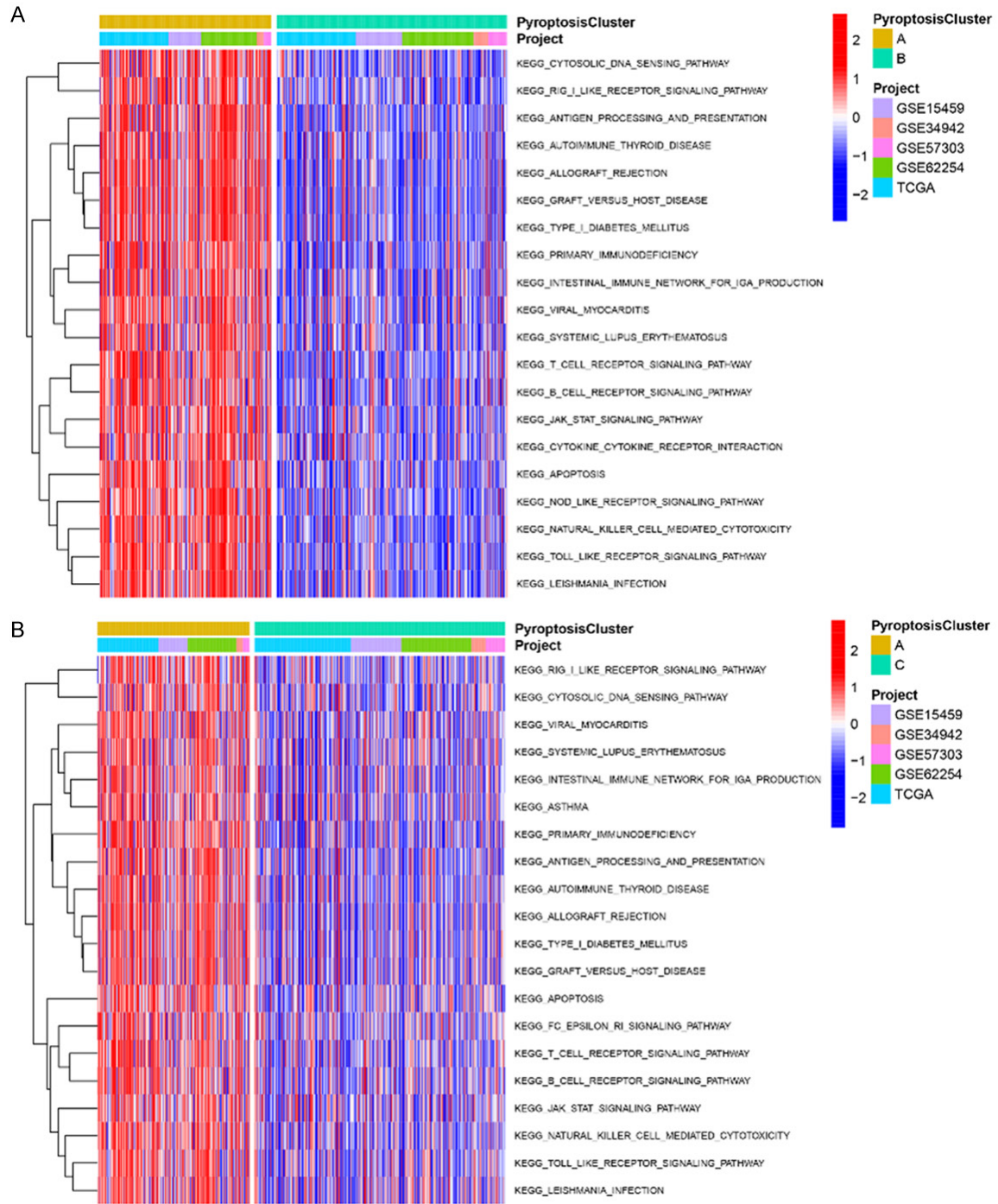
**Figure S8.** Difference in PRGs expression between NLRP3-mutant and wild types. (A-I) Expression levels of CASP3 (A), CASP6 (B), CASP9 (C), ELANE (D), NLRP2 (E), NLRP3 (F), PLCG1 (G), NOD2 (H), and TNF (I) between NLRP3-mutant and wild types.

# Prognostic role of pyroptosis-related genes in gastric cancer

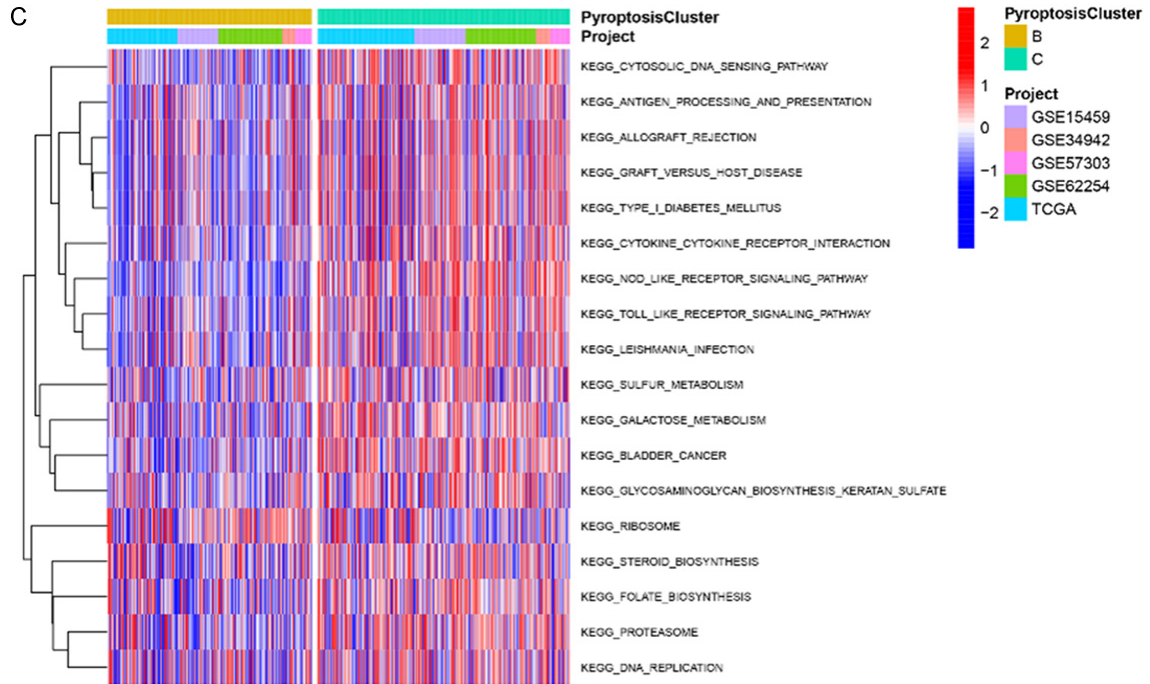


**Figure S9.** Unsupervised clustering analysis for identifying pyroptosis-related molecular patterns. A. Consensus clustering matrix for k=3. B. Relative change in area under CDF curve for k=2-9. C. Consensus clustering cumulative distribution function (CDF) for k=2-9. D. The tracking plot for k=2-9.

# Prognostic role of pyroptosis-related genes in gastric cancer

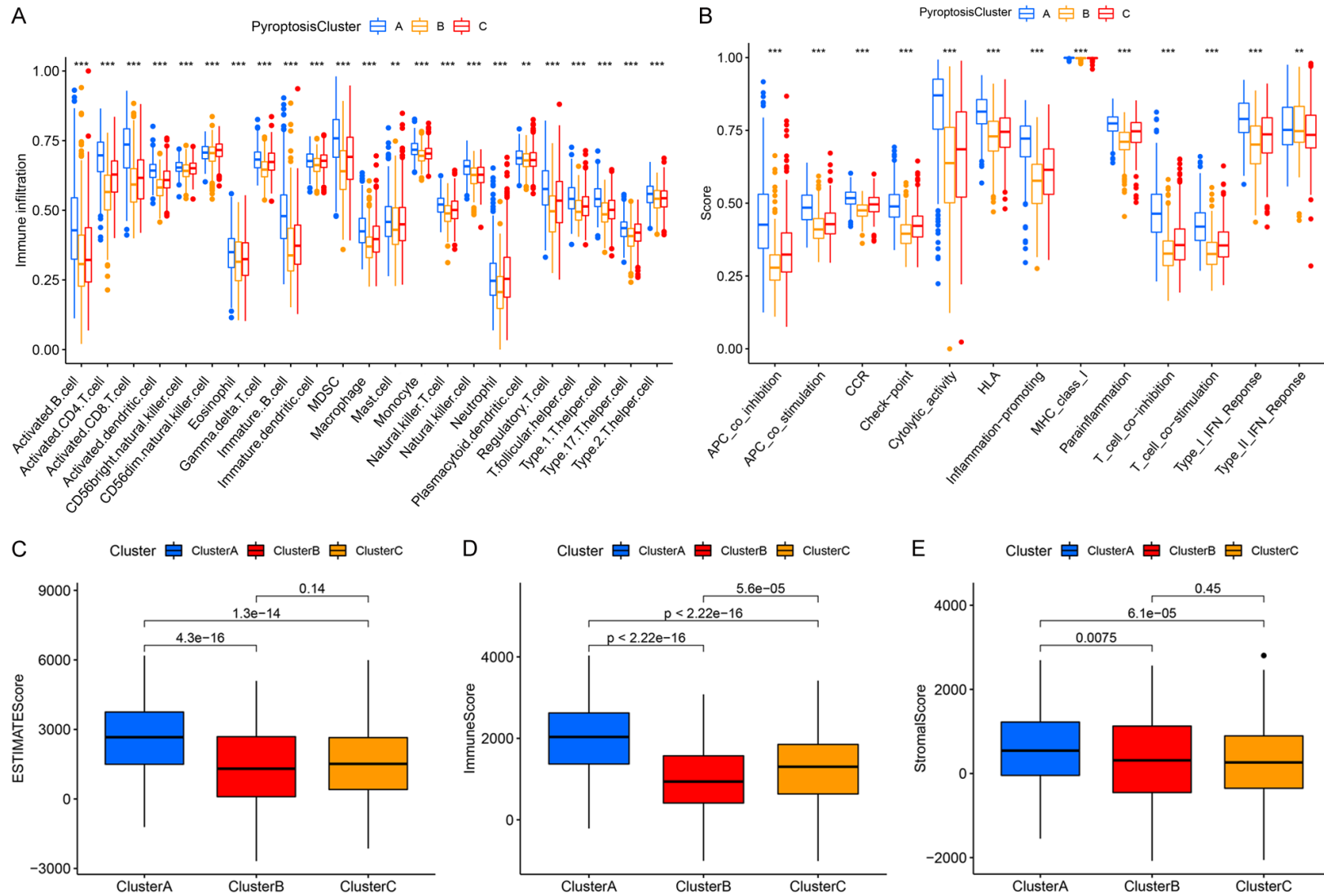


## Prognostic role of pyroptosis-related genes in gastric cancer



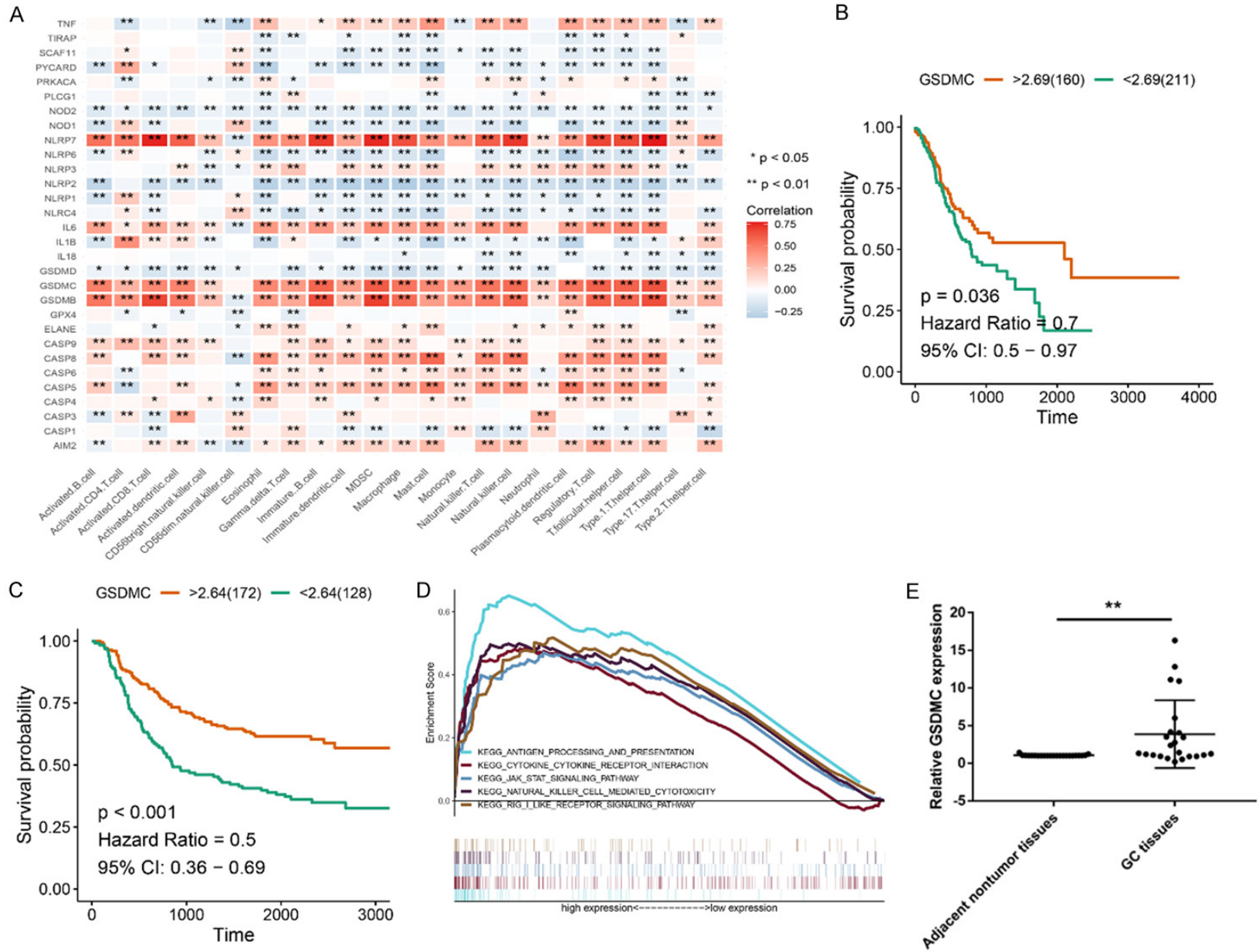
**Figure S10.** Identification of biological pathways by GSVA enrichment analysis in distinct pyroptosis-related molecular patterns. The heatmap was used to show the activation states of biological pathways. Red represents the activated pathways, while blue represents the inhibited pathways. The GC cohorts were used as sample annotations. A. Pyroptosis Cluster A vs pyroptosis Cluster B; B. Pyroptosis Cluster A vs pyroptosis Cluster C; C. Pyroptosis Cluster B vs pyroptosis Cluster C.

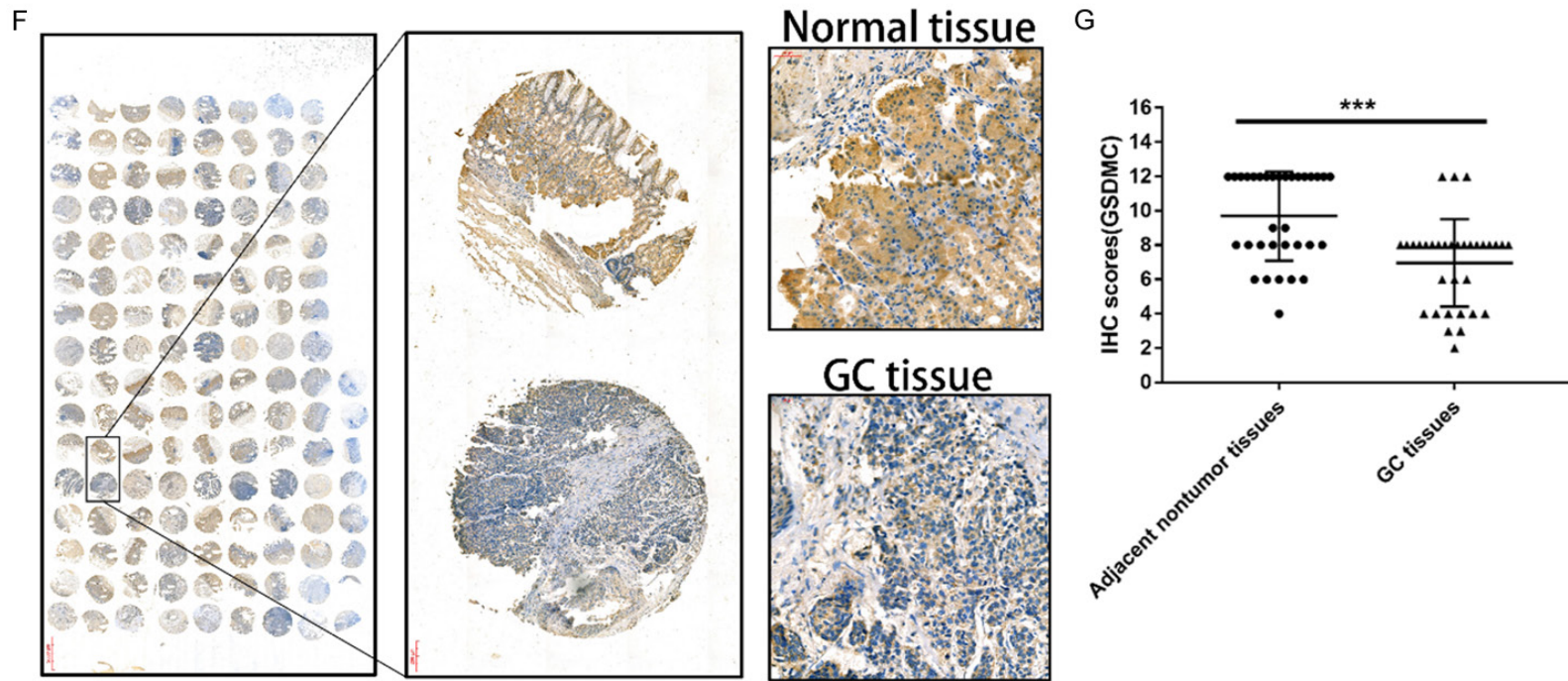
## Prognostic role of pyroptosis-related genes in gastric cancer



**Figure S11.** Correlation between the characteristics of tumor immune microenvironment (TIME) and pyroptosis clusters. (A) Box plots depicts the scores of immune infiltrations among the three pyroptosis clusters. (B) Box plots presents the scores of immune functions among the three pyroptosis clusters. \* $P < 0.05$ ; \*\* $P < 0.01$ ; \*\*\* $P < 0.001$ . (C-E) Box plots shows the differences in (C) ESTIMATE score, (D) immune score, and (E) stromal score among the three pyroptosis clusters.

# Prognostic role of pyroptosis-related genes in gastric cancer

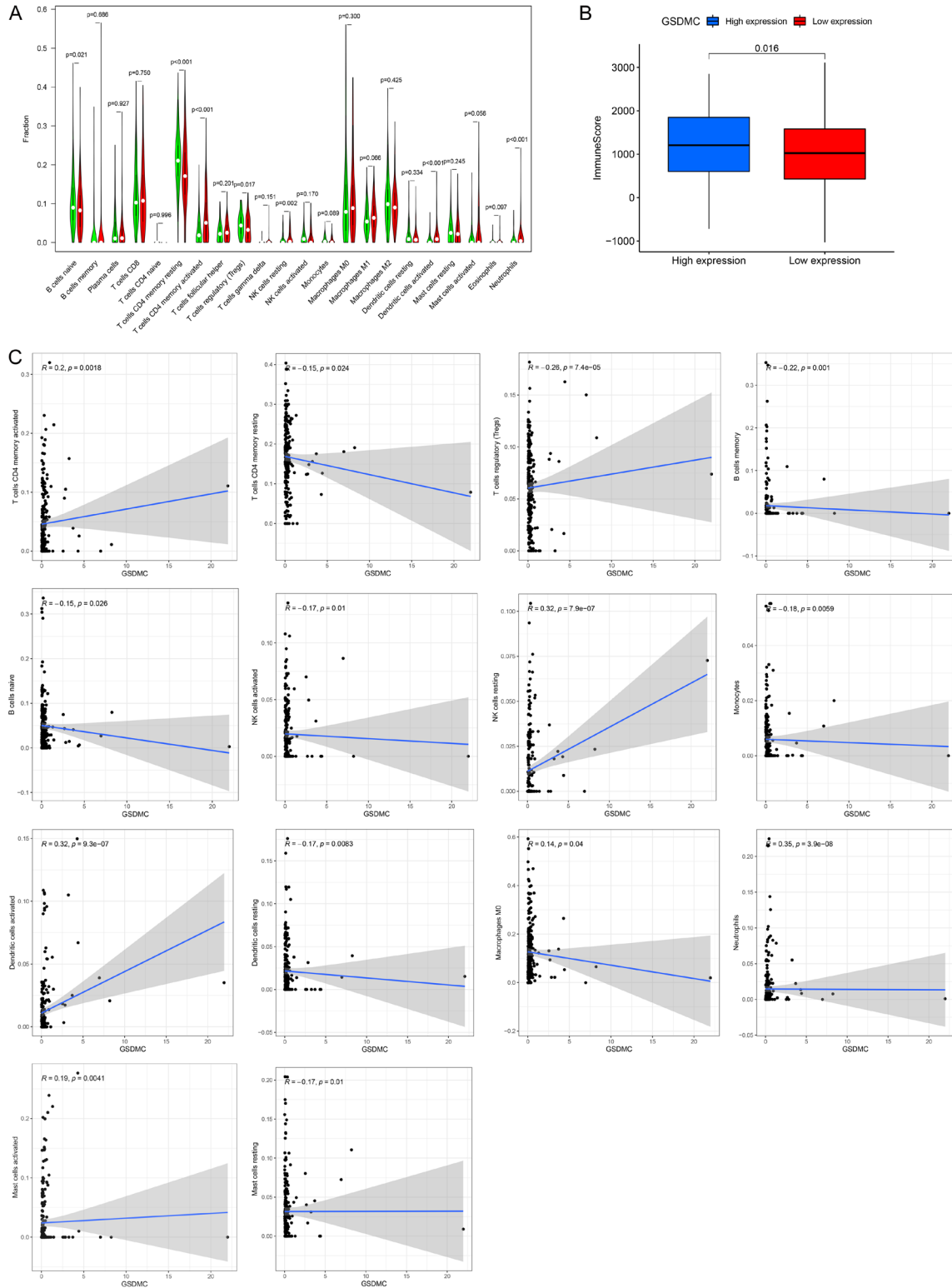




**Figure S12.** Correlation between GSDMC expression and TME infiltration as well as the prognostic role of GSDMC in GC. (A) The correlation between each PRGs and each TME infiltration cell type using spearman analysis. \* $P < 0.05$ ; \*\* $P < 0.01$ ; \*\*\* $P < 0.001$ . (B, C) Survival analyses for patients with low or high GSDMC expression in the TCGA-STAD (B) and GSE62254 (C) cohorts using Kaplan-Meier curves. (D) GSEA analysis indicated that five immune or inflammation-related pathways were enriched in the GSDMC high expression group in the gathered GC cohort. (E) RT-qPCR results showed that the mRNA expression level of GSDMC was higher expressed in GC tissues than adjacent non-tumor tissues. \* $P < 0.05$ ; \*\* $P < 0.01$ ; \*\*\* $P < 0.001$ . (F) GSDMC expression in GC tumor tissues and the paired adjacent non-tumor tissues was evaluated by immunohistochemical staining with tissue microarray. (G) IHC scores of GSDMC staining in GC tissues and adjacent non-tumor tissues. \* $P < 0.05$ ; \*\* $P < 0.01$ ; \*\*\* $P < 0.001$ .



# Prognostic role of pyroptosis-related genes in gastric cancer



**Figure S13.** Correlation between GSDMC expression and immune cells infiltration. A. Difference in the abundance of each TME infiltrating cell between GSDMC high expression (Red) and low expression (Green) groups. B. Box plots shows the differences in immune score between GSDMC high expression and low expression groups. C. Correlation between GSDMC expression and immune cells infiltration.

## Prognostic role of pyroptosis-related genes in gastric cancer

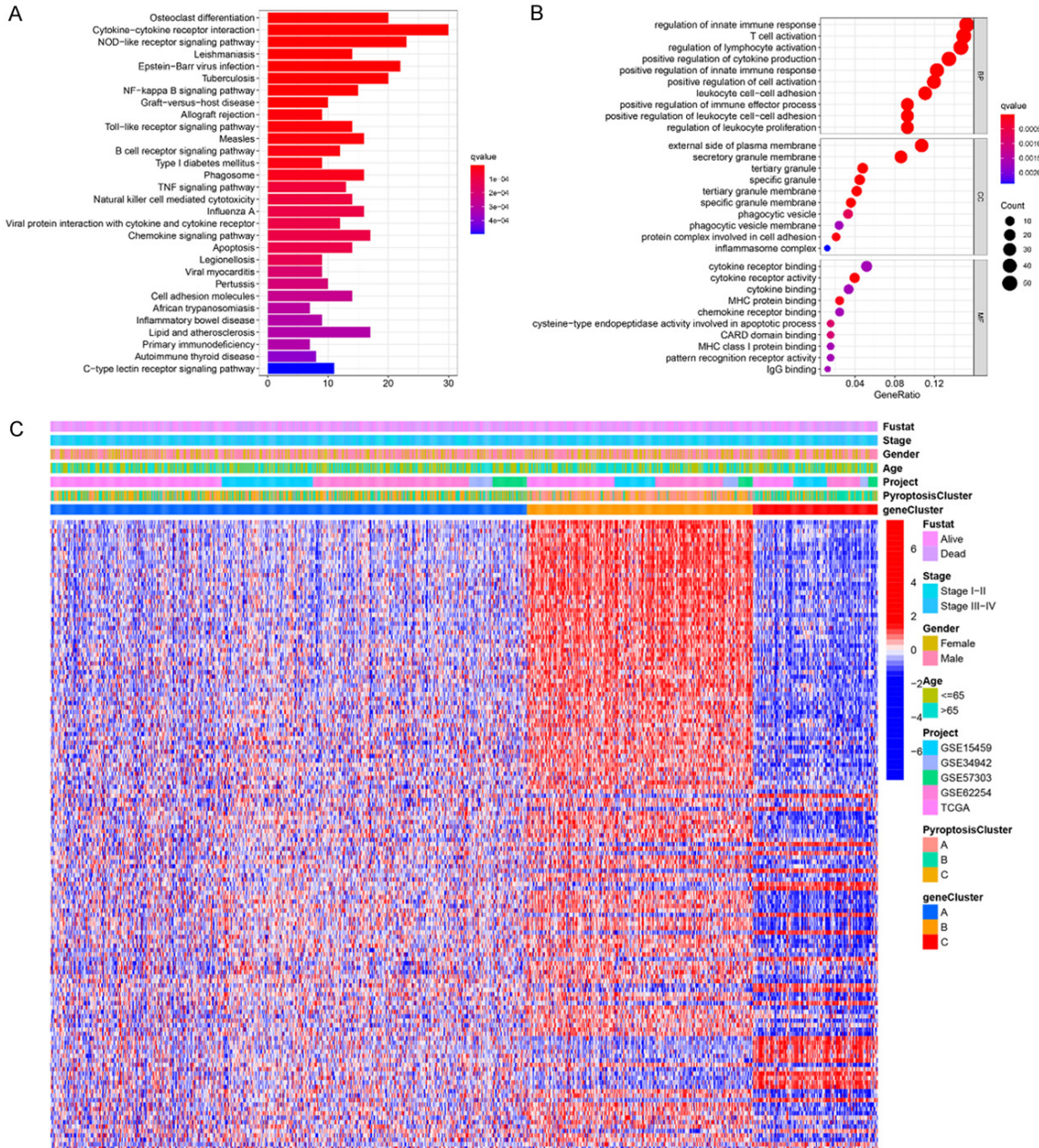
**Table S5.** 346 overlapping DEGs

---

Gene
IRF1 IDO1 CASP1 GBP5 GBP1 CD274 APOL6 IL12RB1 TAP1 TYMP TAP2 IFNG TNFRSF9 PSMB9 RNF213 IL2RB TNFSF13B CARD16 ICOS UBE2L6 IL32 SAMD9L IL2RA ETV7 BATF2 GZMB SLAMF8 SNX20 CXCL11 STAT1 LCP2 CD80 LAMP3 BIRC3 CD300LF IFIH1 CCL4 HAVCR2 IFIT3 ICAM1 SIGLEC10 CXCL10 SNX10 PRF1 PSMB8 TRAFD1 PLEK KLRD1 ZBP1 NCF1 CYBB CD300A ADAMDEC1 RNF19B LAG3 PLA2G7 CD53 IFI35 FLVCR2 CD86 ACP5 LYN IGSF6 NMI IL15RA SAMSN1 KMO OAS2 BCL2A1 CD38 SLAMF1 CLEC7A TFEC SLAMF7 LCP1 LILRB4 HK3 DAPP1 IL18RAP KLHL6 GPR65 TLR8 LILRB1 OAS3 IL4I1 NFAM1 STX11 RAC2 ST8SIA4 CLEC4E CCR1 ITGB2 PARP12 ITGAX MICB CLEC4A TAGAP GNLY FGR CTLA4 DOK3 SLC2A5 PDCD1LG2 LAPT5 KIR2DL4 STAT4 LAIR1 HCK SIGLEC7 PIK3R5 JAK3 CYTH4 RHOH PTAFR CASP5 HPS5 NCF2 PIK3AP1 LST1 MNDA TRAF1 APOL1 USP18 FCER1G GCH1 PILRA NLRC4 PMAIP1 KLHDC7B ALOX5AP LACTB CASP4 SOCS1 TNFAIP3 CSF3R FPR3 OASL CASP10 FCGR1B TNFRSF1B LILRB2 SERPINB9 SLC31A2 ZNF267 MOV10 MMP25 LAIR2 APOBR OSCAR CCR8 CD40 CMPK2 HLA-C PLSCR1 DENND2D MTURN CD69 CD83 SH2D2A SRGN CD7 SELL THEMIS2 LINC01094 CSF2RB LILRB3 RIPK2 LILRA6 ISG20 NFE2L3 CCL18 TNF PRDM1 PREX1 RSAD2 ITGA4 SECTM1 MYD88 HPSE NPL KIF2A LMNB1 GSTO1 TNFRSF4 MLKL SIGLEC9 SPI1 GCA RELT NOS2 FBXO6 TYROBP CYTIP GSDMB CKB RASGRP3 FCGR2A SH2B3 HMOX1 SERTAD4 ITGAM PIM2 CCRL2 TMSB10 CCL22 ADPGK BAK1 RNF149 CDCP1 NFKBIE CNDP2 MCM5 IL12RB2 DNMT1 OAS1 FCGR2C MEI1 UBE2D1 TNIP3 ADAM10 BATF SIGLEC5 ADA KYNU CASS4 NOD2 PBX1 HELZ2 ISG15 WFS1 CD300C EXOSC9 C15orf48 NECAP2 DRAM1 PSMA4 REEP1 IGHG1 TNFRSF18 ACOT7 MYO7A TCEAL4 KCNH2 UHRF1 NCEH1 CASP7 TMPO IKBKE COL4A5 IL17RA HELLS SIRPB1 EZH2 BRIP1 PPP1R14A NUP50 CENPK PTBP3 CEACAM4 ALAS1 DYNC1I1 RHEBL1 DDX60L CD14 SDS ACP2 CAPG OLR1 RAB39A IRF7 CAPZA1 TRIM15 SIRPB2 CENPH NAV2 WLS TPM3 GTF2B HLA-G KNTC1 TRPV2 PRKAB2 EAF2 RGS19 IL7R MCM6 DENND1A CHST11 PRELID1 APBB1IP BATF3 CXCL16 SLC25A22 E2F7 VLDLR TTLL7 DEPDC1B BMPR1B PTGES3L LINC01278 ENAH HNRNPF MREG SLC41A3 PDZRN3 CYP39A1 SLC16A6 PDZK1IP1 GNAZ VNN2 C3orf70 CTSZ MALT1 CDCA2 CDV3 POLD1 MYEF2 GINS3 RAB42 COQ2 PCP4 GPD2 ALOX5 PARP8 M6PR VAMP8 NUP62 SLC15A4 MZB1 ATOX1 RP2 ZNF827 MFSD5 AK2 IL1B CELF2 TK2 RBM43 PROK2 PIK3IP1 NLRP2 ACSM5 BCL2 MBNL1 LNPEP RASD1

---

# Prognostic role of pyroptosis-related genes in gastric cancer



**Figure S14.** Identification of pyroptosis gene clusters. A. KEGG pathway enrichment analysis presents the enriched pathways of 346 overlapping DEGs. B. GO enrichment analysis of biological process (BP), cellular component (CC) and molecular function (MF) terms of 346 overlapping DEGs ranked by adjusted  $p$ -value. C. Heatmap presents the correlation between the three gene clusters and clinicopathological characteristics of GC patients.

Prognostic role of pyroptosis-related genes in gastric cancer

**Table S6.** 143 OS-related DEGs

Gene	HR	HR.95L	HR.95H	P value
IRF1	0.807396	0.715696	0.910845	0.000505
IDO1	0.913376	0.863272	0.966388	0.001646
CASP1	0.813646	0.738252	0.896739	3.23E-05
GBP5	0.925065	0.857991	0.997382	0.042537
CD274	0.859674	0.76913	0.960876	0.007749
APOL6	0.73715	0.642404	0.845871	1.39E-05
IL12RB1	0.804104	0.692594	0.933568	0.004204
TAP1	0.796753	0.717163	0.885175	2.32E-05
TAP2	0.748394	0.64462	0.868875	0.000142
IFNG	0.876235	0.793202	0.967961	0.009294
PSMB9	0.825908	0.744501	0.916216	0.000303
RNF213	0.847019	0.735574	0.97535	0.02107
CARD16	0.817257	0.709925	0.940817	0.004966
UBE2L6	0.850847	0.75684	0.956531	0.006852
ETV7	0.78489	0.704059	0.875	1.25E-05
BATF2	0.819535	0.746162	0.900123	3.20E-05
GZMB	0.870201	0.80528	0.940356	0.000441
LAMP3	0.898799	0.820095	0.985056	0.02249
BIRC3	0.906458	0.827936	0.992427	0.033636
IFIH1	0.787342	0.680068	0.911538	0.001377
PRF1	0.884607	0.79423	0.985267	0.025754
PSMB8	0.761764	0.670688	0.865209	2.81E-05
TRAFD1	0.718729	0.582103	0.887422	0.002139
KLRD1	0.8558	0.738816	0.991306	0.037857
ZBP1	0.864853	0.77625	0.963569	0.008465
RNF19B	0.830844	0.71336	0.967676	0.017201
LAG3	0.86336	0.783926	0.950843	0.002849
IFI35	0.844633	0.735133	0.970443	0.017151
LYN	0.838348	0.720759	0.975122	0.022215
NMI	0.765955	0.651375	0.90069	0.001259
IL15RA	0.842184	0.718375	0.987331	0.03425
OAS2	0.904819	0.820738	0.997514	0.044433
DAPP1	0.869986	0.766543	0.987389	0.031047
OAS3	0.865288	0.773493	0.967976	0.011445
NFAM1	0.829233	0.711609	0.9663	0.016432
PARP12	0.807629	0.694691	0.938928	0.005438
MICB	0.848303	0.761751	0.944689	0.002733
GNLY	0.898997	0.825789	0.978696	0.014016
CTLA4	0.837573	0.735601	0.953681	0.007451
KIR2DL4	0.700891	0.593537	0.827663	2.79E-05
CASP5	0.826208	0.743883	0.917644	0.000364
USP18	0.853709	0.76377	0.954239	0.005359
GCH1	0.730314	0.629373	0.847445	3.46E-05
OASL	0.911778	0.83342	0.997503	0.043957
CASP10	0.672346	0.580646	0.778529	1.12E-07
MOV10	0.784419	0.651599	0.944313	0.010308
MMP25	0.719693	0.614968	0.842253	4.14E-05

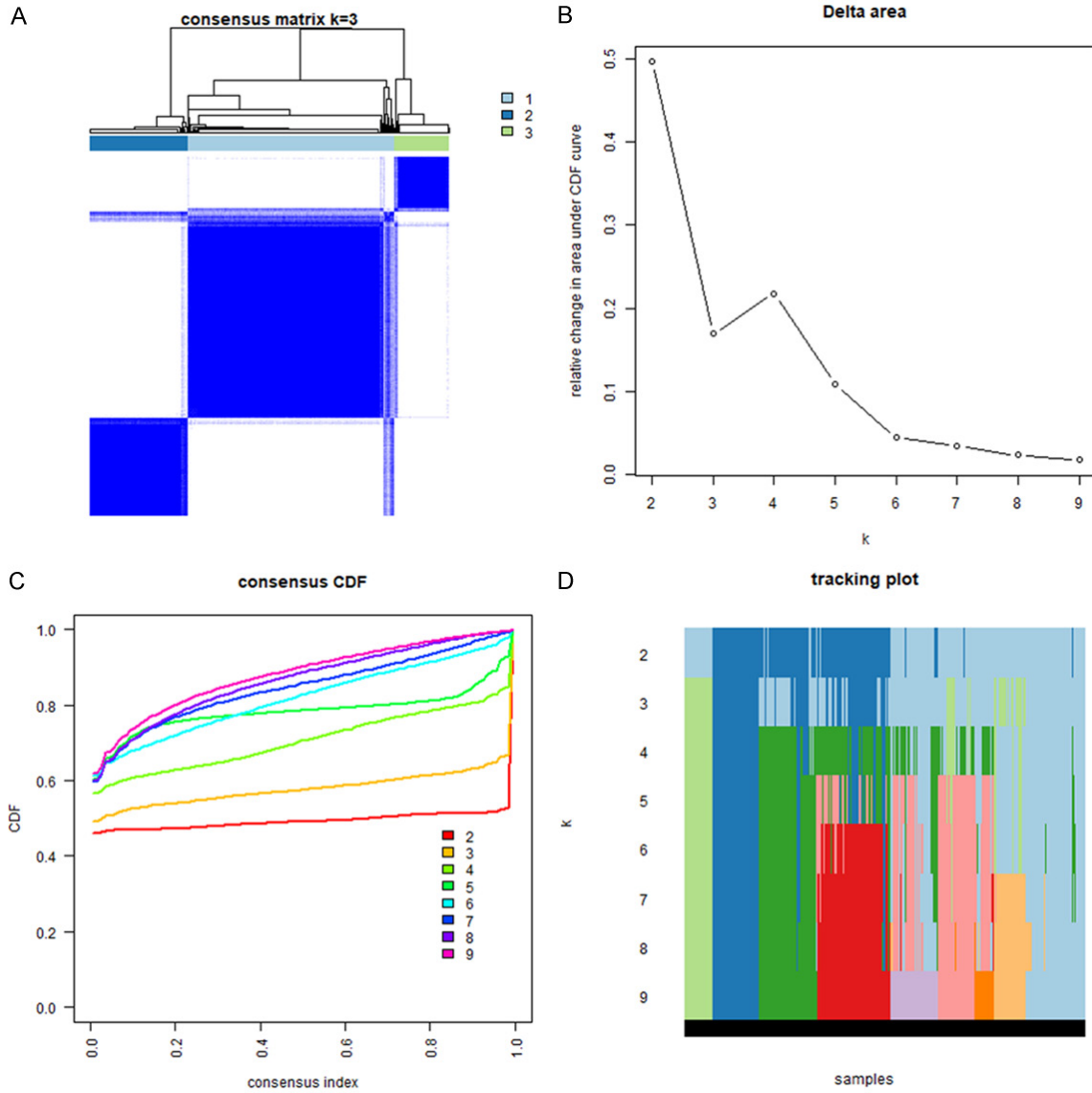
## Prognostic role of pyroptosis-related genes in gastric cancer

LAIR2	0.793559	0.706695	0.891099	9.26E-05
CMPK2	0.891545	0.808428	0.983207	0.021497
DENND2D	0.747292	0.641983	0.869875	0.000171
LINC01094	1.186739	1.038648	1.355946	0.011817
ISG20	0.887751	0.799108	0.986227	0.02653
NFE2L3	0.840868	0.755551	0.935819	0.001498
SECTM1	0.867966	0.783065	0.962072	0.007014
MYD88	0.804417	0.656286	0.985984	0.036091
LMNB1	0.827362	0.744515	0.919428	0.000431
MLKL	0.835612	0.701855	0.994858	0.043603
GCA	0.735403	0.607031	0.890921	0.00169
NOS2	0.885801	0.827356	0.948374	0.000498
FBXO6	0.830328	0.73806	0.93413	0.001977
TYROBP	1.150582	1.04052	1.272285	0.006252
GSDMB	0.86055	0.784177	0.944361	0.001539
CKB	1.094855	1.020508	1.174618	0.011544
FCGR2A	1.171335	1.051725	1.304548	0.004007
HMOX1	1.132562	1.013423	1.265708	0.028158
SERTAD4	1.177681	1.071471	1.294417	0.000695
BAK1	0.778463	0.665738	0.910275	0.001702
CDCP1	0.882331	0.794858	0.979429	0.018765
CNDP2	0.672423	0.567409	0.796873	4.63E-06
DNMT1	0.774564	0.652206	0.919876	0.003591
OAS1	0.889679	0.804738	0.983586	0.022417
ADAM10	0.836061	0.699363	0.999478	0.049333
NOD2	1.163598	1.021308	1.325712	0.022799
PBX1	1.16536	1.048668	1.295037	0.004473
HELZ2	0.811761	0.705668	0.933803	0.003518
WFS1	1.14481	1.016241	1.289645	0.02608
EXOSC9	0.69493	0.564794	0.855053	0.000581
C15orf48	0.926584	0.873933	0.982408	0.010631
PSMA4	0.781498	0.621595	0.982535	0.034789
REEP1	1.186947	1.103541	1.276657	4.02E-06
TNFRSF18	0.830752	0.723653	0.953701	0.00846
ACOT7	0.797017	0.690832	0.919523	0.00187
TCEAL4	1.495561	1.308147	1.709825	3.81E-09
KCNH2	1.179119	1.093046	1.271971	2.04E-05
UHRF1	0.833989	0.755463	0.920677	0.000321
NCEH1	0.869246	0.782718	0.965339	0.00881
CASP7	0.6674	0.572033	0.778668	2.75E-07
TMPO	0.761282	0.652237	0.888558	0.000544
IKBKE	0.706057	0.598759	0.832583	3.50E-05
COL4A5	1.180412	1.085782	1.283289	0.0001
HELLS	0.798777	0.702036	0.908849	0.000647
EZH2	0.774796	0.688768	0.871569	2.15E-05
BRIP1	0.796093	0.692997	0.914527	0.00127
PPP1R14A	1.202651	1.131172	1.278646	3.58E-09
NUP50	0.669595	0.544852	0.822898	0.000137
CENPK	0.865314	0.767958	0.975011	0.017524

## Prognostic role of pyroptosis-related genes in gastric cancer

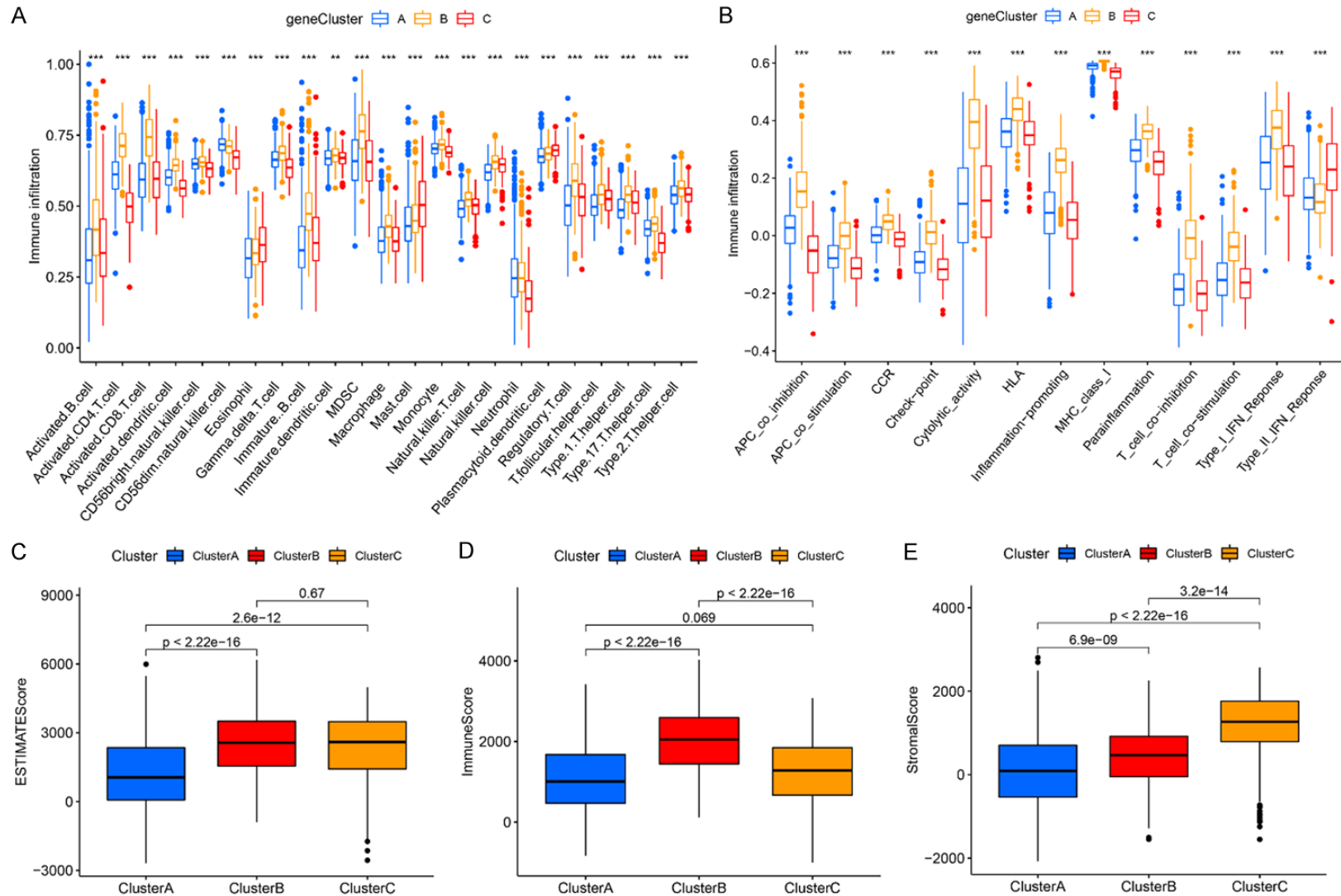
PTBP3	0.835305	0.703892	0.991253	0.039345
CEACAM4	0.8132	0.673753	0.981508	0.031206
ALAS1	0.734179	0.61261	0.879874	0.000821
DYNC111	1.385781	1.241473	1.546863	6.06E-09
CD14	1.185833	1.069669	1.314612	0.001194
SDS	1.130917	1.012385	1.263327	0.029417
OLR1	1.186747	1.097358	1.283418	1.83E-05
CAPZA1	0.698459	0.546468	0.892725	0.004153
TRIM15	0.866508	0.796407	0.94278	0.000872
NAV2	1.198031	1.04816	1.369331	0.008054
WLS	1.308671	1.172479	1.460683	1.60E-06
TPM3	0.721183	0.584335	0.890081	0.00233
KNTC1	0.80263	0.693607	0.92879	0.00316
PRKAB2	1.248247	1.086094	1.434609	0.001789
MCM6	0.80674	0.680872	0.955875	0.013087
DENND1A	0.725169	0.603349	0.871585	0.000615
CHST11	1.227235	1.085619	1.387323	0.001064
PRELID1	0.816181	0.668596	0.996345	0.045939
BATF3	1.226234	1.023152	1.469627	0.027264
SLC25A22	0.758829	0.649719	0.886263	0.000493
E2F7	0.82213	0.726085	0.930879	0.002002
VLDLR	1.242559	1.134498	1.360912	2.89E-06
TTLL7	1.174714	1.08259	1.274677	0.000111
BMPR1B	1.249103	1.140952	1.367507	1.48E-06
PTGES3L	1.23219	1.107465	1.370962	0.000126
LINC01278	1.210759	1.065914	1.375286	0.003262
ENAH	1.291734	1.13575	1.469141	9.67E-05
MREG	0.742326	0.645139	0.854154	3.16E-05
SLC41A3	1.288212	1.030903	1.609744	0.025902
PDZRN3	1.205114	1.112511	1.305425	4.79E-06
CYP39A1	1.154878	1.03603	1.28736	0.009355
GNAZ	1.157637	1.044683	1.282804	0.005198
C3orf70	1.141964	1.059314	1.231062	0.000534
CDCA2	0.815699	0.73714	0.902631	8.06E-05
POLD1	0.81475	0.705986	0.94027	0.005072
MYEF2	1.220187	1.101455	1.351717	0.000139
GINS3	0.721311	0.60262	0.863379	0.000369
COQ2	0.708387	0.577748	0.868566	0.000917
GPD2	0.762171	0.651281	0.891941	0.000711
SLC15A4	1.338972	1.048805	1.709417	0.019163
MZB1	0.935363	0.878006	0.996467	0.038491
RP2	0.751701	0.61416	0.920043	0.005636
ZNF827	1.272892	1.091552	1.484359	0.00209
MFSD5	0.760984	0.596689	0.970516	0.027727
AK2	0.750842	0.59152	0.953077	0.018527
ACSM5	1.321234	1.055818	1.653372	0.014905
RASD1	1.084967	1.010045	1.165447	0.025501

# Prognostic role of pyroptosis-related genes in gastric cancer



**Figure S15.** Unsupervised clustering analysis for identifying pyroptosis gene Clusters. A. Consensus clustering matrix for k=3. B. Relative change in area under CDF curve for k=2-9. C. Consensus clustering cumulative distribution function (CDF) for k=2-9. D. The tracking plot for k=2-9.

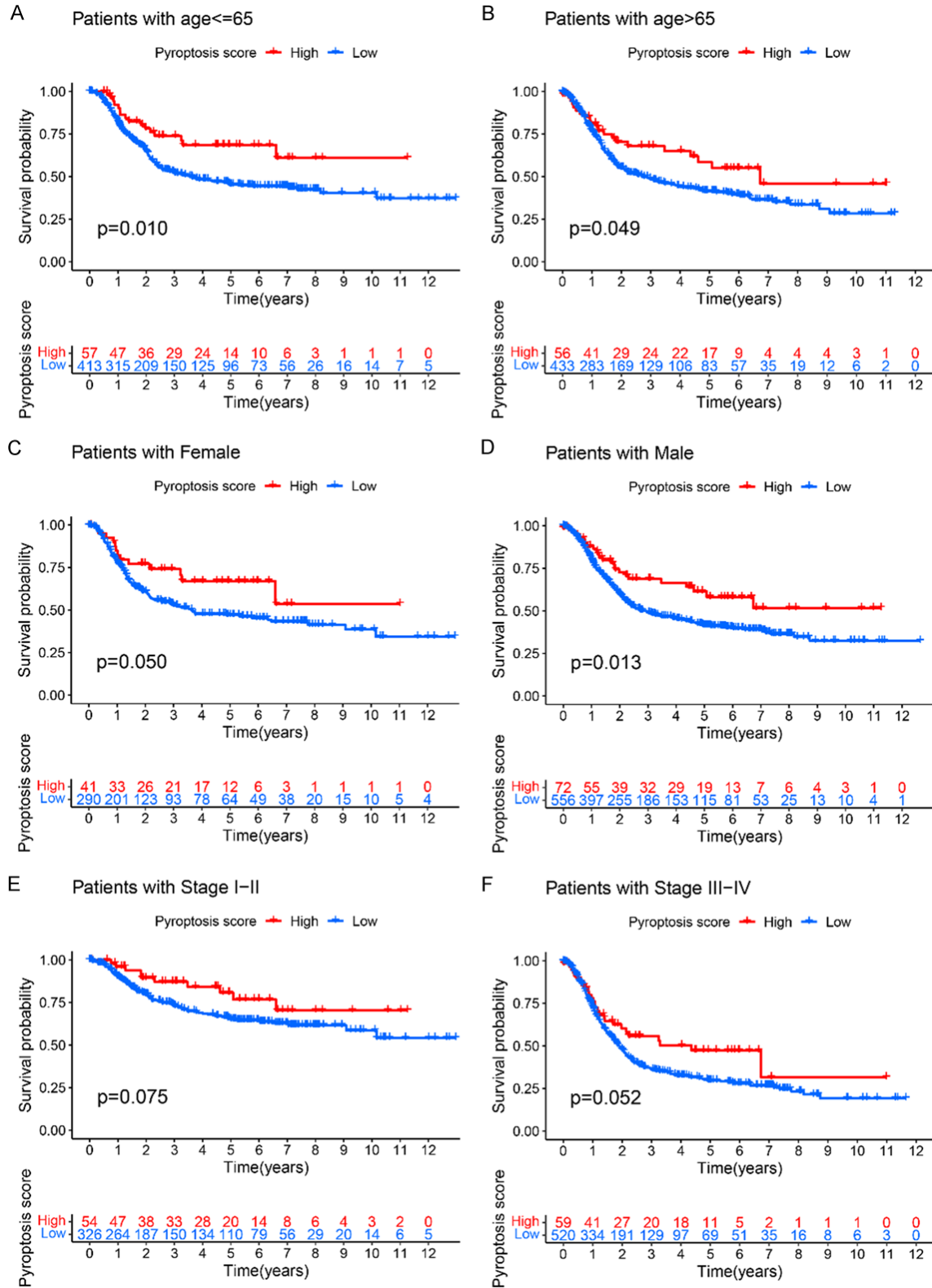
## Prognostic role of pyroptosis-related genes in gastric cancer



**Figure S16.** Correlation between the characteristics of TIME and pyroptosis gene clusters. (A) Box plots depicts the scores of immune infiltrations among the three pyroptosis gene clusters. (B) Box plots presents the scores of immune functions among the three pyroptosis gene clusters. \* $P < 0.05$ ; \*\* $P < 0.01$ ; \*\*\* $P < 0.001$ . (C-E) Box plots shows the differences in (C) ESTIMATE score, (D) immune score, and (E) stromal score among the three pyroptosis gene clusters.

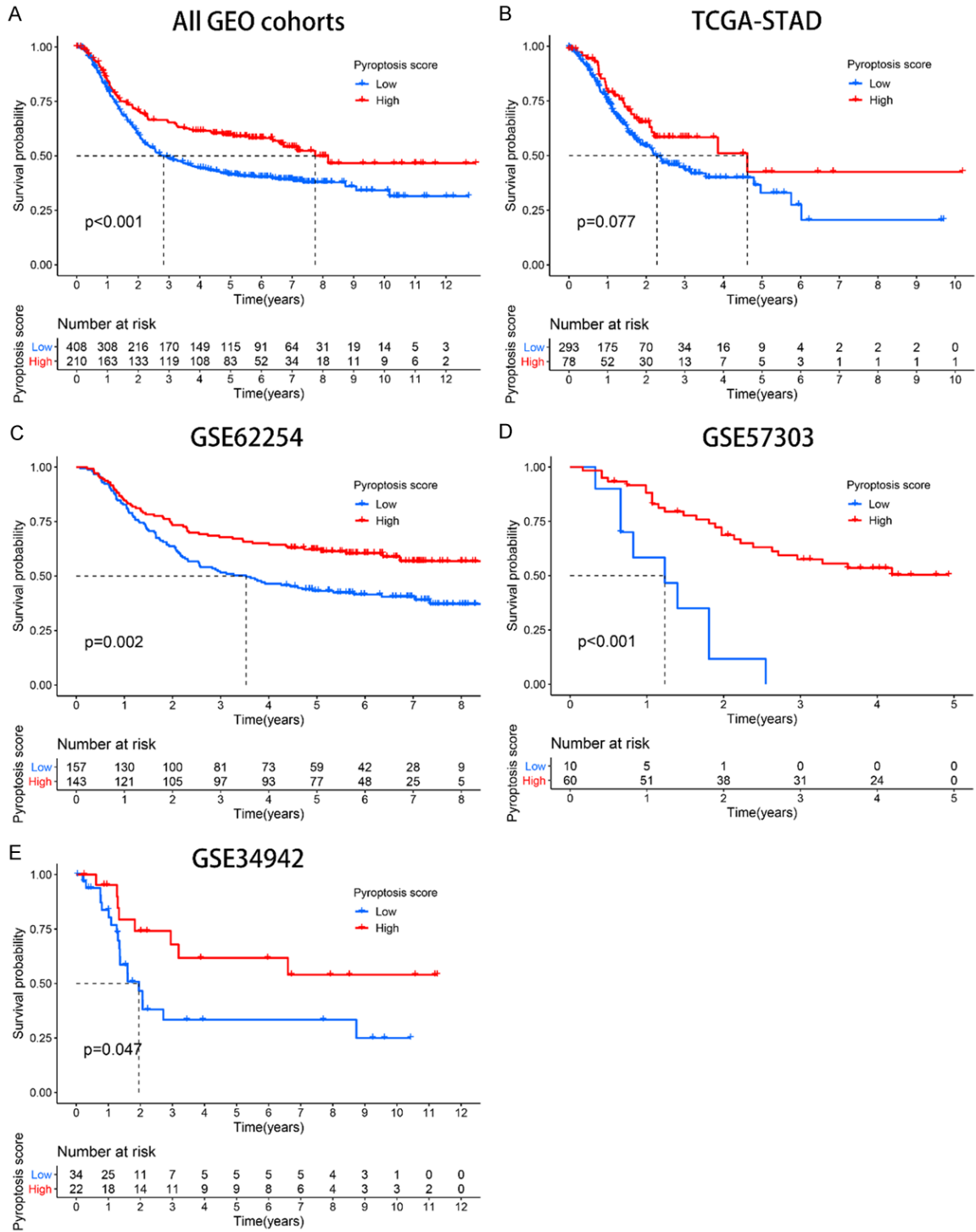


## Prognostic role of pyroptosis-related genes in gastric cancer



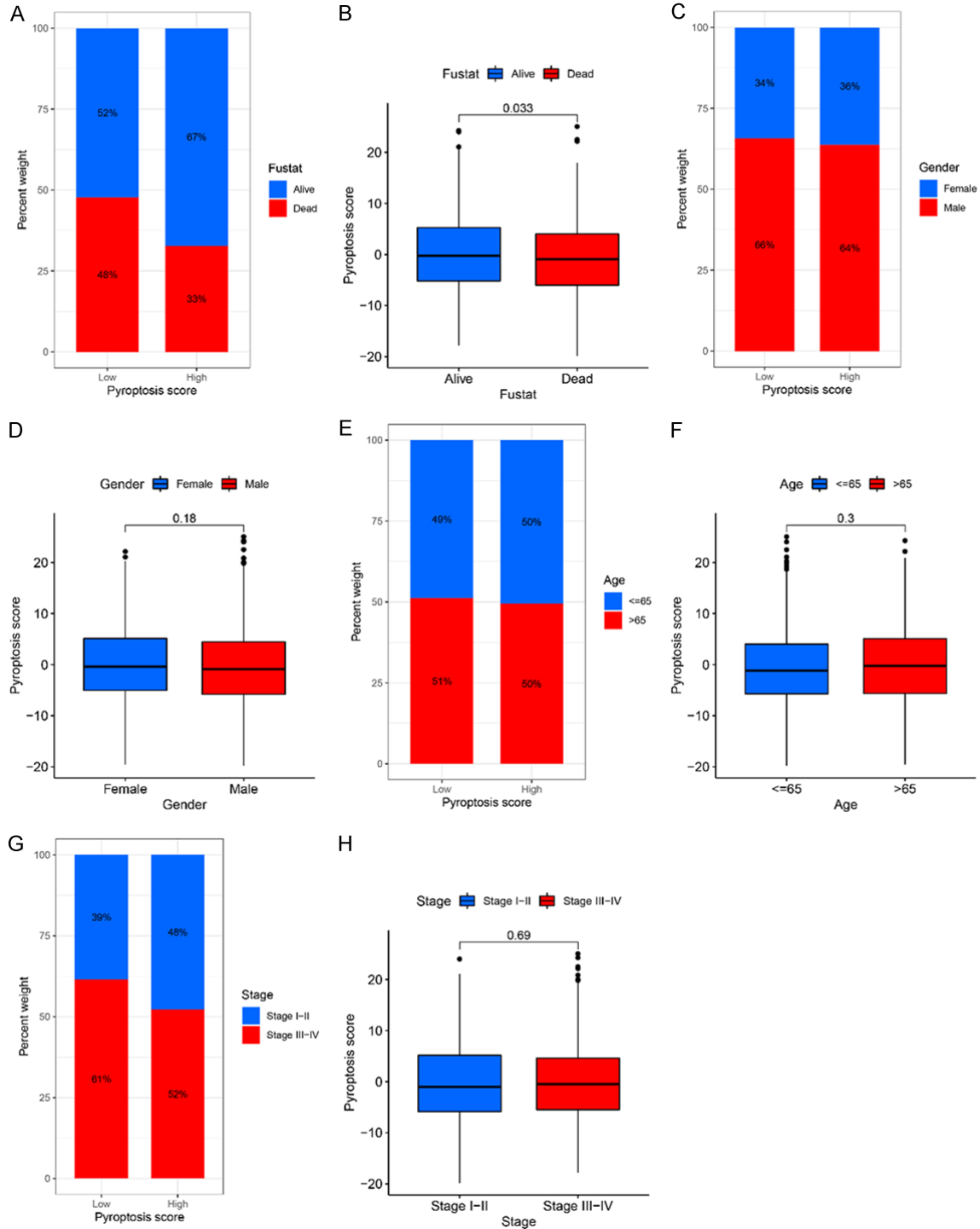
**Figure S17.** Subgroup analysis of the prognostic role of pyroptosis score in GC patients. A, B. Subgroup analysis of the prognostic role of pyroptosis score in GC patients stratified by age. C, D. Subgroup analysis of the prognostic role of pyroptosis score in GC patients stratified by gender. E, F. Subgroup analysis of the prognostic role of pyroptosis score in GC patients stratified by stage.

Prognostic role of pyroptosis-related genes in gastric cancer



**Figure S18.** Survival analysis of the prognostic role of pyroptosis score in different GC cohort. (A-E) Survival analysis of the prognostic role of pyroptosis score in meta-GEO cohort (A, n=618, including GSE15459, GSE34942, GSE57303, and GSE62254 cohorts), TCGA-STAD cohort (B, n=371), GSE62254 cohort (C, n=300), GSE57303 cohort (D, n=70), and GSE34942 cohort (E, n=56).

## Prognostic role of pyroptosis-related genes in gastric cancer



**Figure S19.** Correlation between the pyroptosis score and clinicopathologic features. A, B. Differences in pyroptosis score between patients with different survival state. C, D. Differences in pyroptosis score between patients with different gender. E, F. Differences in pyroptosis score between patients with different age distribution. G, H. Differences in pyroptosis score between patients with different stage.

Prognostic role of pyroptosis-related genes in gastric cancer

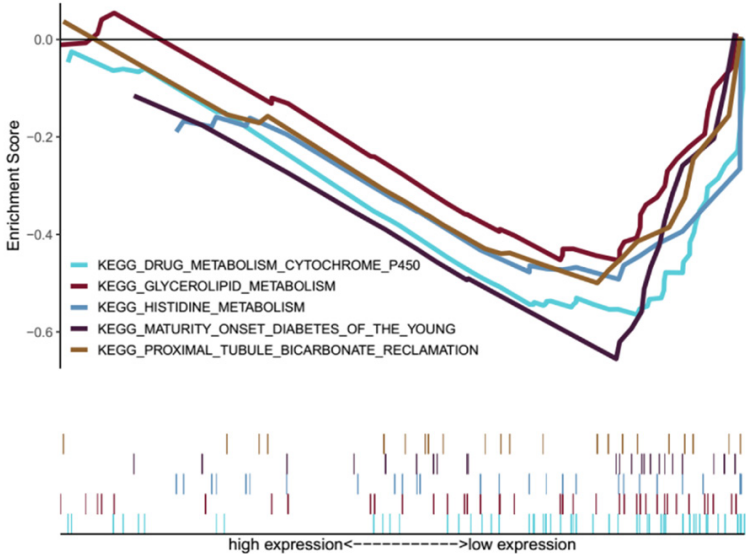
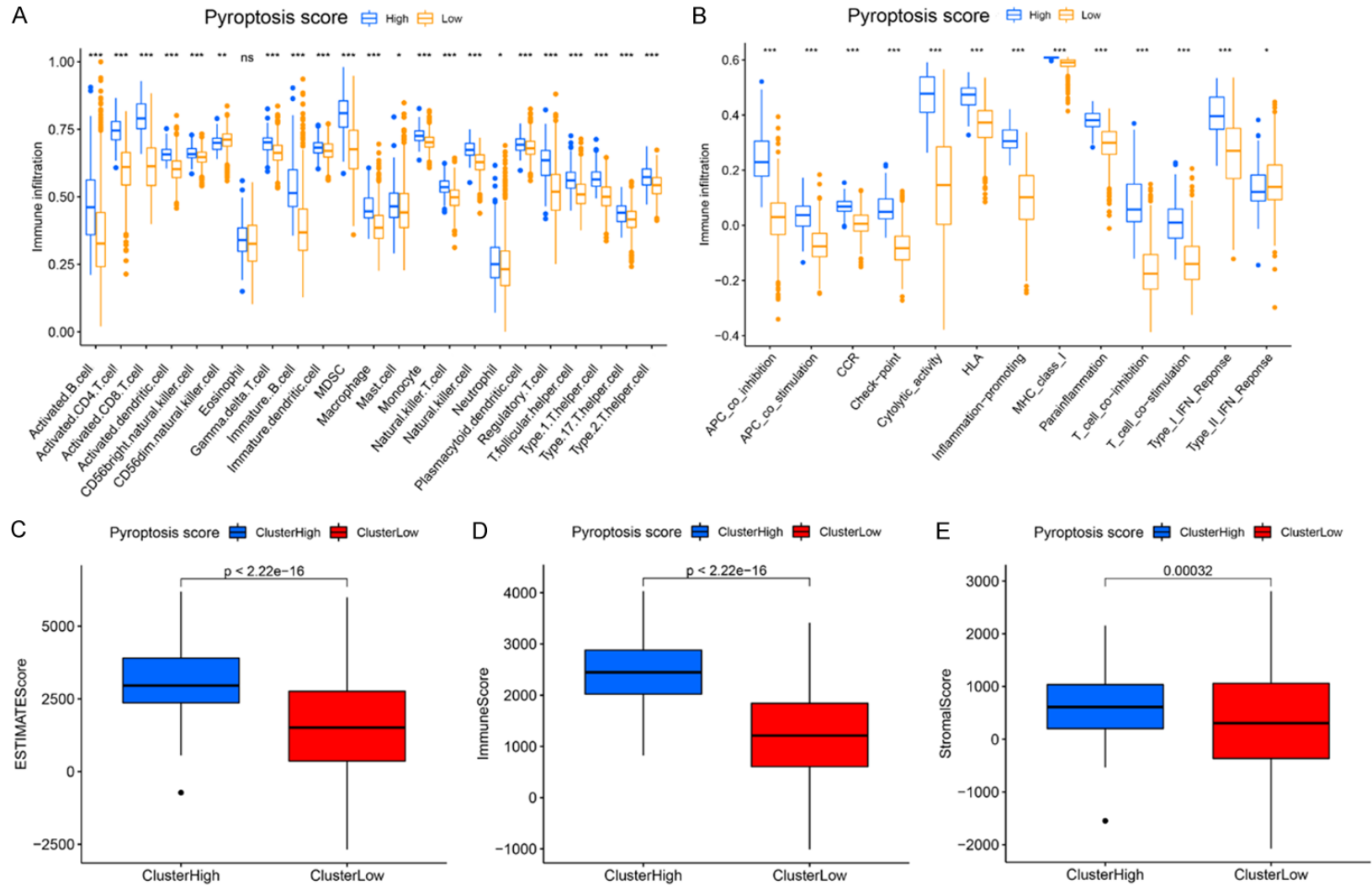


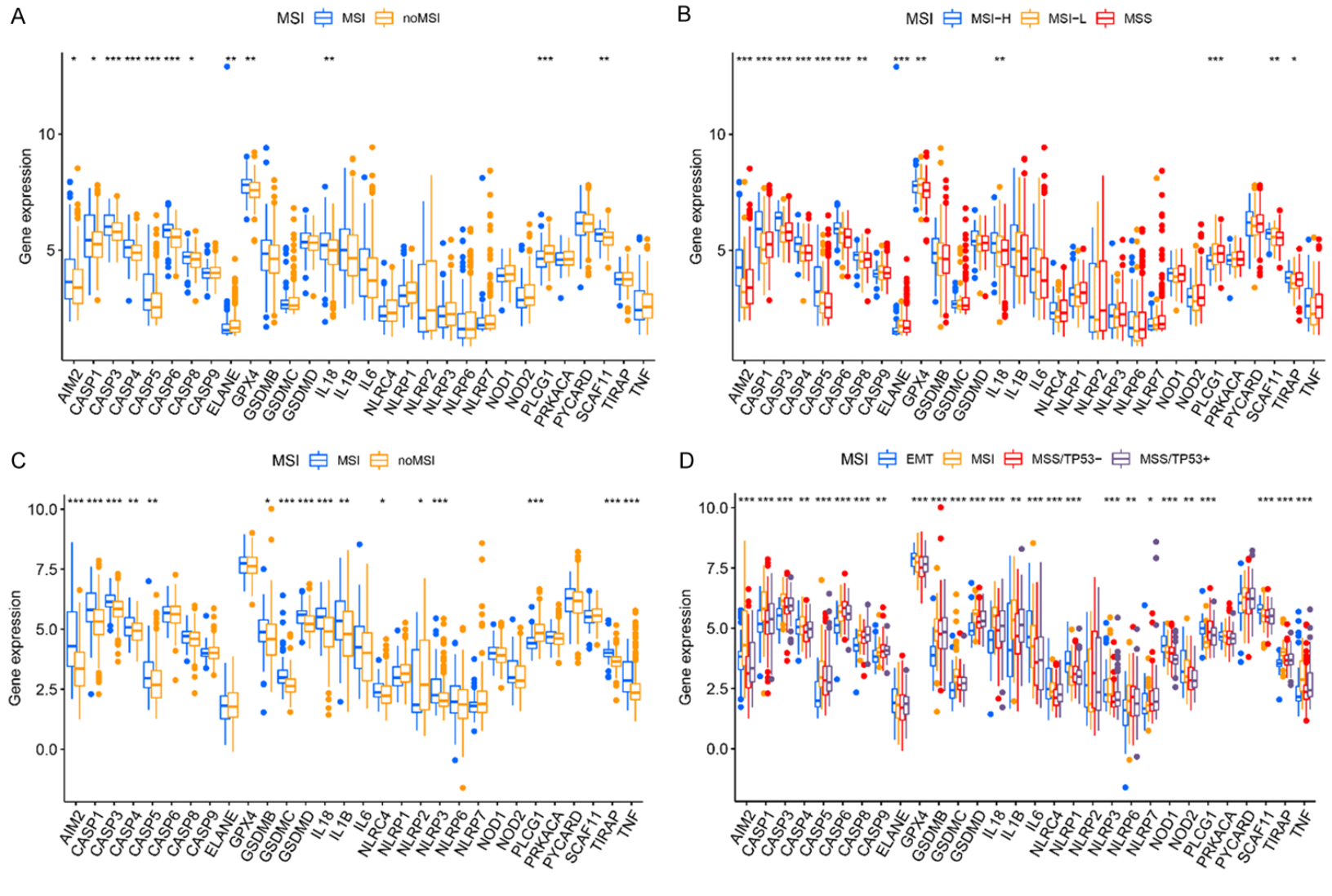
Figure S20. GSEA identified the pathways enriched in the low pyroptosis score group.

## Prognostic role of pyroptosis-related genes in gastric cancer

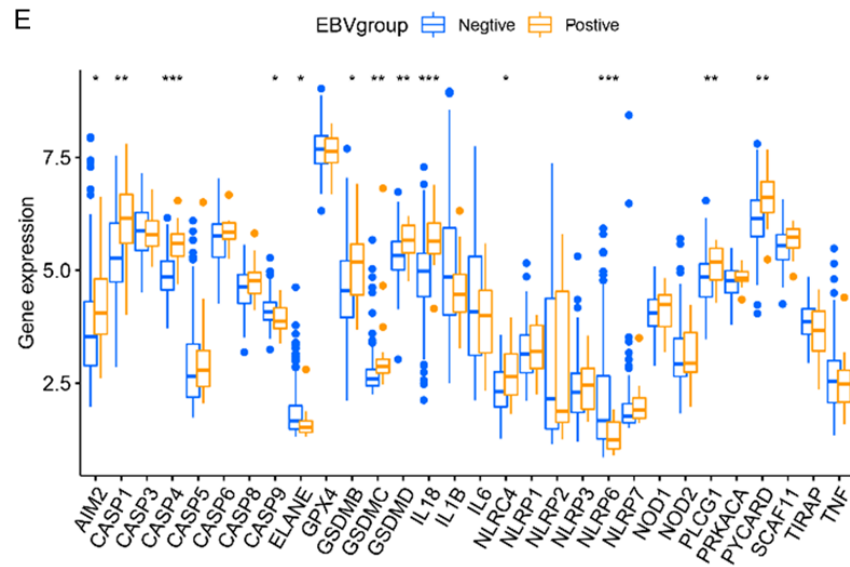


**Figure 21.** Correlation between the characteristics of TIME and pyroptosis score. (A) Box plots depicts the scores of immune infiltrations between the high and low pyroptosis score groups. (B) Box plots presents the scores of immune functions between the high and low pyroptosis score groups. \* $P < 0.05$ ; \*\* $P < 0.01$ ; \*\*\* $P < 0.001$ . (C-E) Box plots shows the differences in (C) ESTIMATE score, (D) immune score, and (E) stromal score between the high and low pyroptosis score groups.

# Prognostic role of pyroptosis-related genes in gastric cancer



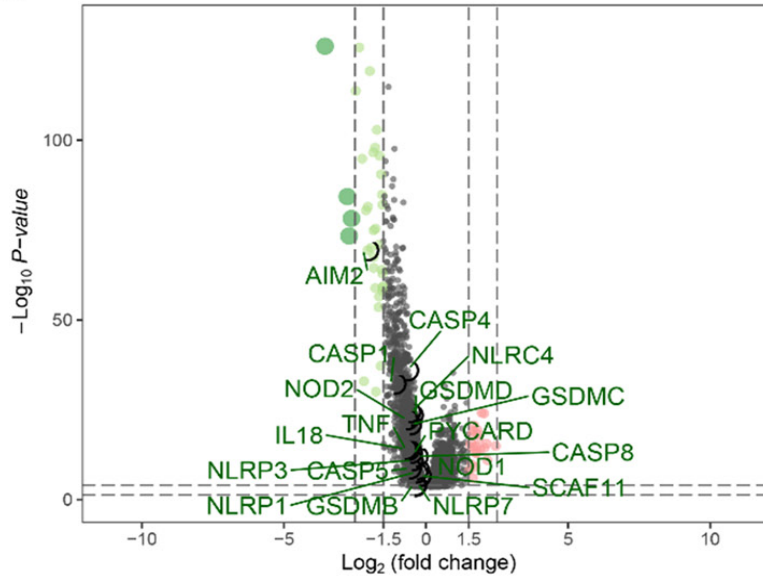
## Prognostic role of pyroptosis-related genes in gastric cancer



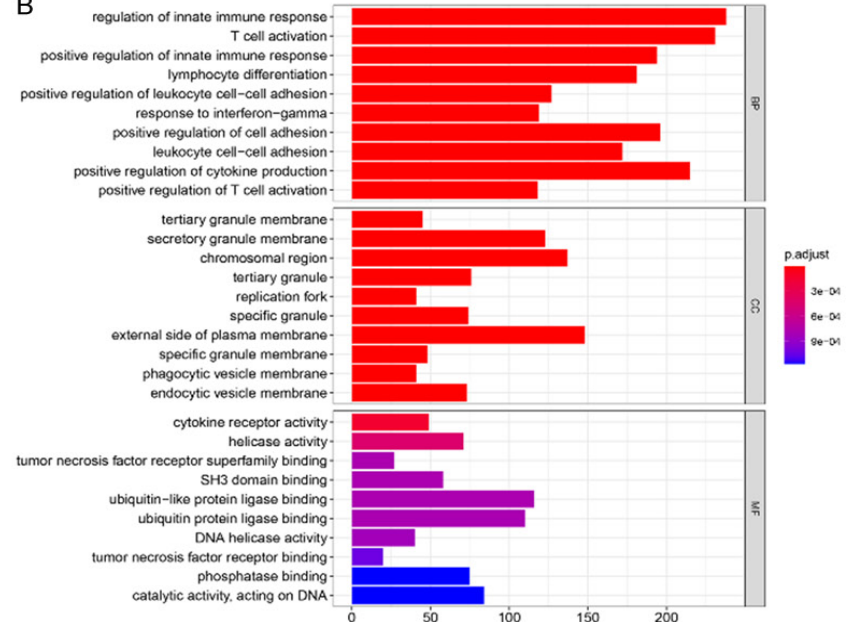
**Figure S22.** The expression levels of PRGs in different subgroups of GC. A. The expression levels of PRGs between the MSI and no MSI groups in TCGA-STAD cohort. B. The expression levels of PRGs among the MSI-High, MSI-Low, and MSS groups in TCGA-STAD cohort. C. The expression levels of PRGs between the MSI and no MSI groups in GSE62254 cohort. D. The expression levels of PRGs among the EMT, MSI, MSI/TP53- and MSI/TP53+ groups in GSE62254 cohort. E. The expression levels of PRGs between the EBV negative and EBV positive groups in TCGA-STAD cohort. \* $P < 0.05$ ; \*\* $P < 0.01$ ; \*\*\* $P < 0.001$ .

# Prognostic role of pyroptosis-related genes in gastric cancer

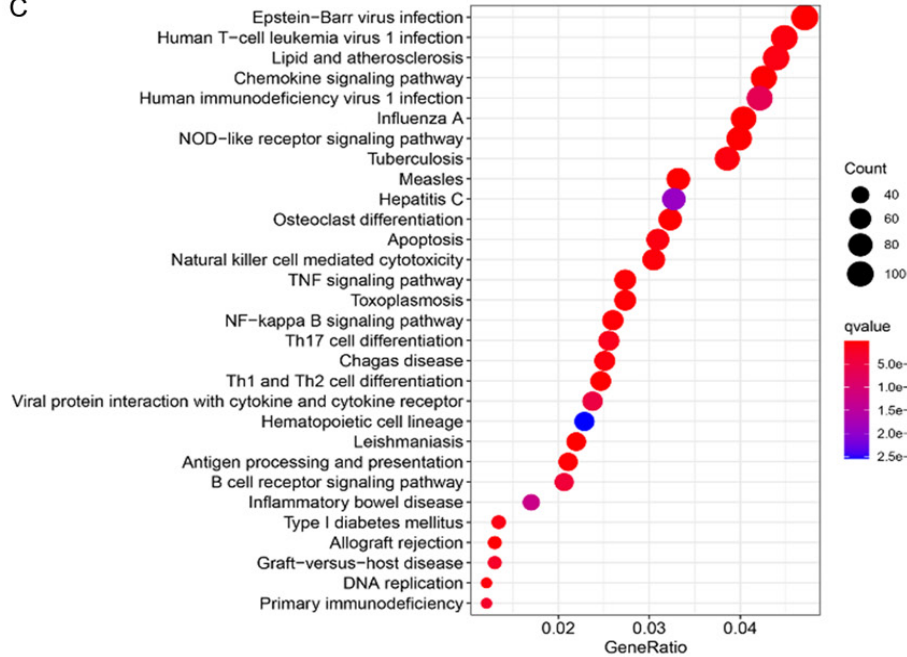
A



B




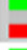









C





Prognostic role of pyroptosis-related genes in gastric cancer

D

rank	cmap name	mean	n	enrichment	p	specificity	% non-null	
1	caffeic acid	0.451	3	0.873	0.00373	0.0000	66	
2	puromycin	-0.636	4	-0.719	0.01255	0.0970	75	
3	alimemazine	-0.618	4	-0.714	0.01355	0.0068	75	
4	memantine	0.418	4	0.683	0.02166	0.0000	50	
5	piperlongumine	0.379	2	0.887	0.02648	0.1364	50	
6	dorzolamide	0.361	4	0.655	0.03284	0.0000	50	
7	bumetanide	-0.384	4	-0.646	0.03744	0.1487	50	
8	0198306-0000	0.422	4	0.643	0.03923	0.0073	50	
9	bacitracin	-0.495	3	-0.728	0.04160	0.0424	66	
10	diprophylline	-0.281	5	-0.569	0.04500	0.0397	60	
11	levothyroxine sodium	-0.213	4	-0.630	0.04603	0.0848	50	

**Figure S23.** Potential small molecule compounds for GC treatment based on the pyroptosis score. A. Volcano plot shows the downregulated genes (green dots) and upregulated genes (red dots) between the low and high pyroptosis score groups. B. GO enrichment analysis of biological process (BP), cellular component (CC) and molecular function (MF) terms ranked by adjusted *p*-value. C. KEGG pathway enrichment analysis presents the enriched pathways. D. Potential small molecule compounds obtains from the CMap database.

Prognostic role of pyroptosis-related genes in gastric cancer

**Table S7.** DEGs between the low and high pyroptosis score groups

Gene	logFC	Average Expression	t	P-Value	Adjusted P-Value	B
IDO1	-3.55431	4.838732	-27.8995	6.69E-127	1.18E-122	278.8428
GBP4	-2.349	4.667764	-27.8471	1.52E-126	1.34E-122	278.0286
IFNG	-1.97693	2.58534	-26.8786	5.58E-120	3.28E-116	262.9997
FASLG	-1.31937	2.644864	-26.2263	1.41E-115	6.21E-112	252.9223
GBP5	-2.4719	4.058779	-26.0607	1.83E-114	6.47E-111	250.3708
CD274	-1.72634	3.513492	-24.4395	1.26E-103	3.69E-100	225.5661
GBP1	-1.78767	5.78937	-23.6833	1.25E-98	3.15E-95	214.1244
TBX21	-1.10858	2.774935	-23.6407	2.38E-98	5.24E-95	213.4834
LAG3	-1.85205	3.377779	-23.4894	2.35E-97	4.60E-94	211.2069
PRF1	-1.63103	4.379355	-23.3453	2.07E-96	3.65E-93	209.0422
GZMB	-2.24618	4.740927	-23.2192	1.39E-95	2.22E-92	207.1524
IRF1	-1.42651	5.666289	-23.1125	6.92E-95	1.02E-91	205.5539
HAPLN3	-1.41129	4.525962	-22.575	2.19E-91	2.97E-88	197.5407
TYMP	-1.58202	5.473206	-22.5498	3.19E-91	4.02E-88	197.1668
KLRD1	-1.14652	2.880229	-22.3416	7.11E-90	8.36E-87	194.0795
LAP3	-1.18876	7.021848	-22.0442	5.90E-88	6.50E-85	189.6866
GBP1P1	-1.54847	2.716381	-21.6716	1.46E-85	1.51E-82	184.2105
CD96	-1.45713	3.042683	-21.6038	3.95E-85	3.87E-82	183.2182
CXCL11	-2.76598	4.432923	-21.5883	4.96E-85	4.60E-82	182.9915
TAP2	-1.12166	4.58346	-21.4417	4.28E-84	3.77E-81	180.8492
USP30-AS1	-1.46041	3.222933	-21.3465	1.73E-83	1.45E-80	179.4613
TAP1	-1.53485	6.901162	-21.2337	9.01E-83	6.91E-80	177.8192
STAT1	-1.37441	6.723666	-21.1809	1.95E-82	1.43E-79	177.051
GZMH	-2.04389	4.030525	-21.1495	3.09E-82	2.18E-79	176.5946
UBE2L6	-1.33854	6.663227	-21.0561	1.21E-81	8.19E-79	175.2394
NKG7	-2.10947	4.714764	-20.9891	3.20E-81	2.09E-78	174.2695
IL18BP	-1.16247	4.251962	-20.6754	3.05E-79	1.92E-76	169.7397
CXCL10	-2.62148	6.017864	-20.629	5.97E-79	3.63E-76	169.0722
JAKMIP1	-1.14945	2.271342	-20.5908	1.04E-78	6.10E-76	168.5229
SLA2	-1.12374	3.334717	-20.5796	1.22E-78	6.94E-76	168.3618
CXCR6	-1.41183	3.686143	-20.5152	3.09E-78	1.70E-75	167.4373
TIGIT	-1.387	3.102083	-20.4872	4.63E-78	2.47E-75	167.0355
IL21R	-1.24281	2.823282	-20.2912	7.78E-77	4.04E-74	164.23
CRTAM	-1.77706	2.507919	-20.1785	3.93E-76	1.98E-73	162.6212
GNLY	-1.84332	3.786585	-20.0977	1.25E-75	6.12E-73	161.4711
CXCL9	-2.70501	5.879483	-19.8492	4.34E-74	2.07E-71	157.9432
ZNF683	-1.49941	3.210272	-19.6149	1.21E-72	5.62E-70	154.6355
BATF2	-1.66725	4.712729	-19.4485	1.27E-71	5.76E-69	152.2963
IL2RB	-1.48553	4.758879	-19.3648	4.14E-71	1.83E-68	151.1233
KLRC3	-1.04734	1.911848	-19.3608	4.39E-71	1.89E-68	151.067
CCL5	-1.92942	6.009196	-19.3162	8.21E-71	3.37E-68	150.4433
ICAM1	-1.43026	5.295064	-19.243	2.30E-70	9.02E-68	149.419
AIM2	-2.05065	3.717292	-19.2081	3.76E-70	1.44E-67	148.9326
IFIH1	-1.0596	4.370766	-19.1052	1.59E-69	5.97E-67	147.4982
SIRPG	-1.39763	2.853407	-19.0969	1.78E-69	6.56E-67	147.3832
APOL3	-1.25584	4.575031	-19.0028	6.66E-69	2.40E-66	146.075
APOL6	-1.06443	5.153018	-18.9589	1.23E-68	4.33E-66	145.4658

## Prognostic role of pyroptosis-related genes in gastric cancer

GZMA	-1.84492	4.949727	-18.8868	3.36E-68	1.16E-65	144.4665
IL12RB1	-1.00177	3.308407	-18.7877	1.33E-67	4.52E-65	143.0962
ETV7	-1.36147	4.23029	-18.669	6.92E-67	2.26E-64	141.4595
RNF213	-1.07039	5.05339	-18.6644	7.37E-67	2.36E-64	141.3973
PSMB9	-1.3798	6.57102	-18.6419	1.01E-66	3.17E-64	141.0869
PTPN22	-1.09793	3.200523	-18.5563	3.29E-66	1.02E-63	139.9112
APOBEC3G	-1.26387	4.206232	-18.4628	1.19E-65	3.63E-63	138.6292
PSMB10	-1.11139	6.118016	-18.4055	2.63E-65	7.85E-63	137.845
CD8A	-1.84211	4.412119	-18.385	3.48E-65	1.02E-62	137.565
HLA-DOA	-1.5506	4.035924	-18.2961	1.18E-64	3.36E-62	136.3505
TNFSF13B	-1.39766	5.195762	-18.282	1.43E-64	4.01E-62	136.1588
KLHDC7B	-1.31388	3.11822	-18.2359	2.70E-64	7.31E-62	135.5312
NLR5	-1.19484	5.043821	-18.2256	3.10E-64	8.30E-62	135.3906
SLAMF8	-1.44643	4.348474	-18.2102	3.83E-64	1.01E-61	135.1816
SAMD9L	-1.53208	4.695359	-18.1228	1.27E-63	3.28E-61	133.9945
KLRC4	-1.17385	1.577925	-17.8906	2.98E-62	7.63E-60	130.8537
ZBP1	-1.35329	2.720734	-17.8425	5.73E-62	1.44E-59	130.2054
LILRB4	-1.21939	3.165039	-17.7503	2.00E-61	4.89E-59	128.9649
THEMIS	-1.31427	2.756617	-17.7282	2.69E-61	6.50E-59	128.6687
SH2D1A	-1.29271	2.986779	-17.565	2.42E-60	5.77E-58	126.4845
IFIT3	-1.51314	5.830556	-17.513	4.87E-60	1.13E-57	125.7907
CXCR3	-1.24504	3.586424	-17.4689	8.80E-60	2.02E-57	125.2029
LAMP3	-1.52723	4.752006	-17.4494	1.14E-59	2.55E-57	124.9426
PLA2G2D	-1.78298	2.619041	-17.4332	1.42E-59	3.13E-57	124.7281
HAVCR2	-1.15342	3.775779	-17.4262	1.56E-59	3.40E-57	124.6339
IL2RA	-1.16975	3.369232	-17.412	1.89E-59	4.01E-57	124.4456
CD3G	-1.31208	3.751683	-17.3951	2.36E-59	4.96E-57	124.2215
PDCD1LG2	-1.25256	2.459625	-17.3669	3.45E-59	7.15E-57	123.8463
GPR171	-1.45689	3.594426	-17.3135	7.03E-59	1.44E-56	123.1388
ZBED2	-1.52848	2.339475	-17.2943	9.08E-59	1.84E-56	122.8842
CCR5	-1.34766	4.425179	-17.2024	3.08E-58	6.18E-56	121.6691
IFI35	-1.02067	5.718356	-17.1801	4.15E-58	8.13E-56	121.3745
CD247	-1.1519	3.651872	-17.1423	6.85E-58	1.31E-55	120.8762
ITGAL	-1.35197	4.10479	-17.083	1.50E-57	2.82E-55	120.0944
EPSTI1	-1.35037	5.480953	-17.0626	1.97E-57	3.64E-55	119.8263
JAK2	-1.20636	4.281729	-17.0622	1.98E-57	3.64E-55	119.8205
CD38	-1.64728	3.864888	-17.0249	3.25E-57	5.90E-55	119.3306
TLR8	-1.29719	3.144036	-16.9794	5.92E-57	1.05E-54	118.7343
IL32	-1.3428	6.439153	-16.9222	1.26E-56	2.22E-54	117.9848
CLEC2D	-1.03037	2.750319	-16.7064	2.14E-55	3.67E-53	115.1692
OAS2	-1.36606	5.098954	-16.6002	8.57E-55	1.44E-52	113.7914
PYHIN1	-1.07541	2.758997	-16.56	1.45E-54	2.40E-52	113.2719
CD2	-1.49103	5.174619	-16.5402	1.87E-54	3.06E-52	113.0153
SLAMF7	-1.66653	4.210657	-16.5037	3.01E-54	4.87E-52	112.5441
CD300LF	-1.25538	3.703832	-16.4993	3.19E-54	5.11E-52	112.4871
ICOS	-1.42521	2.775487	-16.2931	4.59E-53	7.17E-51	109.8361
UBASH3A	-1.27128	2.530287	-16.2522	7.78E-53	1.19E-50	109.3127
SNX10	-1.2003	5.184888	-16.2376	9.40E-53	1.42E-50	109.1251
STX11	-1.04782	3.334425	-16.1826	1.91E-52	2.80E-50	108.4232

## Prognostic role of pyroptosis-related genes in gastric cancer

CD74	-1.30425	8.058649	-16.1321	3.65E-52	5.23E-50	107.7789
SLC15A3	-1.10948	4.826265	-16.1194	4.29E-52	6.10E-50	107.617
SIGLEC10	-1.20916	3.706367	-16.0145	1.64E-51	2.32E-49	106.2837
IL4I1	-1.42906	3.838432	-15.9635	3.15E-51	4.41E-49	105.6372
ZAP70	-1.18635	3.236698	-15.9006	7.01E-51	9.74E-49	104.8424
CTLA4	-1.06892	3.040391	-15.8958	7.46E-51	1.03E-48	104.7813
CMKLR1	-1.08042	3.465696	-15.8368	1.58E-50	2.14E-48	104.0366
HLA-DMB	-1.36654	5.899453	-15.7391	5.44E-50	7.21E-48	102.8075
GBP2	-1.12052	5.741394	-15.6924	9.81E-50	1.29E-47	102.2221
CD3D	-1.37019	5.244348	-15.5937	3.40E-49	4.41E-47	100.9876
FCGR1B	-1.08097	3.328647	-15.5908	3.53E-49	4.54E-47	100.9513
HK3	-1.11209	2.776986	-15.5062	1.02E-48	1.29E-46	99.89639
LCP2	-1.01079	4.096755	-15.4985	1.12E-48	1.41E-46	99.80139
TRAC	-1.37868	5.431936	-15.4854	1.32E-48	1.66E-46	99.6379
CD84	-1.04861	3.534901	-15.4412	2.30E-48	2.86E-46	99.08944
DOK2	-1.03446	4.068926	-15.4261	2.78E-48	3.43E-46	98.9021
CCL4	-1.4232	5.066903	-15.4134	3.26E-48	3.99E-46	98.74386
CYBB	-1.27734	4.497968	-15.3943	4.13E-48	5.02E-46	98.50815
TRAT1	-1.27845	2.727951	-15.3477	7.39E-48	8.92E-46	97.93119
HLA-DMA	-1.33004	6.639855	-15.3179	1.07E-47	1.29E-45	97.56213
SLAMF6	-1.16313	3.664096	-15.2152	3.83E-47	4.50E-45	96.29722
TNFSF10	-1.11654	6.358827	-15.213	3.94E-47	4.60E-45	96.26956
CX3CL1	-1.34592	4.282181	-15.0969	1.65E-46	1.89E-44	94.8457
IGSF6	-1.11907	4.130879	-15.0781	2.08E-46	2.32E-44	94.61581
APOL1	-1.29514	6.285014	-15.0058	5.07E-46	5.59E-44	93.73294
CIITA	-1.08827	3.447376	-14.9976	5.61E-46	6.14E-44	93.63248
NCF1	-1.12414	3.585945	-14.9429	1.10E-45	1.19E-43	92.96622
MAP4K1	-1.08885	3.615022	-14.9097	1.65E-45	1.76E-43	92.56325
ITK	-1.16071	3.538305	-14.8803	2.36E-45	2.49E-43	92.2058
TFEC	-1.0093	2.852336	-14.8109	5.50E-45	5.77E-43	91.36591
LILRB1	-1.1218	3.577598	-14.7662	9.48E-45	9.89E-43	90.82556
TRBC1	-1.15323	4.324132	-14.7539	1.10E-44	1.14E-42	90.67705
TRIM22	-1.21996	5.884855	-14.7296	1.48E-44	1.52E-42	90.38481
BIRC3	-1.3359	5.67084	-14.7056	1.98E-44	2.03E-42	90.09573
C1QA	-1.41323	6.644572	-14.6984	2.16E-44	2.20E-42	90.00893
XAF1	-1.064	4.574723	-14.6928	2.31E-44	2.34E-42	89.94094
HCST	-1.12102	4.906659	-14.6739	2.90E-44	2.93E-42	89.71419
PRKCQ	-1.01174	3.333984	-14.6456	4.09E-44	4.10E-42	89.37383
DHX58	-1.00496	3.562542	-14.615	5.93E-44	5.90E-42	89.00655
ITGB7	-1.09677	3.4338	-14.6038	6.78E-44	6.68E-42	88.87282
IKZF3	-1.29399	3.540706	-14.5683	1.04E-43	1.01E-41	88.4469
PLEK	-1.26028	4.77013	-14.4681	3.47E-43	3.35E-41	87.25112
GFI1	-1.0329	2.90409	-14.3856	9.34E-43	8.90E-41	86.26976
HLA-DPA1	-1.48344	6.963538	-14.3774	1.03E-42	9.76E-41	86.17338
NLRC3	-1.09113	3.450843	-14.2959	2.72E-42	2.57E-40	85.20825
MICB	-1.09486	4.543145	-14.206	7.93E-42	7.40E-40	84.14704
C1QB	-1.45876	6.975558	-14.1872	9.91E-42	9.20E-40	83.92606
EOMES	-1.1428	3.612076	-14.153	1.48E-41	1.36E-39	83.52481
DPYD	-1.05575	4.151208	-14.0794	3.54E-41	3.19E-39	82.66165

## Prognostic role of pyroptosis-related genes in gastric cancer

OAS3	-1.05063	5.337618	-14.0731	3.81E-41	3.41E-39	82.58849
CD3E	-1.13604	4.364999	-14.0507	4.97E-41	4.38E-39	82.32584
P2RY13	-1.26058	3.187418	-14.0465	5.22E-41	4.58E-39	82.27775
SIGLEC1	-1.164	3.79367	-14.0415	5.53E-41	4.81E-39	82.21927
CD86	-1.04523	4.138302	-14.0373	5.82E-41	5.03E-39	82.16927
SIT1	-1.26781	3.610463	-14.0048	8.53E-41	7.23E-39	81.79033
IFIT2	-1.153	4.545695	-13.9961	9.44E-41	7.97E-39	81.68904
HLA-DPB1	-1.24918	6.86552	-13.8675	4.26E-40	3.54E-38	80.19446
AOAH	-1.0955	3.770346	-13.8234	7.12E-40	5.81E-38	79.68517
CLEC4E	-1.01132	3.035083	-13.8134	8.00E-40	6.47E-38	79.56907
ITGB2	-1.20878	4.930908	-13.8074	8.58E-40	6.91E-38	79.49982
TBC1D10C	-1.0571	3.748558	-13.7511	1.65E-39	1.28E-37	78.85092
ACP5	-1.10619	5.737338	-13.7237	2.27E-39	1.72E-37	78.53573
CD40	-1.03237	4.531851	-13.674	4.03E-39	2.97E-37	77.96486
CST7	-1.25411	4.804418	-13.6561	4.96E-39	3.63E-37	77.75864
OASL	-1.25841	4.782212	-13.593	1.03E-38	7.46E-37	77.03657
HLA-DRA	-1.32331	8.887327	-13.5849	1.13E-38	8.15E-37	76.94432
BIN2	-1.11549	3.799017	-13.573	1.29E-38	9.27E-37	76.80911
SLA	-1.01686	4.562465	-13.5669	1.39E-38	9.87E-37	76.73867
PTPRC	-1.25281	4.813935	-13.5327	2.06E-38	1.44E-36	76.34878
CD53	-1.10205	5.209922	-13.5141	2.54E-38	1.77E-36	76.13708
SECTM1	-1.14763	5.39264	-13.5054	2.81E-38	1.94E-36	76.03845
ADAMDEC1	-1.5928	4.835004	-13.4309	6.59E-38	4.54E-36	75.19282
GZMM	-1.11075	2.899223	-13.4248	7.07E-38	4.83E-36	75.12316
RASGRP1	-1.06847	4.045234	-13.424	7.13E-38	4.86E-36	75.1146
HCK	-1.01422	4.53857	-13.339	1.88E-37	1.27E-35	74.15347
CCR1	-1.00579	4.570657	-13.3118	2.56E-37	1.72E-35	73.84712
PLA2G7	-1.26829	5.001209	-13.2754	3.87E-37	2.57E-35	73.43716
SLC1A3	-1.07067	3.316332	-13.2538	4.94E-37	3.26E-35	73.19512
C1QC	-1.26745	7.064372	-13.223	7.00E-37	4.59E-35	72.84923
LCP1	-1.13223	5.967788	-13.1612	1.41E-36	9.09E-35	72.15788
IFITM1	-1.20646	8.076191	-13.1564	1.49E-36	9.56E-35	72.10357
P2RY10	-1.08626	3.05838	-13.0133	7.40E-36	4.63E-34	70.51183
BST2	-1.30007	6.850634	-12.9757	1.13E-35	6.95E-34	70.09505
SASH3	-1.07753	4.703293	-12.9109	2.32E-35	1.42E-33	69.37921
CORO1A	-1.09697	5.201756	-12.823	6.15E-35	3.71E-33	68.41283
CD7	-1.05236	3.817542	-12.7083	2.18E-34	1.28E-32	67.1584
FCER1G	-1.12135	6.371534	-12.6093	6.45E-34	3.70E-32	66.08295
HLA-DOB	-1.06169	3.185148	-12.5935	7.66E-34	4.37E-32	65.91163
CXCL13	-2.18367	5.296091	-12.5497	1.24E-33	6.99E-32	65.43763
TNFAIP2	-1.03107	5.30466	-12.4823	2.57E-33	1.43E-31	64.71153
LCK	-1.09231	4.523586	-12.4418	3.99E-33	2.20E-31	64.27617
CASP1	-1.0913	5.386825	-12.4186	5.13E-33	2.79E-31	64.02712
APOC1	-1.37269	6.093299	-12.2421	3.43E-32	1.79E-30	62.14581
CTSW	-1.14301	3.436921	-12.23	3.90E-32	2.02E-30	62.01783
RSAD2	-1.24958	4.529799	-12.2186	4.41E-32	2.28E-30	61.89669
LAPTM5	-1.03957	7.050242	-12.1701	7.39E-32	3.75E-30	61.38396
FPR3	-1.15369	4.638867	-12.1659	7.73E-32	3.91E-30	61.33958
IFI44	-1.10063	5.035672	-12.1522	8.94E-32	4.51E-30	61.19512

## Prognostic role of pyroptosis-related genes in gastric cancer

HLA-DQB2	-1.19564	3.696556	-12.1256	1.19E-31	5.92E-30	60.91407
CMPK2	-1.03886	5.313313	-12.0827	1.87E-31	9.30E-30	60.46282
IL10RA	-1.01365	4.733931	-12.0713	2.11E-31	1.05E-29	60.34311
CD48	-1.04619	4.388943	-11.9831	5.36E-31	2.60E-29	59.42041
CCL18	-1.76165	5.533357	-11.9295	9.43E-31	4.54E-29	58.86193
TGM2	-1.02922	5.595118	-11.8185	3.02E-30	1.42E-28	57.71029
APOE	-1.28946	6.728426	-11.7887	4.11E-30	1.93E-28	57.40278
GZMK	-1.38006	3.9883	-11.7173	8.63E-30	4.00E-28	56.66841
MX1	-1.09602	5.902376	-11.7065	9.66E-30	4.45E-28	56.55726
HLA-DRB6	-1.32526	4.66653	-11.6931	1.11E-29	5.08E-28	56.42054
IFI44L	-1.36888	4.477214	-11.6419	1.88E-29	8.56E-28	55.89647
EVI2B	-1.06366	5.334309	-11.3804	2.73E-28	1.20E-26	53.24767
MNDA	-1.02138	4.627542	-11.2768	7.79E-28	3.32E-26	52.21128
SOWAHA	1.428179	4.085916	11.23307	1.21E-27	5.12E-26	51.77619
HLA-DQB1	-1.25557	5.420894	-11.2265	1.29E-27	5.45E-26	51.71059
ISG15	-1.05471	7.134546	-11.2247	1.31E-27	5.52E-26	51.69299
CCL8	-1.26084	4.198086	-11.184	1.98E-27	8.20E-26	51.28974
TCEA3	1.012944	4.844596	11.03398	8.81E-27	3.47E-25	49.811
BCL2A1	-1.14247	4.837489	-10.9986	1.25E-26	4.89E-25	49.46505
CD27	-1.11357	4.337048	-10.9985	1.25E-26	4.89E-25	49.46415
PMAIP1	-1.00701	4.749237	-10.9601	1.83E-26	7.07E-25	49.08853
CD52	-1.17849	5.816532	-10.9146	2.86E-26	1.09E-24	48.64567
FMO5	1.015765	3.722771	10.76843	1.19E-25	4.40E-24	47.23269
MUC16	-1.09618	1.747865	-10.7164	1.98E-25	7.22E-24	46.73361
FAM3B	1.961208	4.921229	10.57783	7.52E-25	2.62E-23	45.41261
IL2RG	-1.07946	5.919447	-10.5497	9.84E-25	3.38E-23	45.14604
HMGCS2	2.044358	4.938481	10.54024	1.08E-24	3.69E-23	45.05678
CD163	-1.03511	4.653017	-10.4008	4.06E-24	1.33E-22	43.74501
SUCNR1	-1.10115	3.240811	-10.2724	1.36E-23	4.33E-22	42.55002
NEURL3	-1.10558	3.270631	-9.97601	2.12E-22	6.34E-21	39.83766
GUCY2C	1.688427	4.299357	9.720254	2.15E-21	6.02E-20	37.54908
CHIT1	-1.06803	2.348874	-9.67109	3.34E-21	9.24E-20	37.11474
SCNN1A	1.2684	5.12814	9.507582	1.42E-20	3.82E-19	35.68346
TFF3	1.808903	6.36527	9.38289	4.24E-20	1.09E-18	34.6056
LINC00261	1.671566	3.850185	9.322564	7.16E-20	1.80E-18	34.0884
IGHG1	-1.12929	5.281731	-9.24418	1.41E-19	3.48E-18	33.42053
VSNL1	-1.20523	3.767789	-9.11632	4.21E-19	1.01E-17	32.34135
TM4SF20	1.808621	4.250576	9.095341	5.03E-19	1.20E-17	32.16553
PROM1	1.470239	5.761914	9.06579	6.47E-19	1.52E-17	31.91839
SMIM24	1.635327	5.947574	9.041305	7.96E-19	1.86E-17	31.71414
PLEKHS1	-1.21704	4.017999	-9.03826	8.16E-19	1.90E-17	31.68879
REEP1	1.025573	3.668233	8.962791	1.54E-18	3.52E-17	31.06235
CDH17	1.848436	6.130962	8.676104	1.66E-17	3.55E-16	28.72358
MMP9	-1.09152	5.631714	-8.65634	1.94E-17	4.13E-16	28.56478
NR1I2	1.056265	3.369352	8.539228	5.03E-17	1.03E-15	27.62998
RBP4	1.387906	3.941766	8.435821	1.15E-16	2.34E-15	26.81372
ZBTB7C	1.047288	3.378303	8.413474	1.38E-16	2.77E-15	26.63846
PRAP1	1.580725	4.853674	8.373743	1.89E-16	3.76E-15	26.32784
CKB	1.041133	5.799021	8.35812	2.14E-16	4.22E-15	26.20606

## Prognostic role of pyroptosis-related genes in gastric cancer

REG4	2.131133	5.907702	8.322824	2.82E-16	5.52E-15	25.93163
HLA-DQA1	-1.48851	4.91039	-8.31759	2.94E-16	5.74E-15	25.89105
NROB2	1.181628	4.338953	8.305616	3.23E-16	6.27E-15	25.7982
AOC1	1.282527	5.98737	8.296282	3.48E-16	6.71E-15	25.72593
ERAP2	-1.00117	4.286192	-8.25253	4.91E-16	9.30E-15	25.38809
REG1A	2.45408	6.61988	8.133405	1.24E-15	2.29E-14	24.47619
TM4SF5	1.125104	5.267303	8.104982	1.54E-15	2.82E-14	24.26032
ITLN1	1.757415	4.203511	8.079021	1.89E-15	3.41E-14	24.06373
GGT6	1.229835	4.126859	8.075182	1.94E-15	3.50E-14	24.0347
CLDN3	1.553322	6.148682	8.058748	2.20E-15	3.95E-14	23.9106
TM4SF4	1.663036	4.321273	8.054771	2.27E-15	4.06E-14	23.88059
SLC01B3	-1.26395	2.444378	-8.03629	2.62E-15	4.65E-14	23.74136
IGHM	-1.42255	6.427732	-8.03362	2.67E-15	4.74E-14	23.72123
MMP12	-1.48014	5.93987	-8.00706	3.27E-15	5.75E-14	23.52166
REG3A	2.064028	4.323832	7.978176	4.08E-15	7.08E-14	23.30532
CHI3L1	-1.10976	4.569415	-7.94182	5.38E-15	9.24E-14	23.03393
SPINK4	1.907325	4.637652	7.863413	9.72E-15	1.64E-13	22.45244
MZB1	-1.10917	4.621182	-7.84148	1.15E-14	1.92E-13	22.2907
IGHV1-69	-1.10267	3.221195	-7.76667	2.00E-14	3.29E-13	21.74195
WFDC2	1.298359	4.466244	7.766705	2.00E-14	3.29E-13	21.74221
VSIG2	1.323889	5.238353	7.761152	2.09E-14	3.43E-13	21.70165
IGLL5	-1.25481	5.886437	-7.71162	3.01E-14	4.86E-13	21.34113
PPP1R1B	1.446869	5.513268	7.640876	5.08E-14	7.98E-13	20.82976
FABP1	1.780536	3.796608	7.567355	8.68E-14	1.34E-12	20.30275
CXCL14	1.225398	5.753145	7.550701	9.80E-14	1.50E-12	20.184
SI	1.753095	3.507331	7.520345	1.22E-13	1.86E-12	19.96816
PCK1	1.2203	3.523833	7.490314	1.52E-13	2.29E-12	19.75538
MUC20	1.029919	4.240138	7.476003	1.68E-13	2.51E-12	19.65425
IGKC	-1.10027	7.627939	-7.27102	7.23E-13	1.02E-11	18.22478
SOSTDC1	1.293356	3.245767	7.20267	1.17E-12	1.62E-11	17.75604
SLC44A4	1.000074	6.120378	7.163271	1.53E-12	2.10E-11	17.48767
GSTA1	1.245838	4.737209	7.162771	1.54E-12	2.10E-11	17.48427
HEPACAM2	1.270971	3.182235	7.127144	1.97E-12	2.66E-11	17.24275
MEP1A	1.437369	3.520276	7.120024	2.07E-12	2.79E-11	17.19461
SLC39A5	1.014016	4.136339	7.113774	2.16E-12	2.90E-11	17.15239
CHP2	1.251602	2.899363	7.032034	3.79E-12	4.95E-11	16.60331
C9orf152	1.044916	5.221179	6.916676	8.28E-12	1.04E-10	15.83817
SCGB2A1	1.246862	2.840178	6.883775	1.03E-11	1.28E-10	15.62206
PGC	2.158453	6.577776	6.880866	1.05E-11	1.31E-10	15.60299
IGLV1-44	-1.15993	6.268803	-6.87654	1.08E-11	1.34E-10	15.57466
CDX1	1.427475	4.623075	6.809218	1.70E-11	2.06E-10	15.13578
ANXA13	1.114345	4.383017	6.731995	2.83E-11	3.33E-10	14.6372
DUOX2	1.356959	4.514285	6.634826	5.34E-11	6.07E-10	14.01722
CLRN3	1.127346	5.467898	6.559636	8.67E-11	9.64E-10	13.54314
TFF1	1.599723	7.972554	6.48042	1.44E-10	1.54E-09	13.04902
SERPINB2	-1.01588	2.674147	-6.24823	6.15E-10	6.10E-09	11.63259
TFF2	1.733246	6.38321	6.186997	8.96E-10	8.66E-09	11.26699
IGLV6-57	-1.02998	4.487879	-6.14619	1.15E-09	1.09E-08	11.02518
FOLR1	1.00057	3.658	6.089129	1.62E-09	1.51E-08	10.68959

## Prognostic role of pyroptosis-related genes in gastric cancer

SST	1.230545	3.41636	6.03486	2.24E-09	2.05E-08	10.3731
AKR1B10	1.429791	6.07492	5.876195	5.73E-09	4.86E-08	9.462895
MUC6	1.325998	4.297497	5.873972	5.80E-09	4.91E-08	9.450306
KRT20	1.52244	4.916111	5.795889	9.13E-09	7.50E-08	9.01083
CHGA	1.072955	3.729114	5.778185	1.01E-08	8.23E-08	8.911945
SLC6A14	-1.11978	4.735673	-5.72461	1.37E-08	1.09E-07	8.614453
PCSK1N	1.03438	4.17106	5.708727	1.50E-08	1.19E-07	8.526745
FAM3D	1.030764	5.645195	5.640296	2.21E-08	1.70E-07	8.151506
PSCA	1.397946	5.06099	5.433306	6.96E-08	4.89E-07	7.042353
AGR3	1.033655	6.608379	5.301997	1.41E-07	9.41E-07	6.358992
GKN1	1.658028	4.561589	4.897706	1.13E-06	6.45E-06	4.354491
GKN2	1.370019	4.169295	4.848052	1.45E-06	8.07E-06	4.118723
ADH1C	1.055051	5.590649	4.740801	2.44E-06	1.30E-05	3.617301
MUC5AC	1.119009	4.903346	4.660829	3.58E-06	1.85E-05	3.250387
MAGEA6	1.193754	3.187223	4.57933	5.26E-06	2.61E-05	2.882621
LIPF	1.347958	4.557164	4.157699	3.49E-05	0.000146	1.079622
OLFM4	1.249237	7.033496	3.86787	0.000117	0.000435	-0.06224